University of Southampton

Faculty of Environmental and Life Sciences

School of Ocean and Earth Science

Descent from the Hyperthermals: Persistent Organic-Matter Rich Lakes in the Eocene

by

Amy Louisa Elson

ORCID ID 0000-0002-1220-5674

Thesis for the degree of Doctor of Philosophy

November, 2021

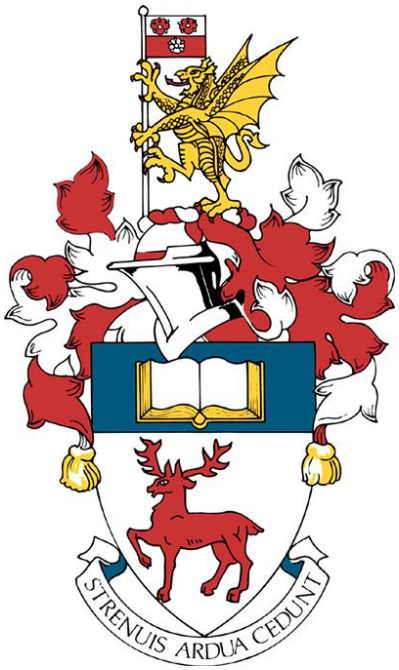

University of Southampton

Abstract

Faculty of Environmental and Life Sciences

School of Ocean and Earth Science

Thesis for the degree of Doctor of Philosophy

Descent from the Hyperthermals: Persistent Organic-Matter Rich Lakes in the Eocene

by

Amy Louisa Elson

In this doctoral thesis, I reconstruct continental paleoclimate from the early Cenozoic, when the Earth's surface experienced a long-term warming trend punctuated by a series of short-lived global warming (hyperthermal) events that culminated in an extended interval of elevated CO_2 and extreme warmth, the Early Eocene Climatic Optimum (EECO, 53.26 to 49.14 Ma). The hydrological cycle's response to climate perturbations is thought to be highly variable, and can promote feedbacks that induce further warming or cooling, thus serving as critical lessons for future warm worlds. However, the response of the hydroclimate regime operating during the EECO is poorly constrained, especially for the mid-to-low latitudes and particularly from continental interior sites.

Here, I adopt a multi-proxy approach, integrating geochemical, organic petrographic, and sedimentological perspectives from organic-rich sediments from the Green River Formation of the Uinta Basin, Utah and the Piceance Basin, Colorado, U.S.A., which were deposited in long-lived, large lakes at ~40ºN. I observed a wide range of organic matter types and distribution, with accumulation of organic matter at the lamination scale controlled by longer term sub-orbital cycles suggesting decadal periodicities in large organic-matter fluxes and associated carbon drawdown. Spatial and temporal variations in salinity conditions were the result of long-term tectonic controls driving the water balance between fresher and brine-rich inputs into the Uinta Basin, increasing ecological stress on biota living in the water column and leading to the cessation of conditions favouring prodigious organic accumulation in the Mahogany Zone, a regionally extensive marker unit. Lastly, hydrogen isotopes from organic molecules indicate that the hydrological cycle operates differently during gradual vs. transient warming events, and that a stable hydrological regime may have supported deep lake development and promoted organic matter preservation. These organic-rich lake systems acted as an important negative feedback during the termination of the EECO, sequestering at least ~76 Gt of organic carbon over the ~400 kyr history of the Mahogany Zone.

Table of Contents

Table of Tables

Chapter 2

Chapter 3

Chapter 4

Appendix D

Table of Figures

Chapter 1

Chapter 2

Chapter 3

Table of Figures

Chapter 4

Research Thesis: Declaration of Authorship

Print name: Amy Louisa Elson

Title of thesis: Descent from the Hyperthermals: Persistent Organic-Matter Rich Lakes in the Eocene

I declare that this thesis and the work presented in it are my own and has been generated by me as the result of my own original research.

I confirm that:

1. This work was done wholly or mainly while in candidature for a research degree at this University;
2. Where any part of this thesis has previously been submitted for a degree or any other qualification at this University or any other institution, this has been clearly stated;
3. Where I have consulted the published work of others, this is always clearly attributed;
4. Where I have quoted from the work of others, the source is always given. With the exception of such quotations, this thesis is entirely my own work;
5. I have acknowledged all main sources of help;
6. Where the thesis is based on work done by myself jointly with others, I have made clear exactly what was done by others and what I have contributed myself;
7. None of this work has been published before submission.

Signature: ..... Date: 05.11.2021

Acknowledgements

It is a genuine pleasure to express my deep sense of gratitude to my mentor and supervisor, Dr. Jessica H. Whiteside for all of her continual support and enlightening insight to our research, and for her trust in extending many fascinating and collaborative opportunities to me during my PhD. I would also like to express my sincere gratitude to my secondary supervisor, Dr. John E. A. Marshall, for particular guidance and wisdom on all thing's terrestrially related, and his heroic efforts to try and dissolve the Mahogany Zone.

Special thanks must go to Sargent Bray for his vital laboratory support, and the equally as important humour he brought to the lab. I would also like to thank the NOCS PhD community but in particular, the Palaeoclimate research group at Southampton for all of the useful conversations, meetings, and support in my development as I moved into the world of geochemistry. Thank you to the NERC CDT Oil and Gas program, who co-funded this project along with the University of Southampton, for the extensive support, for the CDT community, and for the many, *many* courses and fieldtrips that gave me countless good memories.

I would also like to thank my family, particularly my sister, mother, and father, and my friends, especially my friends from my alma mater (Keele University), and the locals in Southampton, for their unwavering support and patience through both the fun and the challenging times.

Last, but not least, I would like to thank the many friends and colleagues I made along the road to this thesis, for the support in my academic development and also the many cherished memories I'll keep.

Definitions and Abbreviations

ACL: Average chain length

am: Amorphous organic matter

AOM: Amorphous organic material

Bi: Bituminite

ca: Calcite

CO_2: Carbon dioxide

CPI: Carbon preference index

Cu: Cutinite

DCM: Dichloromethane

EECO: Early Eocene Climatic Optimum

ENSO: El Niño–Southern Oscillation

ETM2: Eocene Thermal Maximum 2

ETM3: Eocene Thermal Maximum 3

ft: Foot

GC-MS: Gas Chromatograph - Mass Spectrometer

GI: Gammacerane index

Gt: Gigatonne

hb: Herbaceous

In: Inertinite

IPCC: Intergovernmental Panel on Climate Change

Kyr: Thousand years

La: Lamalginite

Ld: Liptodetrinite

Li: Liptinite

Ma: Millions of years

mm: Millimetre

OC: Organic Carbon

OEP: Odd-even Predominace

OM: Organic Matter

OMA: Organo-Mineralic Aggregates

PETM: Paleocene-Eocene Thermal Maximum

Pf: Framboidal pyrite

Ph: Phytane

Pr: Pristane

py: Pyrite

RCP: Representative Concentration Pathway

SEM-EDS: Scanning Electron Microscope- Energy Dispersive X-ray spectroscopy

SEM: Scanning Electron Microscope

sp: Spore

Sp: Sporinite

TAR: Terrigenous-to-aquatic ratio

TL: Transmitted light

TLE: Total lipid extracts

TOC: Total Organic Content

UV: Ultraviolet

Vi: Vitinite

VSMOW: Vienna Standard Mean Ocean Water

w: Woody

wt.%: Weight percent

yr: Year

$\delta^{13}C$: Ratio of two stable carbon isotopes, ^{12}C:^{13}C

$\delta^{18}O$: Ratio of two stable oxygen isotopes, ^{18}O:^{16}O

$\delta^{2}H$: Ratio of two stable hydrogen isotopes, ^{2}H:^{1}H

µm: Micrometre

Chapter 1 Introduction

1.1 Thesis Introduction

Understanding how past rapid warming has affected global precipitation patterns in warm worlds is essential to enhancing our forecasting ability of the impacts of future climate change. The early Eocene (~56-47.8 Ma) represents an interval of peak warmth during the past 65 million years, with global temperatures ~14 ± 3 °C warmer than pre-industrial temperatures and CO_2 concentrations likely exceeding 1000 ppm (95 % confidence; Anagnostou et al., 2016). These levels are similar to predicted outcomes of 'business as usual' scenarios, i.e. RCP8.5, when extended to 2300 (IPCC AR5). The Eocene thus speaks to the effect of rapid warming on hydrological stability and resilience of Earth's Critical Zone. Lakes, particularly closed-basin systems, are more sensitive than the oceans to global change and tend to record more dramatic responses. The Eocene Green River Formation of Utah, Colorado, and Wyoming, USA, is comprised of giant lakes deposited from ~53.5 to 43 Ma, spanning the Early Eocene Climatic Optimum. Drill cores in multiple basin locations through the Parachute Creek Member offer an unprecedented opportunity to explore high-resolution continental records that are well-constrained through improved geochronological estimates from frequent ash layers. The breadth of tools utilised in Chapters 2, 3, and 4 includes field and core observational, microscopic, geochemical, and molecular perspectives and allows for assessment of palaeoclimate conditions of these large long-lived lakes of the Eocene, and implications for the behaviour of the wider terrestrial climate during this transition.

1.2 Early Eocene Climate

The early Eocene (~56 to 47.8 Ma) represents an interval of prolonged Cenozoic warmth that culminated in the early Eocene Climatic Optimum (53.26 to 49.14 Ma; EECO; Figure 1), where CO_2 concentrations reached ~1625 ± 760 parts per million by volume (Zachos et al., 2001, 2008; Jagniecki et al., 2013; Anagnostou et al., 2016; Lunt et al., 2017; Foster et al., 2017; Westerhold et al., 2018a). Superimposed on this longer warming trend is a series of at least twenty gas-induced periods of rapid warming where temperature spikes exceeded 5°C, known commonly as hyperthermal events (examples observed in continental and marine sections include: PETM, ~56 Ma; ETM2, ~53.7 Ma; and ETM3, ~52.8 Ma; Thomas et al., 2000; Cramer et al., 2003; Lourens et al., 2005; Nicolo et al., 2007; Stap et al., 2009; Galeotti et al., 2010; Zachos et al., 2008, 2010; Abels et al., 2016; Zeebe and Lourens, 2019).

Multiple drivers of this extended warmth have been identified and debated, including volcanic outgassing, reduced silica weathering, and the destabilisation of methane hydrates as a result of elevated ocean temperatures (Zachos et al., 2008; Lunt et al., 2011; Hyland & Sheldon 2013; Reagan et al., 2013; Gutjahr et al., 2017). Due to the lack of permanent ice sheets, the ice-albedo feedback mechanism that acts as a prominent amplifier of high climatic variability in the modern world, was non-existent. Despite this, the Eocene displays a surprising amount of climate variability which requires strong feedback mechanisms not observed in the Earth system today, or the presence of very strong and variable orbital forcing, or both (Röhl et al., 2004; Lourens et al., 2005; Nicolo et al., 2007).

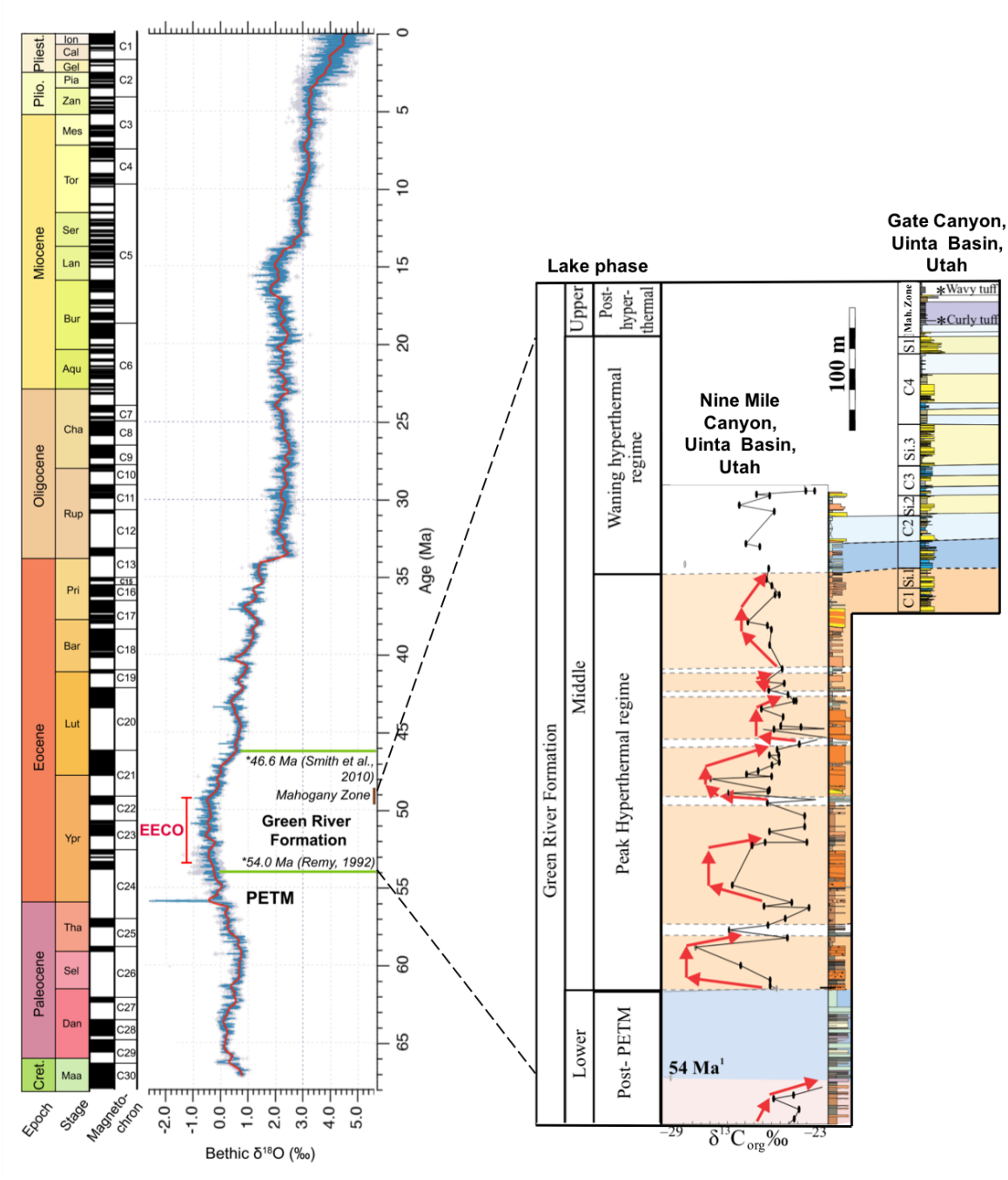

Figure 1: (Left) Benthic foraminifera $\delta^{18}O$ record forming part of the Cenozoic global reference benthic carbon and oxygen isotope dataset (CENOGRID; Modified from Westerhold et al., 2020). Deposition of the Green River Formation in the Uinta Basin is bracketed by dated tuff beds (*Remy, 1992; Smith et al., 2010) and encompasses the EECO (53.26 to 49.14 Ma), with the Mahogany Zone spanning the latest EECO (Smith et al., 2010; Westerhold et al., 2020). (Right) $\delta^{13}C_{org}$ sampled from fluvial floodplain-derived siltstone and paleosol units, and stratigraphic columns of Nine Mile Canyon and Gate Canyon of the Uinta Basin. At least four negative shifts in $\delta^{13}C_{org}$, ranging from 2.5‰ and 5‰, identify hyperthermal events in the Middle Green River Formation (Modified from Birgenheier et al., 2019). Hyperthermal events have also been identified in a $\delta^{13}C_{carb}$ and lacustrine lithologic

record from the Greater Green River Basin of Wyoming, and argued to occur during the eccentricity minima (Smith et al., 2014).

The large-scale changes in early Eocene climate and ocean circulation are recorded by evolutionary turnovers and extinction events in the marine and terrestrial record (McKenna, 1983; Wolfe, 1985; Huber and Caballero, 2011). Isotope excursions in oxygen and hydrogen indicate a major hydrological perturbation and increased continental runoff accompanying global warming (Pagani et al., 2006; Kraus and Riggins, 2007; John et al., 2008). The latitudinal temperature gradient in the early Eocene was at least 32% lower than modern while surface temperatures were substantially higher (Lunt et al., 2012; Evans et al., 2018).

Large amounts of methane were released in the early Eocene, mostly from wetlands, forests and other swampy environments, themselves more expansive because of the warmer climate (Sloan, 1994). More recently, it has been argued that hydrothermal vents associated with interaction between magmas and organic-rich sediments may have released large amounts of methane, potentially driving warming in the early Eocene (Svensen et al., 2004; Jones et al., 2018). In the Great Plains and northern Rocky Mountains of North America, deciduous plants flourished and diversified in the late Palaeocene. Flora in the early Eocene was markedly different to the temperate woodlands of the late Palaeocene, with families that are characteristic of extant megathermal rainforest extending far to the north and south (Wolfe, 1981, 1985; Wing and Greenwood, 1993). The largest lakes present in the early Eocene were lakes Uinta and Gosiute of the Green River Formation, analogous in area to the Great Lakes of North America today (Bradley, 1929; Johnson, 1985; Tänavsuu-Milkeviciene and Sarg, 2012; Feng et al., 2016; Vanden Berg and Birgenheier, 2017; Johnson et al., 2018; Birgenheier et al., 2019). The response of the North American continental interior to the early Eocene

hyperthermals has been contrasting, revealing strong local controls (Wing et al., 2005; Clechenko et al., 2007; Foreman et al., 2012; Kraus et al., 2013; Wang et al., 2017).

1.3 Lake-basin fill models

Based on the observation of numerous lacustrine successions in the geological record, Carroll and Bohacs (1999) proposed and refined (Bohacs et al., 2000) three lacustrine facies associations reflecting the three general deposit types observed. The principal controls on lake-basin type and the related successions preserved is the potential accommodation space that determines the volume a lake can occupy, and the combined water and sediment fill which fills this accommodation space. The interplay between these two primary controls determine the lake basin type, which can be defined as under-filled, balance-filled and over-filled. In this lake model, under-filled basins are related to evaporitic facies associations, showing dominantly aggradation cycles of sedimentation in saline-hypersaline lakes which may experience desiccation, evaporation, and aeolian input. Balanced-filled basins are characterised by fluctuating profundal facies associations, with mixed aggradational to progradational cycles and can deposit rich oil-shale systems (Birgenheier et al., 2019). Over-filled lake basins often have the most stable lake-levels and are filled with fluvial-lacustrine facies associated with sedimentary packages more progradational in nature and containing a mix of freshwater lacustrine mudstones and fluvio-deltaic deposits. These lake basin classifications are useful over time-averaged successions but their applicability can break down when applied to short time spans and complex or interconnected lacustrine systems.

Lacustrine basins such as the Uinta Basin, the focus of this doctoral thesis, can be endorheic in nature, where water only leaves via evaporation. Due to the lack of

outflow, lake chemistry may become enriched in dissolved salts, leading to high pH and salinity which can fluctuate with water inflow variations (Tuttle and Goldhaber, 1993). Organic-rich sediments in lacustrine environments are often laminated as a result of seasonal variation in precipitated carbonate material and blooms of organic matter, which together form a 'varve' or lacustrine 'couplet' (Crowley et al., 1986; Ripepe et al.1991). Paler-coloured laminations are from lacustrine whiting events, where spring and summer precipitation of carbonate follows organic-rich darker laminations from algal blooms that destabilises the bicarbonate equilibrium in the upper water column (Allen and Collinson, 1986).

Terrestrial records can have high sedimentation rates on the order of m kyr^{-1} compared to deep-sea records, which typically have sedimentation rates closer to the order of <cm kyr⁻1 but more continual deposition (Westerhold et al., 2018b; Walters et al., 2020). Deep lacustrine environments allow for an expanded section without the high likelihood of hiatuses and erosion, which may affect floodplain and palaeosol reconstructions (Hyland et al., 2018).

1.4 Green River Formation

The Green River Formation was deposited in a network of continental interior lakes during the early-middle Eocene over ~10 million years (~53.5-43 My; Sheliga 1980; Remy 1992; Smith et al., 2008; Figure 2). Named after a tributary of the Colorado River, the ancient lake systems of the Green River Formation record widespread economically important resources of oil shales and trona, along with a wealth of fauna and flora (MacGinitie 1969; Wilf 2000; Smith et al., 2008; Vanden Berg and Birgenheier. 2017). The Green River Formation also provides one of the most extensive terrestrial records of the EECO; 53.26 to 49.14 Ma, the peak of Cenozoic warming and greenhouse conditions (Zachos et al., 2001, 2008; Smith et al., 2008;

Westerhold et al., 2018a). These intermittently alkaline and saline lakes have been argued to record a range of temporal variability from orbital pacing (20-2400 kyr) and sub-orbital periodicities at the quasi-decadal (8-18 year) and sub-decadal (2-8 year) timescales (Sayles 1922; Bradley 1929; Fischer and Roberts 1991; Ripepe et al., 1991; Cole 1998; Machlus et al., 2008; Meyers 2008; Whiteside and Van Keuren, 2009; Aswasereelert et al., 2013) despite the tectonic influence usually held to persist through long-lived lacustrine basins, including the Green River Formation (Kelts, 1988; Pietras and Carroll, 2006). Improved geochronological dates from frequent ash layers of the Challis and Absaroka volcanic fields have permitted inter-basin correlation of the formation's various sedimentary expressions (Smith et al 2008; 2010), allowing for a deeper understanding of the Green River Formation lake system in a broader palaeogeographic and climatic context.

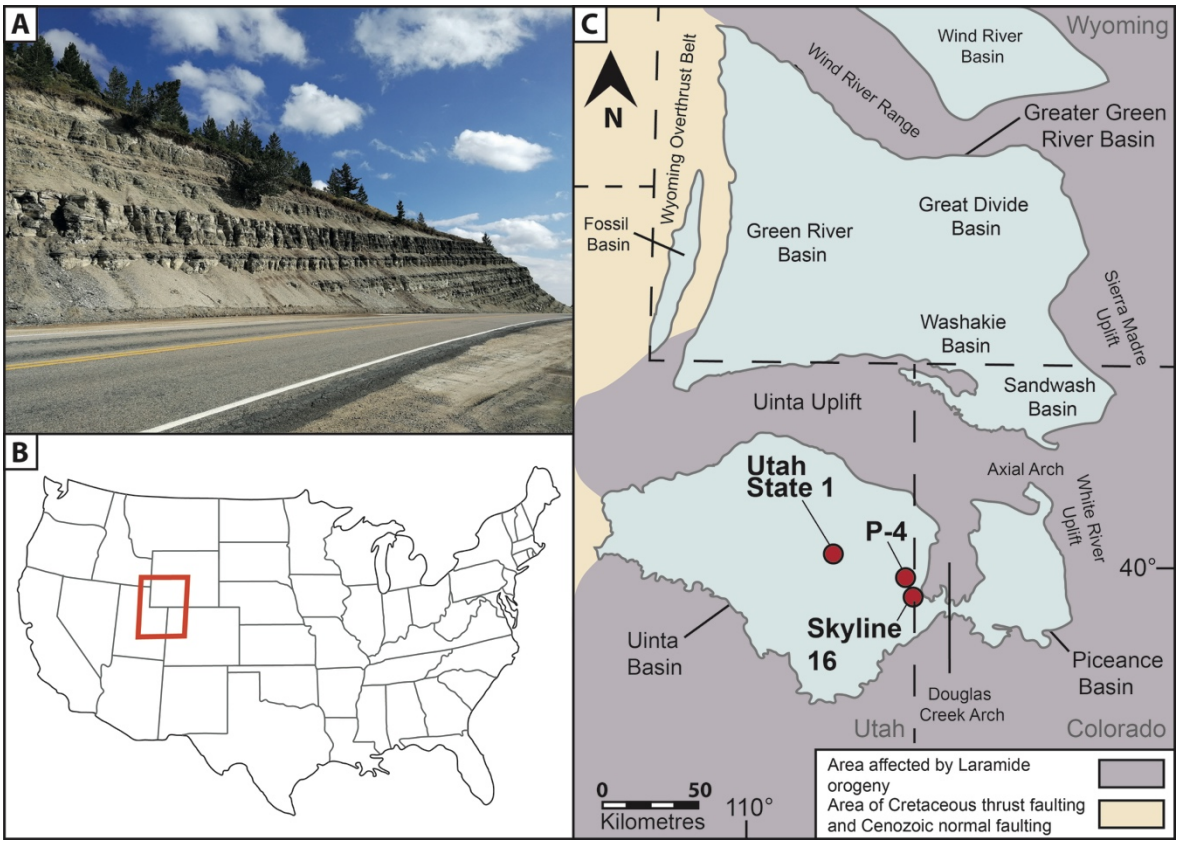

Figure 2: (A) The Mahogany Zone in outcrop at Indian Canyon, Uinta Basin, Utah. (B) Location of the Green River Formation, spanning Utah, Colorado, and Wyoming. (C) Overview of the Green River Formation basins and locations of Utah State 1, P-4, and

Skyline 16, the three Uinta Basin cores in this thesis (Modified from Grande, 1964; Johnson et al., 2019).

1.4.1 Basins of the Green River Formation

Late Cretaceous Laramide-related deformation resulted in four structural basins situated around the Uinta Uplift: the Uinta; Piceance; Greater Green River; and Fossil basins (Figure 2). Each record a wide variety of lithofacies resulting from changes in depositional environments, including but not restricted to: lake depth and chemistry, sedimentary supply, and ecological variations (Bohacs et al., 2003; Smith et al., 2008; Rosenberg et al., 2015). Around the margins of the lake system, interfingering with the primarily alluvial facies of the Uinta, Wasatch, Bridger, Colton and DeBeque formations, is common. The southern basins were occupied by Lake Uinta, the focus of this thesis, which was partially split by the low Douglas Creek Arch into the eastern Piceance Basin of Colorado and the western Uinta Basin of Utah (Cashion, 1967; Carroll and Bohacs, 1999).

1.4.1.1 Greater Green River and Fossil basins

Towards the north, the Greater Green River Basin is divided by intra-basin anticlines into four structural sub-basins, occupied by the large ancient Lake Gosiute. The Rock Springs uplift, the largest anticline, trends north-south across the centre of the greater Green River Basin and separates it into the Green River Basin to the west and the Sand Wash, Washakie, and Great Divide basins towards the east (Baars et al., 1988; Mederos et al., 2005). Anticlinal structural separators such as the Cherokee Ridge divided the southern Sand Wash Basin from the central Washakie Basin, which is separated from the Great Divide Basin in the north by the Wamsutter Arch. To the west of the Greater Green River Basin lies the Fossil Lake deposits of

the Fossil Basin. These basins are all predominately found in Wyoming (Bohacs et al., 2000).

The first deposition of Green River Formation in the Greater Green River Basin is the Luman Tongue, a freshwater lacustrine environment with lean oil shale deposits. Above this lies the Tipton Shale Member, which represents the transition from a freshwater lake with less-rich organic mudstones to a saline lacustrine environment with organic-rich mudstone deposition. Increasingly evaporitic conditions led to widespread deposition of evaporitic minerals in the Green River Basin during the Wilkins Peak Member, which comprises cyclic evaporitic mudflat environments during shallower intervals and organic-rich mudstones representing deeper lake depths. Around the basin margin and in the contemporaneous sub-basins of the Greater Green River Basin, strata indicative of saline lacustrine and mudflat deposits, including organic-rich oil shale deposits, are present during deposition of the Wilkins Peak Member. In the youngest member of the Green River Formation in the Greater Green River Basin, widespread oil shale deposition in saline conditions transitioned to freshwater leaner oil shale deposits in the eastern basins. Contemporaneously, in the western Green River Basin there is an absence of organic-rich material, where floodplain and freshwater lacustrine mudstones and channel sandstones predominated (Roehler, 1993).

One of the richest palaeontological sites on Earth, Fossil Basin is divided into three members: the Road Hollow Member at the base, the Fossil Butte Member, and the overlying Angelo Member. Lacustrine deposits of the Green River Formation are ~400 feet thick and comprised of laminated, organic-rich beige-brown carbonate mudstone, limestone, siltstone, sandstone, and evaporites, with frequent oil shale and volcaniclastic beds (Buchheim, 1994). The famed fossil fish beds of Fossil Basin

are found in the Fossil Butte Member, before the freshwater lake turned hypersaline in the Angelo Member (Oriel and Tracey, 1970).

1.4.1.2 Uinta and Piceance basins

Towards the south, the long-lived Lake Uinta occupied the Uinta and Piceance basins, with the freshwater Uteland Butte Member representing the base of the Green River Formation in the Uinta Basin (Figure 3). Transitioning to a saline

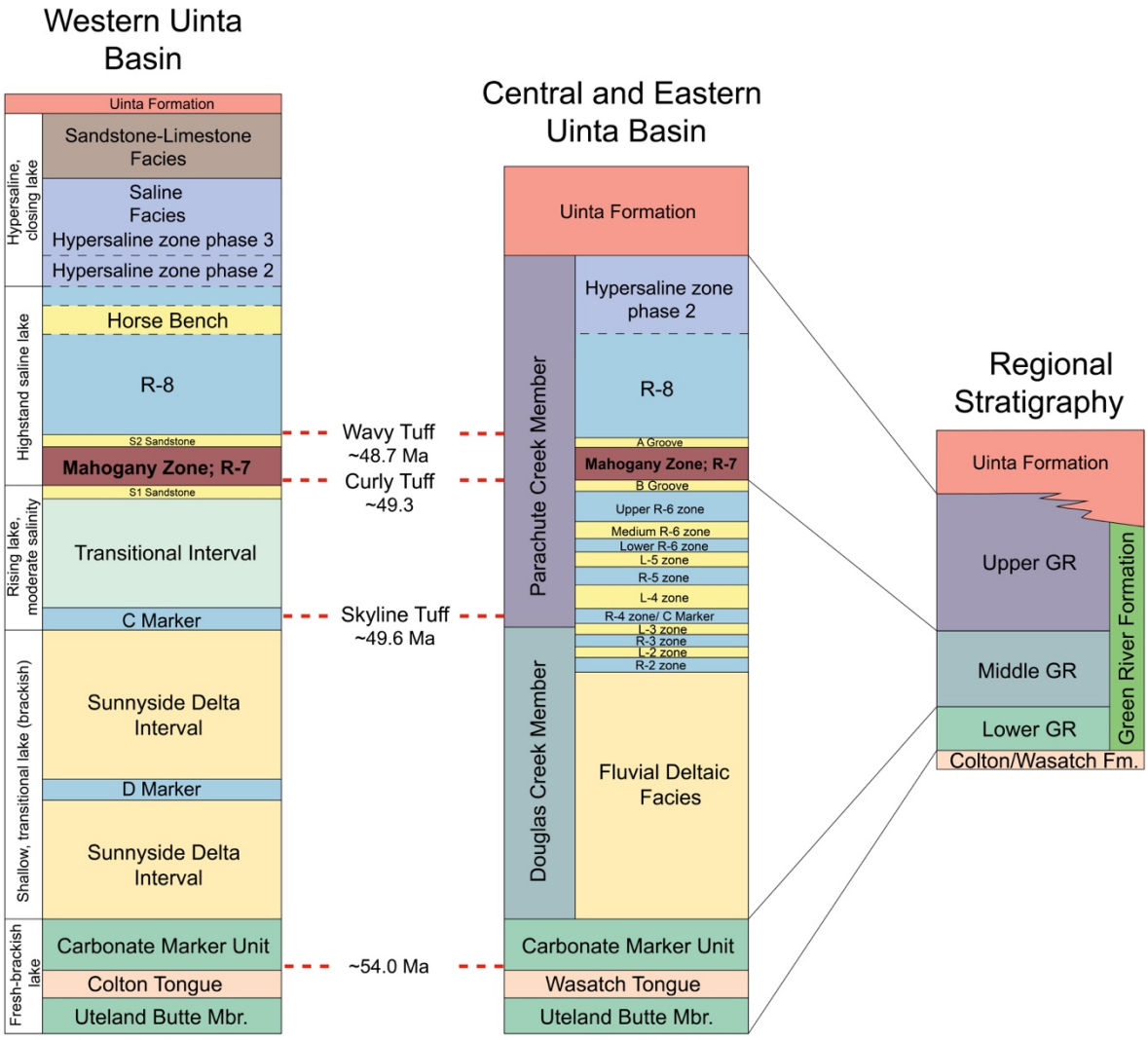

Figure 3: The regional stratigraphy of the Western Uinta Basin (left) and the Central and Eastern Uinta Basin (middle), in the context of the generalized stratigraphy for the Green River Formation in the Uinta Basin (right). The study interval, the Mahogany Zone, represents the base of the Upper Green River Formation and lies in the Parachute Creek Member of the Green River Formation. (Modified from Vanden Berg and Birgenheier, 2017; Johnson et al., 2018; and Birgenheier et al., 2019).

environment in the Carbonate Marker Unit, the middle Green River Formation comprises a series of lacustrine mudstones and ephemeral fluvial sandstones associated with hyperthermal events of the EECO (Gall et al., 2017; Birgenheier et al., 2019; Birgenheier et al., 2020). The Mahogany Zone is bounded by two laterally extensive sandstones known as the 'S1' and 'S2' sandstones, deposited during periods characterised by fluvial incursions from the south (Gall et al., 2017). These sandstones represent two of many marker beds present through the Green River Formation. Much of the Mahogany Zone is comprised of continuous parallel laminated to minorly undulose laminated mudstone with little bioturbation (Roehler, 1993; Whiteside and Van Keuren, 2009; Figure 4). The oil-shale rich sections have a mottled undulose appearance, which in outcrop, results in a paper-thin weathering style. In the underlying B-Groove, and overlying the Mahogany Zone in the A-Groove, lie two tuffs that bracket the Mahogany Zone. The Curly Tuff (49.32±0.3 Ma) and younger Wavy Tuff (48.67±0.23 Ma; Smith et al., 2008; 2010) are considered ash-flow deposits and sourced from the north-eastern Absaroka and Challis volcanic provinces (Smith et al., 2010; Rosenberg et al., 2015). Above the

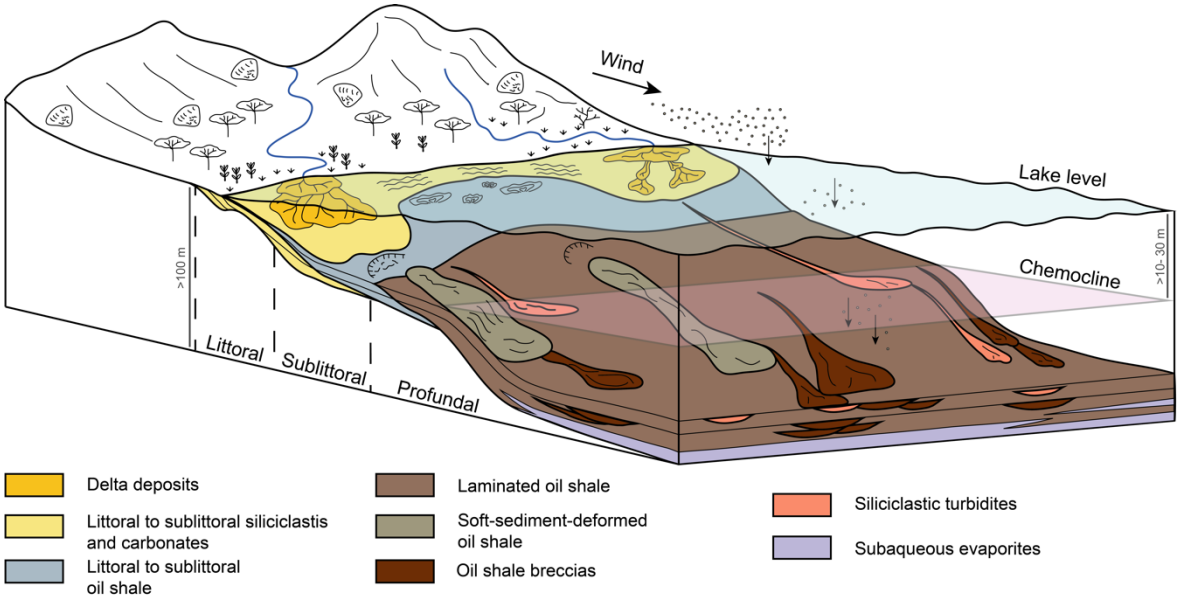

Figure 4: Green River Formation facies model for lacustrine-fluvial deposits and corresponding facies associations. (Modified from Tänavsuu-Milkeviciene and Sarg, 2012).

Mahogany Zone, the lake transitions into an increasingly saline environment, as the terminal basin infilled with water and sediment before the alluvial facies of the Uinta Formation became established. During peak deposition of the Mahogany Zone, the lake- depocentre was in the east of the basin, shifting westwards in the upper Green River Formation as the Lake Uinta was infilled from the east to the west (Bohacs et al., 2000).

1.5 Organic Geochemistry

Several key biomarkers were discovered in the Green River Formation, including perhydro- beta-carotene, various steranes and triterpanes and their aromatic forms, and gammacerane. However, biomarkers and their isotopic composition have not been analysed in an extensive stratigraphic context—the existing literature has worked on isolated data from limited samples from a few beds (Collister et al., 1994). In this thesis, I examined over 500 meters of core from multiple drill holes of varying distance from the palaeoshore. I specifically focus on the Mahogany Zone interval—*the* quintessential oil shale, containing one of the highest kerogen concentrations of any Paleogene, or indeed any, oil shale in the world.

Within the Mahogany Zone of the Green River Formation, four common categories of lipid biomarkers dominate: terrestrial leaf wax-derived *n*-alkanes; hopanoids (including bacterial); chlorophyll-derived isoprenoids; and algal-derived steranes (Tissot, 1987; Collister et al., 1994). Higher plants synthesise hydrocarbons with a strong predominance of odd over even numbered *n*-alkanes, which when preserved in the rock record can inform about terrigenous organic matter input. In particular, *n*-C_{27}, *n*-C_{25}, and *n*-C_{31} are indicative of vascular plant material, which when transported into local lacustrine basins are considered to be minimally transported by fluvial systems and to represent <2000 years of deposition (Davies-Vollum and

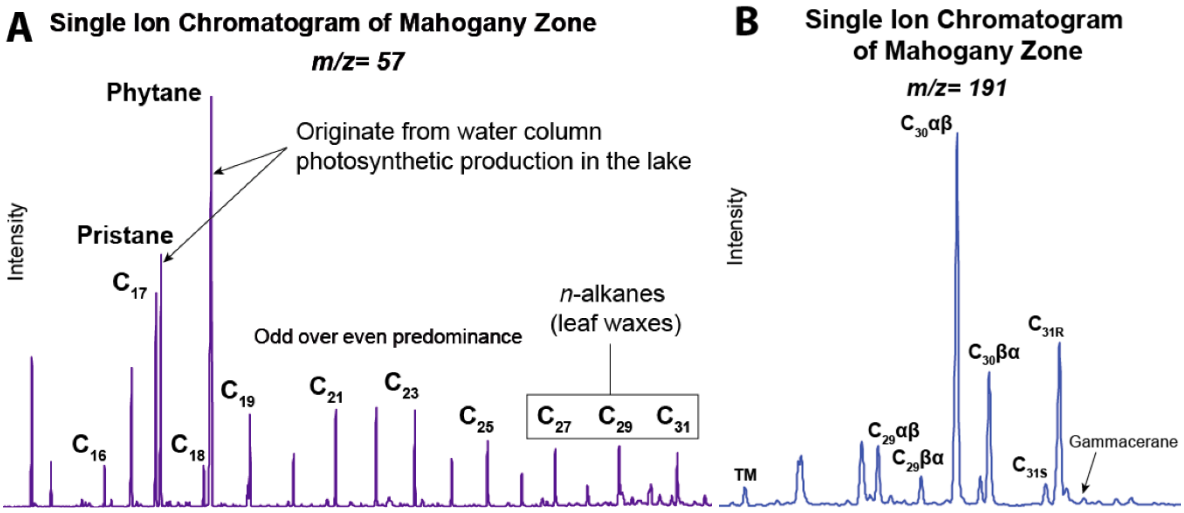

Figure 5: Representative GC-MS Single Ion Current chromatogram of a Green River Formation sample from the Mahogany Zone showing *n*-alkanes identified at m/z=57. High amounts of pristane and phytane, derived from water column photosynthetic production in the lake, are present. Odd/even predominance of *n*-alkanes is clear. (B) Single ion chromatogram at m/z=191, showing hopanes of the Mahogany Zone and gammacerane, a salinity stratification biomarker.

Wing, 1998). Pristane and phytane are derived from chlorophyll-*a*, the photoautotrophic pigment and precursor molecule involved in oxygenic photosynthesis during the light absorption and transfer into chemical energy. Phytane contains an extra carbon atom, unlike pristane which is formed through the dehydroxylation of phytol, with increasing ratios between pristane and phytane long used as a general indicator of redox conditions (Didyk, 1978; ten Haven et al., 1987; Witkowski et al., 2018). Lower molecular weight *n*-alkanes (e.g. *n*-C_{17}) are frequently attributed as aquatic in origin and comparison with terrestrially-derived material through various indices (i.e. average chain length; carbon preference index; terrestrial-to-aquatic ratio) can be a powerful tool for fingerprinting organic matter sources (Collister et al., 1994; Bourbonniere and Meyers, 1996; Ficken et al., 2000; Bi et al., 2005; Figure 5). The presence of gammacerane (the daughter molecule of tetrahymanol, which is considered to be derived from bactiverous ciliates living at the chemocline) in large amounts suggests the presence of a stratified water column

and potential hypersalinity in the depositional setting (Venkatesen, 1989; ten Haven et al, 1989; Sinninghe Damste et al., 1995; Peters et al., 2005).

Studies on modern plants have shown a strong correlation between the hydrogen isotopic ratios ($^2H/^1H$) of leaf wax lipids and the isotopic composition of meteoric water (Chikaraishi and Naraoka, 2003; Sachse et al., 2004, 2012; Sessions et al., 2004; Smith and Freeman, 2006; Hou et al., 2007; Feakins and Sessions, 2010). In this thesis, compound-specific *n*-alkane δ^2H data allow for inferences of hydrological change over the mid-latitudes during the deposition of a key oil shale interval. Leaf waxes conserve the δ^2H of the source water from the surrounding vegetative environment, and the δ^2H of phytane may give an insight into the lake hydrology as it is considered to derive from chlorophyll present in autotrophic aquatic micro-organisms.

The extremely organic-rich facies of the Green River Formation presents an ideal opportunity to interrogate the controls on the deposition and preservation of an organic-rich section during the termination of the EECO, through organic geochemical tools unavailable in less organic-rich sections.

1.6 Thesis aim, objectives and hypotheses

This dissertation aims to determine multiple aspects of paleo-reconstructions of the hydrological cycle during the EECO: the role of large, extremely organic-rich lakes in regulating greenhouse climate; competing drivers of the development, peak and waning of large organic carbon deposits; and multiple co-located sites for a single event. Specifically, this thesis has three main objectives:

1) An evaluation of the sedimentary character and organic petrography to assess the vertical- and micro-scale variation in sources of organic matter (Chapter 2).
2) The recovery of lipid biomarkers from multiple lacustrine sites to constrain productivity controls and burial indications during accumulation of a section exhibiting highly variable organic content (Chapter 3).
3) The recovery of compound-specific hydrogen isotopes from multiple lacustrine sites in the mid-to-low latitudes to constrain the hydroclimate regime during the terminal phase of the EECO (Chapter 4).

The underlying premise is that the hydrogen isotope composition of higher terrestrial plants and aquatic organisms record source water δ^2H variations reflecting a variety of climatic parameters, such as temperature, evaporation and water vapour source. A correlation between environmental waters and $\delta^2H_{(lipids)}$ allows inferences to be made about hydroclimate variation. However, the interpretation of δ^2H signals is complicated by significant ecological and environmental differences reported among existing studies (Sachse et al., 2004, 2012; Sessions et al., 2004), and by uncertainty about how the hydrological cycle might have differed during gradual vs. transient warming events. Conflicting processes from ecological, environmental, and geological processes may be integrated into the isotopic signal, further limiting understanding of meteoric water transport.

Disentangling these spatial and temporal processes is critical to interpreting the hydrogen isotopic signal, and for proper comparison to the results of other palaeoclimate investigations of the hothouse climate of the EECO. Controls of organic matter production and distribution, and the high levels of micro-scale heterogeneity exhibited in the organic-rich mudstones of the Mahogany Zone remain unresolved, further compounding successful isotopic interpretation. To

address this, in Chapter 2, I evaluate the organic matter distribution through detailed organic petrography and SEM analysis coupled with more traditional sedimentological characterization, all at high-resolution. I hypothesised that:

H_1 – ***Variations in the organic matter type follow predictable patterns, and that influxes of terrigenous material identifiable at the micro-scale are reflected in lower TOC values.*** Understanding the sedimentary character of the sections supported organic geochemical investigation as it allowed those results to be placed in the context of the larger depositional system, confirming intervals where material had been transported to the sample core locations from elsewhere in the basin and therefore were not indicative of original conditions at the sample location.

Persistent anoxic water column conditions and a low sediment supply existed throughout deposition of Mahogany Zone in the Uinta Basin, indicating other controls on TOC variability through section. Quantifying these controls, and the degree to which thermal maturation may have affected the character of organic compounds of the Mahogany Zone, is essential to the successful interpretation of hydrogen isotope signals. To address this, in Chapter 3, I generated lipid biomarkers through three cores to allow for disentanglement of multiple drivers and evaluation of water column conditions, including variations in salinity, redox, and remineralisation conditions. I hypothesised that:

H_2 – ***Fluxes in primary productivity, reflecting water column conditions rather than variable dilution and/or preservation of organic matter, are the key driver of TOC levels through the Mahogany Zone.*** After quantification of biomarker compounds for source delineation and water column conditions, I was then able to use compound specific stable isotopes to differentiate features reflecting wider climatic change from those reflecting more local processes.

Given that the distribution of terrestrial *n*-alkanes in the lacustrine record may vary temporally and spatially in response to ecosystem shifts, *n*-alkane hydrogen isotope values may reflect changes in the dominant vegetation type surrounding the lake instead of a hydroclimate signal. To address this concern, in Chapter 4, I generated compound-specific hydrogen isotopes in both *n*-alkanes and phytane through the Mahogany Zone at three different sites. In particular, I hypothesised that:

H_3 – ***N-alkanes and phytane in the lacustrine rock record capture temporal variations in the original source water signal, reflecting the behaviour of the hydroclimate operative during the termination of the EECO.*** These results provide the first high-resolution compound-specific hydrogen isotope records in the North American continental interior during the termination of the EECO.

Chapter 2 Controls on organic matter variation during deposition of the Mahogany Zone of the Parachute Creek Member, Green River Formation, Utah

Authors: Amy L. Elson[1], John Marshall[1], Jessica H. Whiteside[1]

[1] Ocean and Earth Science, National Oceanography Centre Southampton, UK

This chapter is modified from an invited research article accepted for publication in the peer-reviewed 2021 Utah Geological Association guidebook 'The Lacustrine Green River Formation: Hydrocarbon Potential and Eocene Climate Record': Elson, A, L., Marshall, J, E. A., and Whiteside, J. H. 2021. Controls on organic matter variation during deposition of the Mahogany Oil Shale Zone of the Parachute Creek Member, Green River Formation, Utah (Accepted). A. Elson conducted preliminary fieldwork and described the cores, retrieved rock plugs and undertook organic petrographical and SEM analysis of the thin sections, and wrote the manuscript. All the co-authors provided editing and feedback. Total organic content values for Skyline 16 were generated by Mike Vanden Berg (Utah Geological Association, Salt Lake City) and Justin E. Birdwell (USGS, Denver).

Abstract

The Green River Formation of Utah, Colorado, and Wyoming represents a ~10 million-year early-middle Eocene record of an unusually large, productive lacustrine system composed of several interconnected basins. This system gave rise to one of the largest oil shale deposits in the world, which preserves a rich trove of information about the climate and ecosystems that prevailed during the Early Eocene Climatic Optimum. This study uses multiple analytical approaches, including both traditional methods and novel proxies, to determine what brought about the accumulation of the unusually-rich oil shales (>40% TOC) of the Mahogany Zone in the Uinta Basin portion of the Green River Formation.

The organic-rich mudstones of the Mahogany Zone exhibit strong micro-scale heterogeneity, indicating complex controls on organic matter production and distribution. Petrographic observations indicate highly variable amounts of terrestrial organic matter (spores, wood and plant debris), with the most abundant being amorphous organic material in thin organic-rich laminae. Biomarker ratios indicate

that the organic-rich laminae consist of different types of microbially derived organic matter, primarily bituminite and organo-minerallic aggregates of the fluorescent liptinite group. These largely lacustrine-derived laminated deposits are argued to have been produced by large intra- to inter-annual algal blooms and other enhanced microbial productivity events paced by longer-term sub-orbital cycle fluctuations, such as El Niño–Southern Oscillation or sunspot variations. The Mahogany Zone deposits appear to have sequestered enough carbon (~76.07 Gt estimated) to suggest that, in aggregate, they were large enough to cause a draw-down of terrestrial CO_2 and exert a significant negative feedback effect on climatic warming. During the climatic cooling that occurred on the declining limb of the Early Eocene Climatic Optimum, the sedimentary provenance in the Uinta Basin shifted from southerly sources dominated by large ephemeral fluvial systems, to northerly sources rich in feldspathic and carbonate detritus derived from northern sites in Wyoming. The latter were delivered to the Uinta basin via a network of interconnected lacustrine basins. Increasing volcaniclastic material delivered from these northerly basins infilled the Uinta Basin from east to west, and their arrival heralded the end of organic-rich deposition, most notably the prolific oil shales for which the Green River Formation is renowned.

2.1 Introduction

The terrestrial carbon cycle has absorbed ~25% of anthropogenic carbon emissions over the last 50 years, but future behaviour under increasing pCO_2 is uncertain with terrestrial reservoirs potentially acting as either a net CO_2 source or sink (House et al., 2003; Keenan et al., 2016). Two key uncertainties in this system are variation in the lateral riverine transport of terrestrial organic carbon from upland terrestrial

ecosystems to lakes, and variation in the primary productivity in the lacustrine environment.

The early Eocene (~56-47.8 Ma) Green River Formation in Utah, Colorado, and Wyoming provides a ~10-million-year record of unusually large, productive lakes, Lake Uinta in the Uinta and Piceance basins of Utah and Colorado, and Lake Gosiute in the Greater Green River Basin of southwest Wyoming and northwest Colorado, that capture the Early Eocene Climatic Optimum, the warmest climate interval in the Cenozoic (Zachos et al., 2008, 2001; Bradley, 1929; Smith et al., 2008; Smith and Carroll, 2015; Westerhold et al., 2018a). Lake Uinta reached a highstand in the Mahogany Zone, representing an interval of prolific productivity, preservation, and sequestration of organic matter. Here, a combination of approaches from organic petrology and geochemistry are integrated to characterize this organic matter (OM), and the controls on its production and burial during this interval, shedding light on both lateral transport and the primary productivity of large continental lake systems.

2.1.1 The Green River Formation

Late Cretaceous (Maastrichtian) Laramide-related deformation resulted in the formation of three intermontane basins filled by alluvial and open- to marginal-lacustrine sediments of the Green River Formation. Lake Uinta was sited over Piceance Basin of Colorado on the east and the Uinta Basin of Utah on the west, and during lake lowstands was split by the low Douglas Creek Arch (Cashion, 1967; Carroll and Bohacs, 1999). The Douglas Creek Arch flooded over during lake highstands, and during the highstand represented by the Mahogany Zone, Lake Uinta reached ~14,900 km^2 in areal extent (Cashion, 1967). Bathymetrically, the Uinta Basin is highly asymmetric with a gently sloping southern flank, and a deep

northern structural trough where it abuts the southern flank of the Uinta Mountains (Johnson et al., 2019). The Uinta Basin was infilled from east to west during the final lacustrine phase (Smith et al., 2008).

In the Uinta Basin, the Mahogany Zone provides a ~400 kyr record during which unusually organic-rich sediments accumulated (Smith et al., 2008; Whiteside and Van Keuren, 2009). The Mahogany Zone is comprised of continuous organic-rich mudstones with parallel to slightly undulose laminations and little bioturbation, deposited in the profundal zone of the paleo-lake. Within the Mahogany Zone, the unusually organic-rich Mahogany Bed marker (Figure 2) has peak total organic carbon (TOC) of 45 wt.% (Whiteside and Van Keuren, 2008).

The long-term evolution of the Uinta Basin was driven by continental-interior tectonics and the balance of sediment and water fill, as postulated by models of Carroll and Bohacs (1999) for the Greater Green River Basin of Wyoming (see Section 1.3). Time constraints on the depositional interval of the Mahogany Zone are provided by $^{40}Ar/^{39}Ar$ ages of two prominent bracketing tuffs: 49.32 ±0.30 Ma for the older Curly Tuff and 48.67 ±0.23 Ma for the basal Wavy Tuff (Smith et al., 2008; 2010). As Eocene-aged continental sections with comparable age constraints are rare, these precise ages for the well-preserved highly organic-rich sections of the Mahogany Zone enable novel insights into the complex controls on organic matter variation in a large continental interior basin.

2.1.2 Paleoclimate

The Early Eocene Climatic Optimum (EECO) represents the zenith of the long-term warming trend in the early Cenozoic, when global temperatures were elevated ~5-10°C above present levels. The EECO was punctuated by at least twenty intervals of rapid warming, termed hyperthermal events, induced by large releases of gases

such as carbon dioxide and methane to the atmosphere. Hyperthermal events identified in continuous ocean records and therefore well-constrained through orbital tuning include the PETM (~56 Ma), the ETM2 (~53.7 Ma) and ETM3 (~52.8 Ma) (Nicolo et al., 2007; Stap et al., 2009).

The base of the Mahogany Zone, considered the largest and most economically important oil shale of the Green River Formation (214.5 billion barrels of oil in potential reserves for the Mahogany Zone; Vanden Berg, 2008; Birdwell et al., 2015), represents a major climatic shift marking a transition out of the greenhouse world of the EECO (Birgenheier and Vanden Berg, 2011). The transition into a modern cooler icehouse climate occurs against a background of declining atmospheric CO_2 concentrations through the Eocene (Pearson and Palmer, 2000). The associated reduction of weathering and high sedimentation rates facilitated the development of higher lake levels and a significant decrease in the preservation of episodic fluvial-deltaic facies in the Uinta Basin (Gall et al., 2017; Birgenheier et al., 2019).

2.1.3 Organic Matter Inputs During the Mahogany Zone

Lacustrine laminated organic-rich sediments are commonly the result of seasonal variation, showing annual couplets. The Mahogany Zone sediments are strikingly laminated on a sub-millimeter scale (Fischer and Roberts, 1991), representing hypolimnial strata deposited in an anoxic setting, with little to no bioturbation (Bradley 1929, 1931). Couplets (doublets and triplets) of organic ooze, interlayered with fine particles of precipitated carbonates (organic-rich calcimicrites), are thought to represent annual varves (μm to mm scale) and have afforded estimates of accumulation rates (Bradley, 1929; Crowley et al., 1986; Ripepe et al., 1991). Paler-coloured laminae (often called ‘whiting events’; see Section 1.3) represent spring

and summer production of carbonate which follow phytoplanktonic blooms that destabilise the bicarbonate equilibrium of the upper water column. These blooms lead to the formation of darker organic-rich laminae when organic matter settles out of the water column (Allen and Collinson, 1986; Johnson et al., 2018), and are typically carbonate-poor (Washburn et al., 2015). Terrestrial organic material such as leaf wax material, spores and pollen and plant debris also occur in locally significant amounts in the Mahogany Zone.

The factors that control the marked fine-scale heterogeneity observed in oil shales such as those in the Mahogany Zone are poorly understood. The tight timing constraints on Mahogany Zone deposition provides a unique opportunity to investigate an extremely organic-rich interval with a multitude of tools that will permit a better understanding of organic matter production and preservation and carbon sequestration in an unusually organic-rich Eocene lake basin.

2.2 Methods

Core plugs were obtained from Mahogany Zone sections from three drill cores located in central and eastern parts of the Uinta Basin: Utah State 1, the P-4 Chevron White Shale Project core, and Skyline 16. Detailed lithological descriptions and organic geochemical analyses (figure 1, 8) were made using this material.

The Utah State 1 core is in the central part of the Uinta Basin, drilled by TOSCO (The Oil Shale Corporation) and represents the most offshore of the three (Location: T9S, R21E, Sec. 26, UTM 12T 627029 4429992). The P-4 Chevron White Shale Project core (herein referred to as P-4) was drilled in the eastern part of the basin, targeting a more marginal, lacustrine environment of the Mahogany Zone than the former (Location: T10S, R25E, Sec. 19, UTM 12T 659426 4421812). The final core, Skyline 16 (Location: T11S, R25E, Sec. 9, UTM 12T 661444 4415107), was drilled

by the Utah Geological Survey, and represents the shallowest lake water levels and the most marginal of the three. It consists of a section of the Mahogany Zone which is thinner than that in P-4 and Utah State 1.

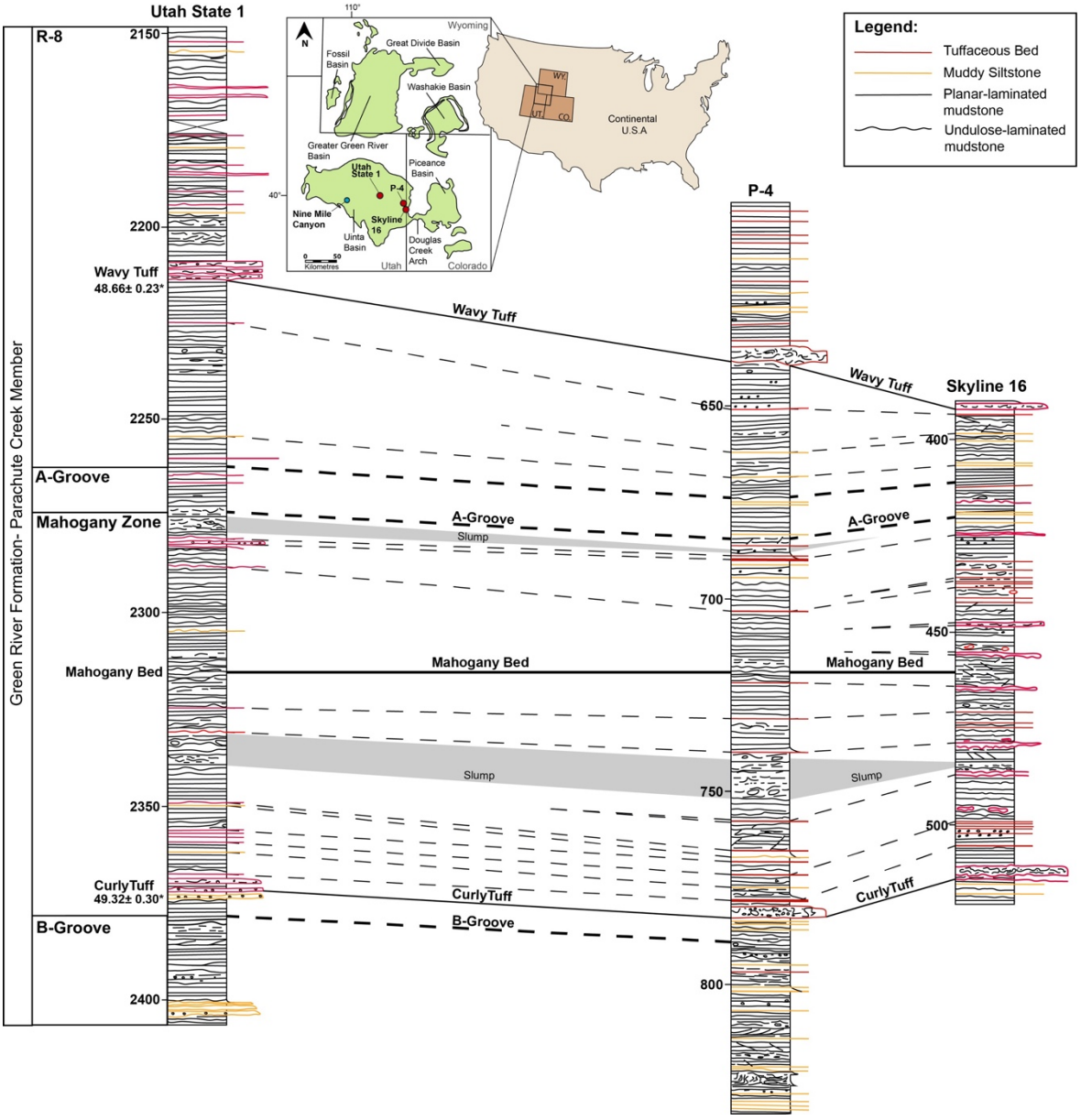

Figure 1: Comparison of the sedimentological descriptions of the three drill cores used in this study: Utah State 1, P-4 and Skyline 16. Bolded correlation lines represent important marker beds that run through the cores, including the Mahogany Bed Marker and the Curly and Wavy tuff beds. Present location of the drill sites shown in map inset in top center. Map modified after Grande, 1984. *Radioisotopic dates from Smith et al., 2010 (See Appendix A, B, C for full sedimentary logs).

Skyline 16 is a pristine core slabbed in 2010 and its proximity to the paleoshore-line coupled with the presence of highly organic-rich facies makes it ideally situated to

capture the full range of organic matter variation in the Mahogany Zone. Thin sections were cut at the National Oceanography Centre Southampton's Rock Preparation and Thin-Sectioning Laboratory and selected to capture the range of heterogeneity present in mudstone petrology. These sections were carbon coated for scanning electron microscope (SEM) analysis using a Leo 1450VP SEM and an Oxford Instruments X-Act 10 mm^2 area SEM-Energy Dispersive Spectrometer utilising the AZtec Energy software system. Along with SEM analysis, energy dispersive X-ray spectroscopy (EDS) was performed through a lamina set. Differences in X-ray response to the electron beam allowed for elemental mapping, and then the grouping together of elements for mineral identification. Once minerals were identified, they were assigned colors for creation of thin section maps. Bulk element analysis allowed for the calculation of several paleo-proxies for these intervals.

For petrological analysis, the carbon coat was removed by polishing with alumina powder. Two microscopes with multiple capabilities were used for this analysis, enabling us to investigate the biological origin of Mahogany Zone organic matter in the three classical methods of organic petrology. The first is a Zeiss UMSP 50 that can be flipped between incident white light tungsten illumination and incident light fluorescence illumination with filter set 9 (band pass excitation at 450-490 nm, with a dichroic beam splitter at 510 nm and a 520 nm long pass filter). This excitation wavelength provided a weak visible light fluorescence of liptinitic macerals. The second is an Olympus BHS equipped with blue excitation (band pass excitation at 380-490 nm, dichroic beam splitter at 500 nm and a 515 nm long pass) that gave a stronger fluorescence, and then can be flipped into transmitted white light mode. All images were captured with a Canon EOS 70D SLR attached to a phototube and operated with the EOS utility software.

To isolate biomarkers for the identification of relative amounts and sources of lacustrine organic matter, total lipid extracts (TLE) were isolated from powdered rock samples of Skyline 16 using a Thermo 350 Accelerated Solvent Extractor with the following program: preheat = 5 min; heat = 5 min; static = 5 min; pressure = 1500 psi; flush = 70%, purge = 300 s.; cycles = 3; solvent = dichloromethane:methanol (9:1, *v/v*). Solvent extracts were placed in a Genevac EZ-2 vacuum centrifuge until dry and then pipetted to small vials, where excess solvent was evaporated under a stream of N_2 gas. Once the samples had been gravimetrically quantified, TLEs were separated into fractions using small silica gel columns. Samples were de-asphaltened and then eluted with hexane, hexane: dichloromethane (DCM) (4:1, *v/v*), and DCM: methanol (MeOH) (1:1, *v/v*) yielded aliphatic, aromatic and polar fractions, respectively.

Identification of plant and algal biomarkers was made with a Thermo Trace 1310 gas chromatograph (GC) coupled to a Thermo TSQ8000 triple quadrupole mass spectrometer (MS). The GC used a DB-5 column (30 m ×0.25 mm inner diameter, 0.25-µm film thickness) with the following oven program: 40°C (held for 2 min), increased at a rate of 6°C/min to 310°C, and then held for 20 minutes. Compound identification of n-alkanes were made using mass spectra and comparison with an in-house reference oil (North Sea Oil-1; Weiss et al., 2000).

2.3 Results

2.3.1 Core Correlation

Core logs through the Mahogany Zone from the basin center (Utah State 1) to the basin margin (P-4 and Skyline 16) have many correlatable surfaces (Figure 1, 2). The thickness of the Mahogany Zone varies, from 83 ft in Skyline 16 to 102 ft for P-4 and Utah State 1. This difference in thickness is largely from slump deposits

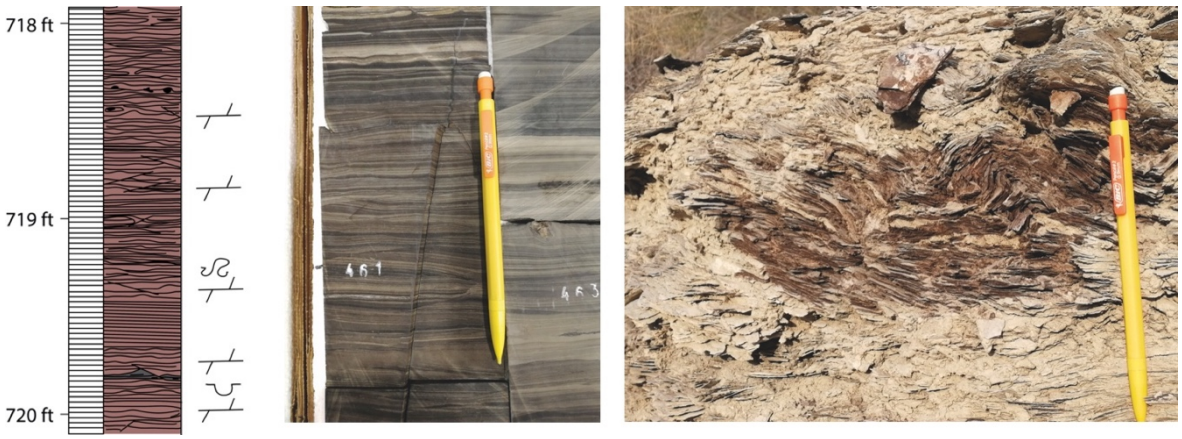

Figure 2: (Left) Schematic log of the Mahogany Bed Marker in core P-4. (Middle) Mahogany Bed Marker in core Skyline 16. Clear minor faulting and slip/deformation is common due to high organic content. (Right) Highly contorted paper-thin laminae and box folding in the Mahogany Bed Marker at Nine Mile Canyon, Utah.

present in P-4 and Utah State 1, which are much thinner in Skyline 16. These slump deposits are thickest at P-4 and thin towards the basin center. Tuffaceous material is present in higher amounts in Skyline 16, with several tuff layers thinning out before reaching the location of P-4.

2.3.2 SEM

2.3.2.1 Organic Matter Variation

Multiple styles of organic matter have been preserved in Skyline 16, varying from distinct laminations of organic-rich material (Figure 3-l), to isolated lenses of organic matter (appearing black in figure 3), to microbial mat textures (Figure 3-i), commonly in close association with carbonate minerals and pyrite. Discontinuous kerogen laminae are also common.

The microbial mats are highly undulose in form, usually warped around larger silt-sized grains. In organic-rich laminations, the microbial mat textures layer on each other, often connected vertically as well as horizontally. In leaner laminations (lighter grey in figure 3), there is some horizontal connectivity of the more-dispersed organic matter present, but very little vertically.

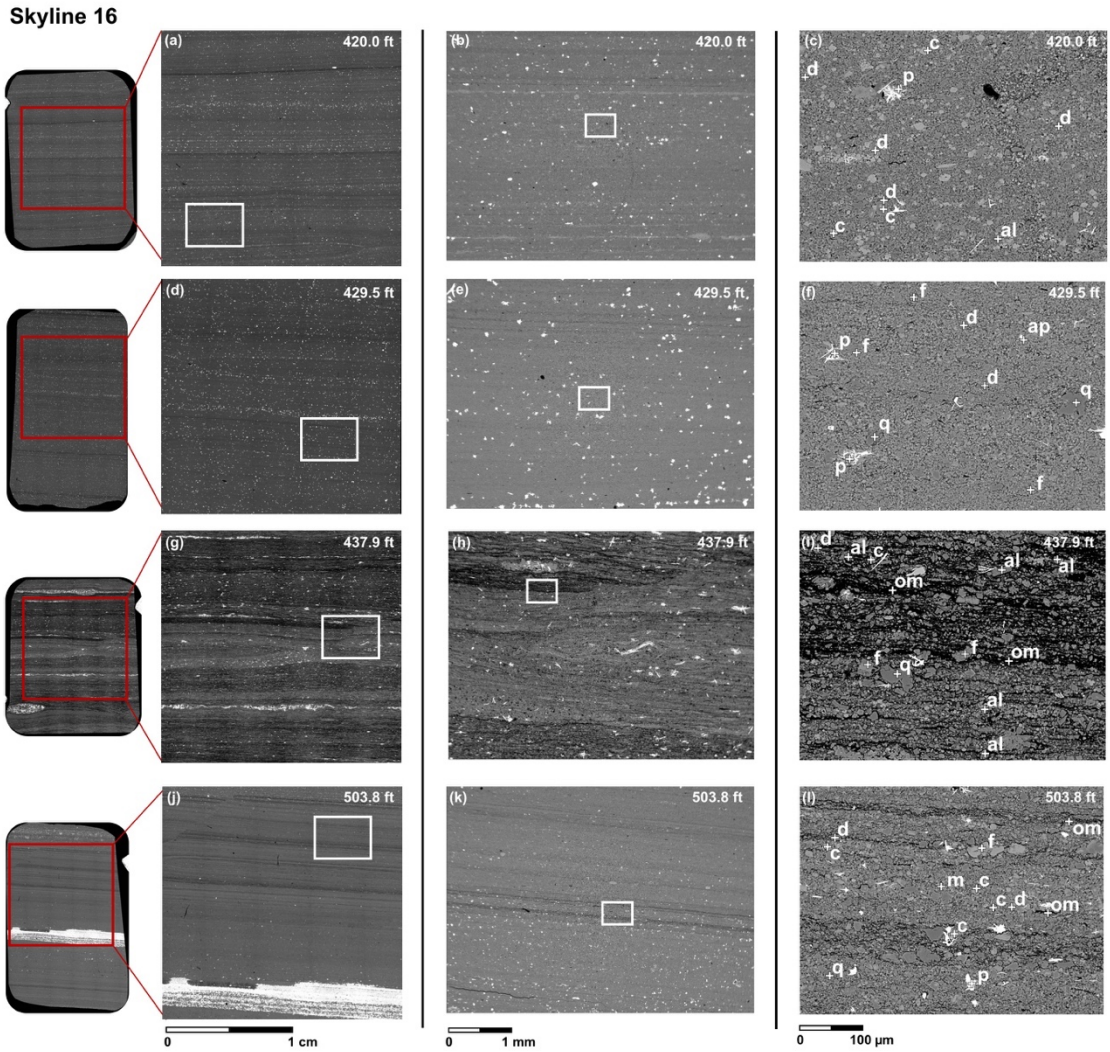

Figure 3: Scanning Electron Microscope (SEM) analysis images of thin sections from the Skyline 16 core, ranging from centimeter scale (left), millimeter scale (middle) and micrometer scale (right). Thin sections were selected by visual inspection to capture the range of heterogeneity present in mudstone petrology. White squares show the location of the increased magnification image immediately to the right. (a) 420.0 ft- Planar laminations with loop bedding and interspersed pyrite. (b) 420.0 ft - Common highly reflective pyrite and planar laminations. (c) 420.0 ft - Common grains of calcite, dolomite and albite. (d) 429.5 ft - Parallel laminations with loop bedding and both pyrite dispersed through the section and concentrated in bedding planes. (e) 429.5 ft - Fibrous iron sulfide, in the form of marcasite, very common along bedding planes. (f) 429.5 ft - Altered feldspars and weathered grains of quartz, with marcasite common. (g) 437.9 ft - Organic rich section with undulose pyrite rich laminations, with pyrite lenses and occasional thin pyrite laminae. Loop bedding is common. (h) 437.9 ft - Lenses of microbial mats and undulose laminations of organic matter-rich material (black) with common marcasite. (i) 437.9 ft - Organic matter rich laminations and lenses throughout, with microbial mat textures in the upper half of the frame. Marcasite is dispersed throughout. (j) 503.8 ft - Parallel laminations with loop bedding and pyrite rich

laminations and a 3mm band of pyrite across lower half of section. (k) 503.8 ft - Parallel laminated mudstone with small pyrite grains. (l) 503.8 ft - Organic-rich and clast-rich alternating laminations, with quartz, feldspar, calcite and dolomite common. Labels are as follows: c- calcite, d- dolomite, p- pyrite, f- plagioclase feldspar, al- albite, q- quartz, om- organic matter, ap- apatite, m- muscovite mica.

2.3.2.2 Mineralogy

Pyrite has variable habits (Figure 3), ranging from being disseminated to aligning along laminae or being in high-enough quantities to form pyritic framboids, lenses and laminations (Figure 3-g). Orthorhombic forms of iron sulfide, known as marcasite, are commonly spread through the matrix and are joined together in larger aggregates.

The silt-sized grains mostly comprise euhedral dolomite, calcite (from whiting events), highly altered feldspars (including albite), and large grains of quartz. A portion of the silt-sized grains form coarser clast-rich laminae, alternating with OM-rich and clay-rich lamina, while other grains are disseminated through the matrix. The clay-rich groundmass has high amounts of illite and amorphous organic matter (AOM).

2.3.2.3 Sedimentology

Appearing parallel laminated at the coarsest scale (Figure 3), many of the laminae at fine scale are disrupted by silt-sized grains. Loop bedding is particularly common in organic-rich levels (Figure 3-g), and is likely the result of the stretching of unlithified to progressively more lithified, laminated sediments of deep lacustrine facies in response to successive minor seismic shocks (Rodriguez-Pascua et al., 2000).

2.3.3 SEM-EDS

Organic-rich layers are filamentous and undulose, and organic-rich laminae bundle together to form OM-rich and OM-lean sections, which express as the darker and lighter laminations at core scale (Figure 4). In organic-lean laminae, alternating bands of silt-enriched and clay-dominated mudstone are clear. The silt-sized

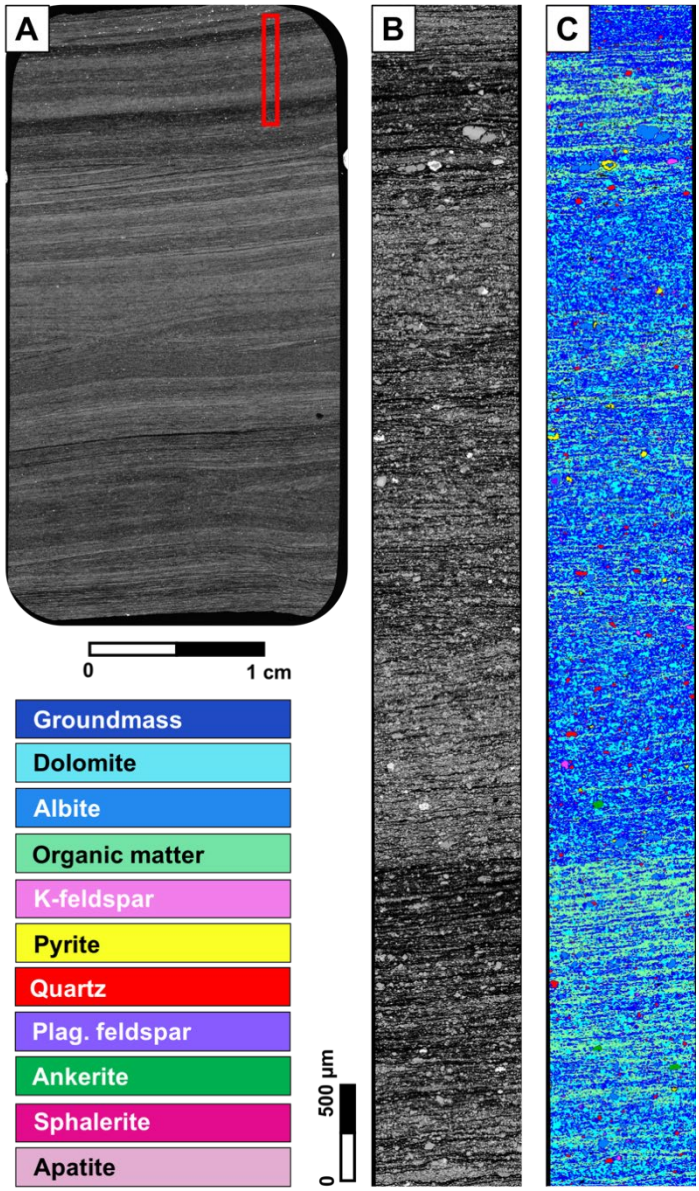

Figure 4: (A) Scanning electron microscope (SEM) analysis of a thin section at 463.9 ft depth from the Skyline 16 core. The highlighted box indicates the location of panels B and C. (B) Backscattered electron image of one frame (magnification x 40) of a SEM analysis through a sequence of polished laminae from the Skyline 16 core (at 463.9 ft). **(C)** Energy Dispersive X-Ray Spectroscopy image through the same laminae set as B with a classified, grouped, and color-coded presentation. See legend in the lower left for mineral identification.

components are composed of euhedral dolomite, irregular grains of quartz, albite, ankerite, plagioclase and orthoclase feldspars, pyrite and sphalerite. Many quartz grains appear subhedral, and are present along with weathered feldspar minerals and ankerite. Pyrite is present as individual grains dispersed through the laminae-set, but some have encrusted dolomite and albite. Similarly, some albite encrusts cores of plagioclase feldspar, and outer rings of ferroan dolomite are present (Figure 4-c). Clay-rich groundmass and laminations are mostly comprised of illite.

2.3.4 Organic Petrology

Organic macerals and kerogen are typically analysed by reflected and transmitted light respectively. Organic maceral types can be broken into the five following groups: (1) amorphous, (2) exinite, (3) vitrinite, (4) inertinite, (5) liptinite. Kerogen type is usually defined by the relative proportions of these maceral groups, and can be sub-divided into the following types: sapropelic, humic-sapropelic, sapropelic-humic and humic. In this study, two microscopes and three different illuminations result in different expressions of the organic matter in thin section. The nomenclature used for different illuminations in this study is depicted in Table 1.

Table 1: Organic petrography nomenclature for the microscopic illuminations used in this study (Teichmüller and Ottenjann, 1977; Burgess 1974; Van Gijzel, 1979; Senftle et al., 1987).

Reflected light	**Transmitted light**	**UV light**
Huminite/Vitrinite	Woody	Vitrinite
Inertinite	Coaly	Inertinite
Liptinite -Sporinite -Cutinite -Liptodetrinite -Alginite	Herbaceous Algal	Liptinite Sporinite Cutinite Liptodetrinite Alginite

-Bituminite	Amorphous	Bituminite
Mineral-bituminous groundmass	Amorphous, pore filling with negative pseudomorphs	Bituminous mineral groundmass solid bitumen

2.3.4.1 Organic Matter Variation

Organic matter fluoresces under excitation from UV light, attesting to the low thermal maturity of the Mahogany Zone, and ranges from orange to bright greens and yellows. Terrestrial organic matter is commonly seen here, with frequent woody debris and collapsed spores oriented along bedding (Figure 5-d, 5-h, 6-g, 6-h). Thin undulose plant remains, resembling cutinite (tenuicutinite?), commonly lie along laminations and separate more OM-rich and OM-lean layers, and the original internal structure of wood remains are commonly preserved and visible in incident UV light.

Algal organic matter is seen as brightly fluorescent filamentous lamalginite, liptodetrinite, and liptinite (Figure 7-e, 7-f), and is deformed around larger silt-sized grains and woody plant material. Filamentous liptinite is a very common form of OM throughout the Mahogany Zone.

Much of the OM in the photomicrographs is dispersed in the matrix, present as amorphous organic material (AOM; transmitted light) or bituminite (reflected/UV light), resulting in much of the background fluorescence (Figure 5-b). In laminations that are darker brown, the OM comprises non-fluorescing bands of bituminite in close association with pyrite and carbonate minerals.

Large organo-mineralic aggregates (OMA) are common (Figure 7-a, 7-b), fluorescing brightly and varying in shape from undulose and bleb-like, to flatter

more-lenticular shapes. The OMA commonly deflects liptinite and cutinitite filaments, loading onto the laminae and deforming them.

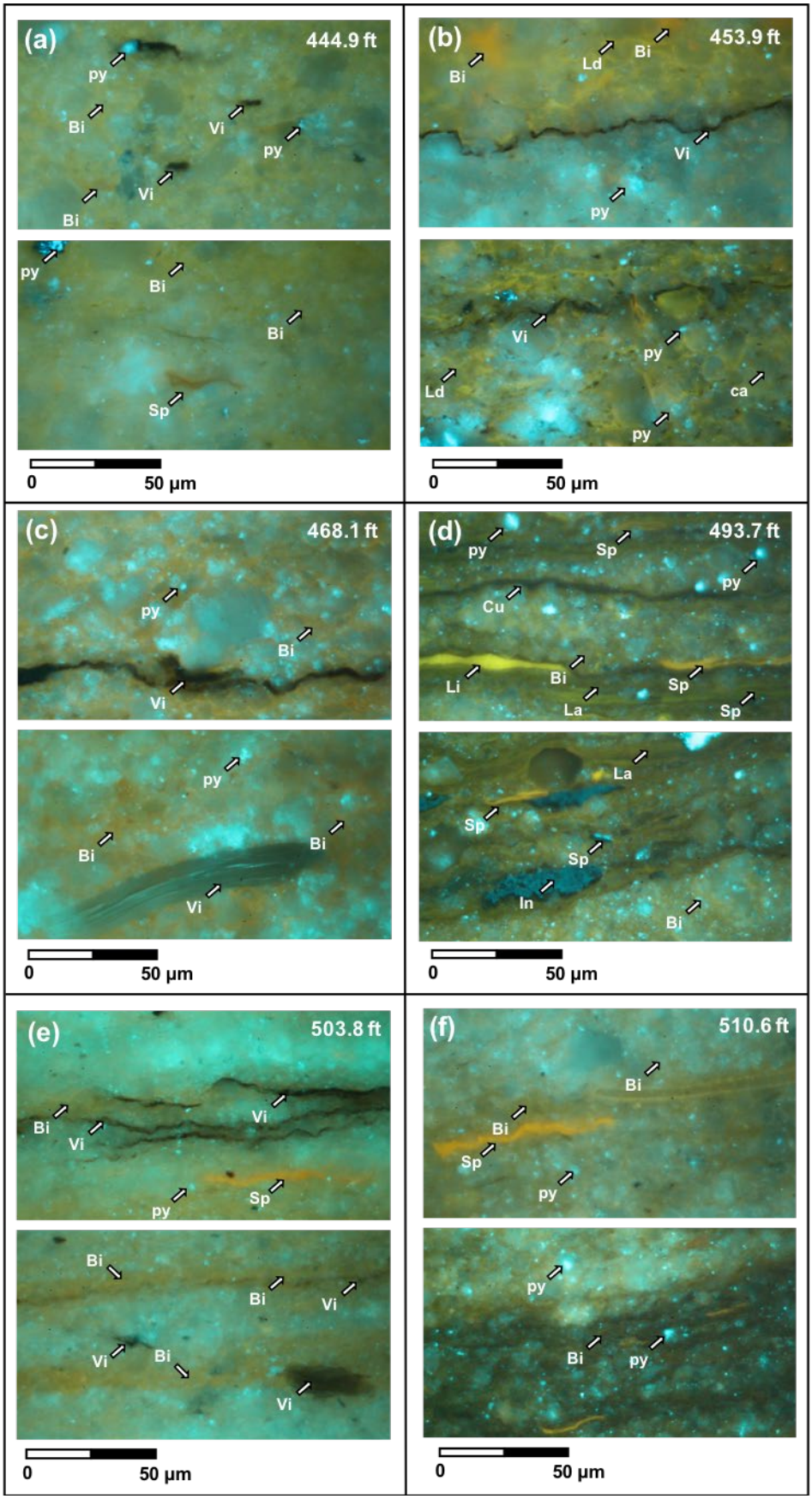

Figure 5: Photomicrographs from the Skyline 16 core, under incident UV light from a Zeiss microscope. (a) Common wood fragments oriented along bedding. Dispersed organic matter (orange fluorescence) through the upper and lower frames, as well as pyrite (reflecting bright blue). Spore in lower frame. (b) Thin undulose plant remains (black), commonly along laminations and separating organic matter-rich and carbonate-rich layers (see arrow in the upper frame). (c) Euhedral calcite grains common (upper frame arrow) and large woody material with internal structure preserved can be seen (lower frame). (d) Laminations of organic-rich and carbonate-rich material, with common spores (arrows) through the upper and lower frames. Organic-rich laminae are warped around large grains (calcite and quartz in the lower frame) and woody remains (dark blue-grey). (e) Discontinuous plant material (upper frame arrow) and clear alternating laminations of organic-rich and carbonate rich material (lower frame). (f) Collapsed spore (upper frame) and a transition from a light stronger fluorescing band to a dark brown band that fluoresces less, with common pyrite, marcasite and carbonate grains throughout (lower frame). UV: Bi-bituminite; Li-liptinite; Ld- liptodetrinite; Sp- sporinite; La- lamalginite; Cu- cutinite; Vi-vitinite; py- pyrite; In- inertinite.

2.3.4.2 Mineralogy

Siliceous material is commonly in close association with OM throughout the studied section. Pyrite is commonly observed, in varying morphologies including large framboids and overgrowths around grains and OM; filaments of marcasite are also observed. The most common habit of pyrite is in the form of very small (<5 μm) disseminated pyrite framboids, with infrequent small (<0.1 mm) disseminated pyrite grains.

Occasionally, small pyrite grains are observed along OM-rich laminae (Figure 7-c, 7-d), with siliceous bands present above and below. Silt-sized components which form the coarser laminae are observed to include quartz, euhedral calcite and

dolomite. The matrix is composed of amorphous organic carbon and dispersed clay minerals.

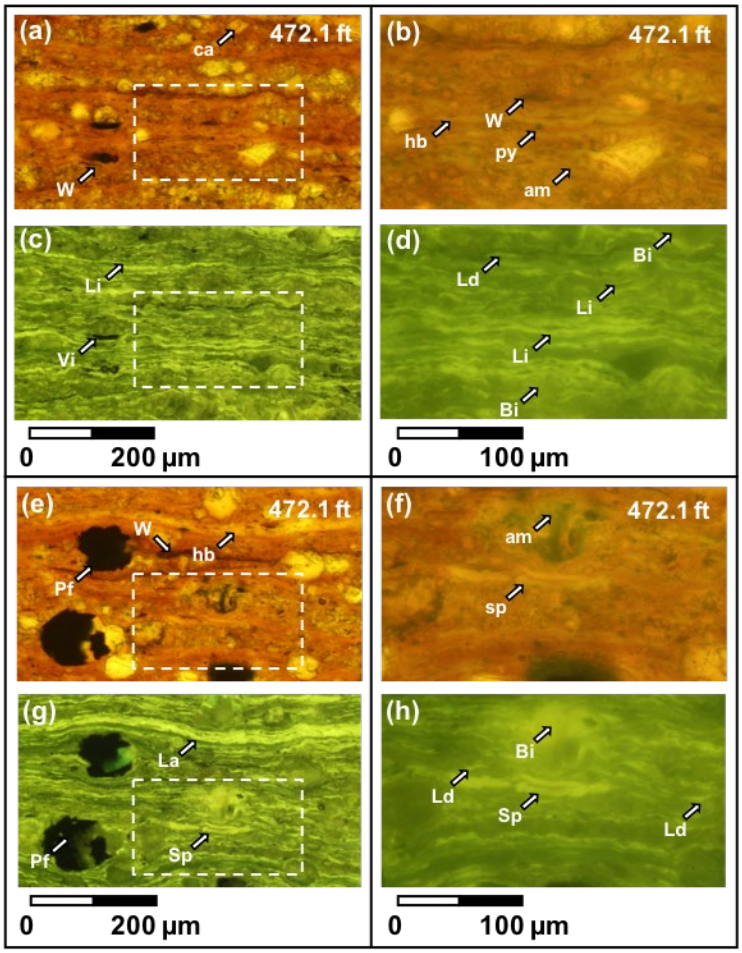

Figure 6: Photomicrographs from Skyline 16 core samples, under white transmitted light (TL, top) and then incident UV (bottom) at x 20 magnification on the left-hand column and x 40 magnification on the right-hand column, from an Olympus BHS microscope. (a) Visible light. (b) Visible light, grains. (c) UV. (d) UV, spores, OM-rich laminations (fluorescing bright green). (e) Visible light. (f) Visible light, collapsed spore in center of frame (orange). (g) UV, large pyrite grains (black) and wavy laminae of fluorescing organic matter. (h) UV, collapsed spore fluorescing brightly. TL: ca- calcite; w- woody; py- pyrite; am- amorphous organic matter; sp- spore; hb- herbaceous; Pf- framboidal pyrite. UV: Bi- bituminite; Li-liptinite; Ld-liptodeterinite; Sp- sporinite; La- lamalginite; Vi- vitinite.

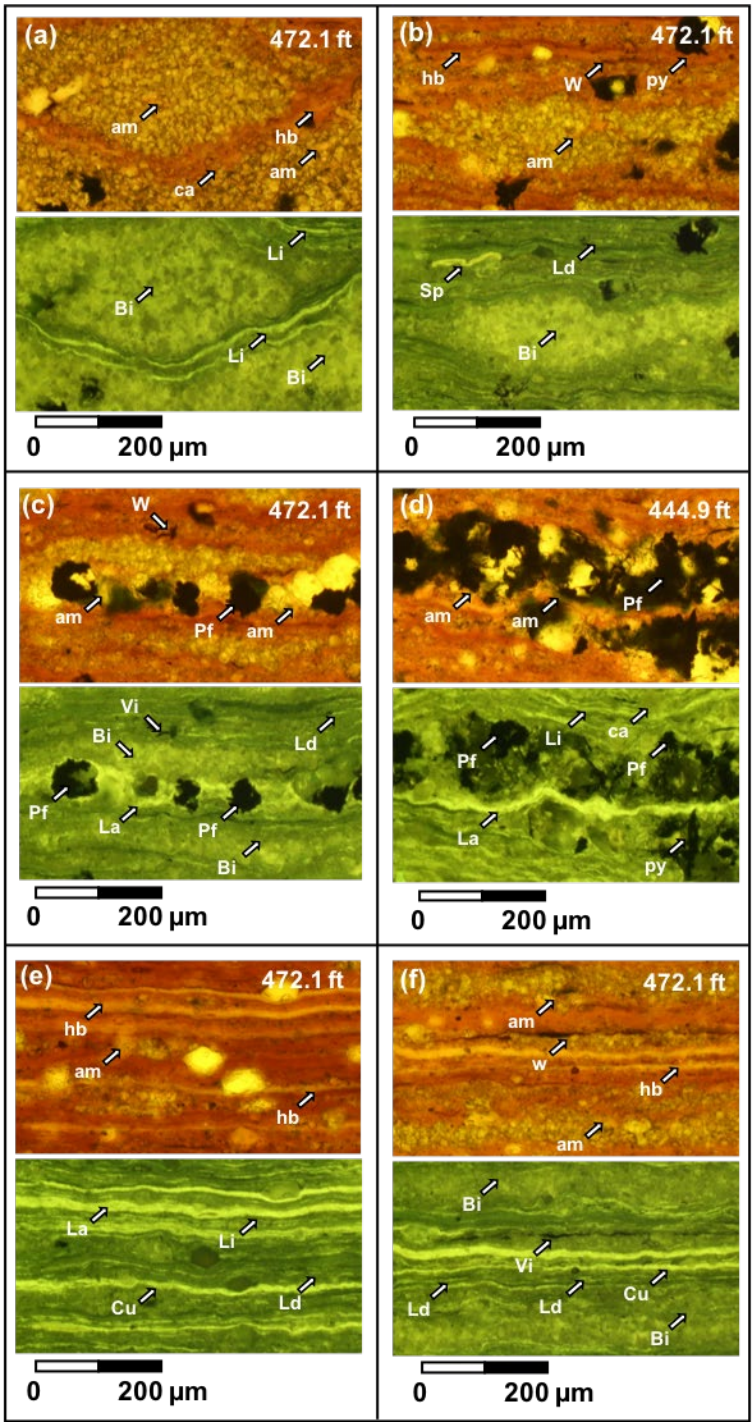

Figure 7: Photomicrographs from Skyline 16 core samples, under white transmitted light (upper pane) and then incident UV (lower pane) at x 20 magnification, from an Olympus BHS microscope. (a) Large OMA with fluorescing OM laminations being deflected (bright fluorescent laminae in lower pane). (b) AOM and grains, collapsed spore on upper left. (c) Large grains of pyrite in an organic-rich layer, with siliceous bands above and below. (d) OM-rich laminations (fluorescing bright green) with large pyrite overgrowth. (e) Wavy laminations of brightly fluorescing organic matter, with carbonate-rich and siliciclastic-rich

laminations inter-layered. (f) Siliceous layers at the base and top of the frames, with brightly fluorescing OM in the middle, and occasional wood material along bedding. TL: ca- calcite; w- woody; py- pyrite; am- amorphous organic matter; hb- herbaceous; Pf- framboidal pyrite. UV: Bi- bituminite; Li-liptinite; Ld- liptodeterinite; Sp- sporinite; La- lamalginite; Cu- cutinite; Vi- vitinite.

2.3.4.3 Sedimentology

Laminae of siliciclastic material are composed of sets of intercalated clay minerals and quartz-rich layers. Although parallel laminated at core scale, at micron level, many of the laminae are undulose in nature, and the clear laminations evident in hand specimens become indistinct at higher magnifications. Lens-shaped aggregates of quartz are common, ~100 μm thick and varying in lateral extent.

2.3.5 Geochemical Analysis

2.3.5.1 Organic Geochemistry

Total organic carbon (TOC) (generated by M. Vanden Berg, of the Utah Geological Association, and J. Birdwell at the USGS, Denver) is elevated throughout the Skyline 16 section, peaking in the middle of the Mahogany Zone where the water column is assumed to be the most stratified (Table 2). TOC is highly variable throughout the Mahogany Zone, with values fluctuating from 1.1 to 29.2% (figure 8-a).

The ratio of terrigenous-to-aquatic *n*-alkanes (TAR index; Bourbonniere and Meyers, 1996) was used to quantify relative inputs of organic matter:

$$TAR = (C_{27}+C_{29}+C_{31})/(C_{15}+C_{17}+C_{19})$$

The TAR index is based on the assumption that odd-numbered longer-chained *n*-alkanes are derived from vascular plants ($C_{27\text{-}31}$), whereas short-chain *n*-alkanes

(C_{15-19}) are derived from photosynthetic algae and bacteria in the water column. Typically applied to data from marine settings, TAR values >1 indicate substantial terrigenous organic matter contributions (Silliman et al., 1996). It has been observed that the TAR index may result in the over-representation of terrestrial sources, but despite this, it is still useful as a qualitative proxy for defining relative inputs of terrestrial versus aquatic organic matter contributions. The TAR results for the Mahogany Zone (Figure 8-b) reveal variability in the dominant source of OM through the section. Although algal input is always dominant, there are four episodes of relatively high terrestrial input which also correlate to lows in TOC and increased terrestrial material in thin section (Figure 8-g), peaking at 453.9 and 477.9 ft, reducing to negligible values by 493.7 ft (Figure 9). Peaks in TOC are concurrent with intervals where the relative contribution of aquatic organic matter is highest.

Higher plants (i.e. vascular tissue containing) synthesize hydrocarbons with a strong predominance of odd over even numbered *n*-alkanes, so the odd over even predominance (OEP) of longer-chain *n*-alkanes can be used to evaluate terrestrial organic matter input (Scalan and Smith, 1970):

$$OEP = (C_{27}+(6xC_{29})+C_{31})/(4xC_{28}+(4xC_{30}))$$

OEP values are elevated, ranging from 4.14 up to 10.23, with the highest values towards the top and the base of the Mahogany Zone (Figure 8-c; 425.2 ft and 515.6 ft) during intervals of lower TOC. The OEP and TAR records are broadly similar. The highest TOC values correspond to the lowest OEP values, indicating the organic matter mixture is comprised of little terrestrial material. Low TOC values do not systematically correspond to high TAR or OEP values although intervals with the highest TOC have lower terrestrial organic matter (Figure 9). This scatter observed at lower TOC values implies that there were multiple controls dominating the TOC

values, likely a result of the high sensitivity of lacustrine basins to variations in primary productivity of different photoautotrophs in the water column, dilution of organic matter, and preservation conditions.

Table 2: Skyline 16 TOC, TAR and OEP. (Left) Total organic content (TOC) vs. depth, with elevated, but highly variable TOC throughout the Mahogany Zone (*generated by Vanden Berg and Birdwell, at the USGS, Denver). (Middle) Terrigenous/Aquatic ratio vs. depth, a biomarker ratio used to quantify algal lipid vs. plant material inputs. (Right) Odd Over Even Predominance vs. depth, is used to quantify terrestrial organic matter input.

Depth (ft)	TOC*	TAR	OEP
420	3.32	1.28	8.74
422.1	2.33	0.96	9.09
425.2	2.14	0.82	10.12
429.5	2.74	2.20	7.14
431.5	5.02	1.46	7.93
437.9	13.18	0.56	4.14
444.9	11.04	1.46	5.34
453.9	7.54	3.00	8.33
463.9	26.57	1.58	6.96
468.1	8.14	1.18	5.82
472.1	29.18	1.03	5.29
477.9	4.44	3.23	7.78
485.8	13.71	2.02	5.43
493.7	23.76	0.41	6.32
496.3	2.38	1.98	7.61
503.8	3.01	2.90	7.88
508.1	1.12	2.94	8.76
510.6	8.99	1.16	5.99
515.7	1.61	0.97	10.43

2.3.5.2 Inorganic Geochemistry

The K/Al ratio ranges from 0.22 to 1.07 (Figure 8-d), revealing small variations in weathering input. This is supported by invariant Si/Al ratios (3.40-4.89; Figure 8-f; Table 3), which indicate a lack of coarser grains and low levels of aeolian transport as a source of quartz silt into the basin (Weltje and von Eynatten, 2004; Plewa et al., 2012). Very low Ti/Al ratios (0.040- 0.056; Figure 8-e) reveal a very low sediment input, at levels suggestive of sediment starvation (Young and Nesbitt, 1998; Whitlock et al., 2008). Ca/Al ratios are relatively low, varying from 1.02 to 10.99 (Figure 8-g),

indicating high lake levels through the Mahogany Zone with potential shallowing towards the top of the section (Sun et al., 2008). The Mn/Fe ratio is essentially zero (0.009- 0.035; Figure 8-h), revealing that the lake floor was continually anoxic (Davison, 1993; Loizeau et al., 2001).

Table 3: Elemental microanalysis for thin sections analyzed by SEM.

Depth (ft)	K/Al	Ti/Al	Si/Al	Ca/Al	Mn/Fe
420.0	0.74	0.059	3.94	3.15	0
429.5	1.03	0.045	3.80	0.83	0
437.9	0.31	0.073	4.54	2.40	0
463.9	0.41	0.049	3.78	1.51	0.0069
503.8	0.95	0.052	3.58	1.55	0

2.4 Discussion

2.4.1 Organic Matter Distribution

The different forms of organic matter observed in the Skyline 16 samples strongly influence the facies, structural competence and TOC values. Organic matter distributed in the matrix varies from amorphous organic material to discrete interlayers with siliciclastic-rich and carbonate-rich laminations.

The processes by which large amounts of primary organic productivity in lakes can be gathered from surface waters are coagulation and the binding of aggregates to mineral matter (Alldredge and Silver, 1988; Graf 1992; Simon et al., 2002). These processes ultimately result in a flux of organic carbon to the lake floor, which is estimated at ~76.07 Gt during Mahogany Zone deposition. This estimate comes from ~214.5 billion barrels of oil reserves in the Mahogany Zone for the Uinta Basin and ~191.7 billion barrels of oil reserves in the Mahogany Zone for the Piceance Basin, based on the Fischer Assay oil yield from Birdwell et al., (2015) and does not take into account carbon sequestered as carbonate minerals. Collectively, this

represents a significant sink of terrestrial carbon into Lake Uinta during the termination of the EECO.

The close association of algal material and clay minerals and the presence of blebs (thin laterally discontinuous lenses of silt and sand) in the deposits studied here suggest that some sediment was delivered to the lake floor as organo-mineralic aggregates (OMA), consistent with previous suggestions (Johnson et al., 2018). Lacustrine organic matter removed by the formation of OMA could provide an important carbon source for heterotrophs in the water column (Kiørboe et al., 2001). The drifting and sinking of algal-rafted debris have been hypothesized as mechanisms for the transport and deposition of sand-sized grains, as well as faecal matter, in a deep carbonate mudstone facies during a lake transgression (Olsen et al., 2018). The mechanism for algal-rafted debris involves mats of cyanobacteria or green algae growing in the littoral zone, where they trap sand- and silt-sized particles, plant material and other debris, prior to breaking free as smaller rafts. Photosynthesis, through the release of O_2 as a waste product, imparts a buoyancy to such algal-rafted debris, permitting the debris to drift into the more distal zones of the lacustrine system, eventually sinking and wrapping around sandy material. It is hypothesised that heavier clasts (mm-size) contract together when the algal mat founders, forming blebs which sink, leaving no visible trace of the mat. Such structures are commonly observed in the Mahogany Zone (Figure 3-l, 4-b), and along with OMA contained in smaller clasts, suggest that algal-rafted debris and OMA are important components of the organic-rich intervals. Very thin laminae and lenses of liptinite (<30 μm) likely represent intra-annual events, whereas thicker laminae are indicative of seasonal algal blooms (Ripepe et al., 1991).

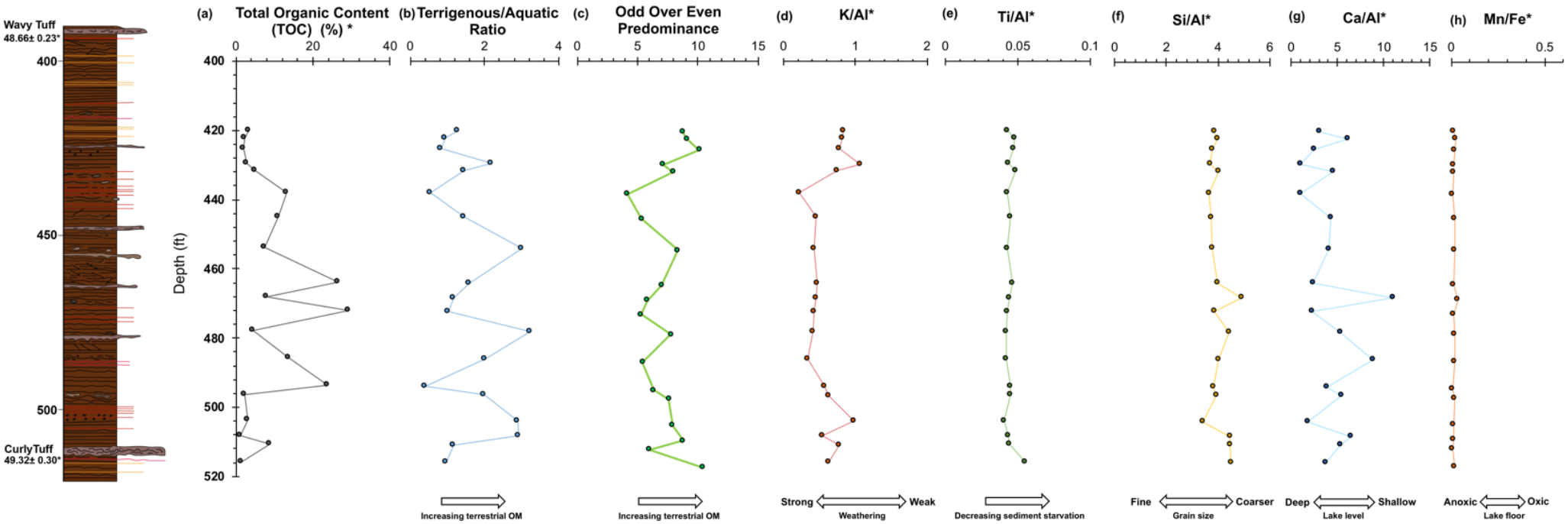

Figure 8: Stratigraphic and geochemical data through the Mahogany Zone of the Skyline 16 core. (a) Total organic content (TOC) vs. depth, with elevated, but highly variable TOC throughout the Mahogany Zone. (b) Terrigenous/aquatic ratio (TAR) vs. depth, a biomarker ratio used to quantify algal lipid vs. plant material inputs. (c) Odd/even predominance (OEP) vs. depth. (d) K/Al ratio showing small variations in weathering input. (e) Ti/Al ratio, indicating low levels of sediment input. (f) Si/Al ratio with very low values through the section, indicating a lack of coarser grains. (g) Ca/Al ratio showing low values indicative of a deep lake level through the Mahogany Zone, and shallowing towards the top of the section. (h) Mn/Fe ratio showing continually anoxic lake floor conditions.

Dark laminations of organic matter at the millimeter-scale are comprised of bundles of bituminite and liptinite, representing multiple intra- and inter-annual events. As such, traditional ‘varves’ observed at the core-level likely represent longer-term sub-orbital-scale climate cycle fluctuations that affect primary productivity in lake surface waters, possibly linked to solar spot periodicities at the decadal and sub-decadal scale (Kuma et al., 2019) or El Niño–Southern Oscillation.

Several studies that have addressed the deposition of the organic-rich zones within the Green River Formation estimate a thickness of 100-200 μm for an annual lacustrine couplet (Bradley, 1929; Washburn et al., 2015; Walters et al., 2020). In thin section, many laminations and lenses of organic matter and carbonate precipitates are thinner and discontinuous, suggesting significant intra-annual variability in the deposition of these components.

The organic matter content in the Mahogany Zone is heterogenous at the millimeter- to micrometer-scale, both vertically and horizontally. Organic matter type varies, with large amounts of AOM dispersed throughout the matrix. In sections containing bituminite, large organo-mineral aggregates and liptinite laminae are commonly present. Terrestrial organic input is represented by common woody debris, plant remains, and spores, and intervals with large relative proportions of terrigenous input correspond to lows of TOC (Figure 9). This may be related to higher energy events washing in large quantities of terrigenous matter, organic matter and sediments together, resulting in a lower proportion of algal lipids in these discrete intervals due to the dual effects of increased leaf wax contribution and sediment dilution.

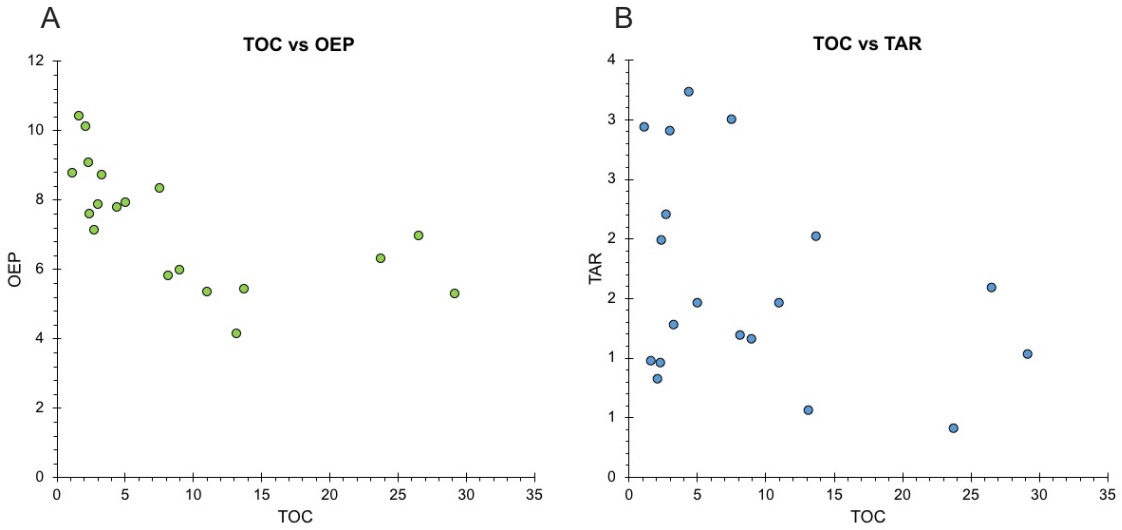

Figure 9: (A) Total organic content vs. odd/even predominance. Very high TOC (>10 wt.%) corresponds to the lowest OEP values with the least organic-rich samples (<5% wt.% TOC) clustering in the higher OEP range, indicating more terrestrial organic matter at these intervals. (B) Total organic content vs. terrigenous/aquatic ratio. The highest TOC values correlate with lower TAR values similarly to the OEP; however, a large amount of scatter exists due to low TOC, low TAR values that are absent in the OEP record.

2.4.2 Lake Chemistry

The formation of pyrite requires a supply of terrigenous iron, organic matter, and sulfate under relatively high pH conditions, although marcasite formation is favoured at lower pH. The majority of pyrite observed was in the form of very small (µm-scale) disseminated framboids, indicative of a persistently anoxic-sulfidic water column supersaturated in sulfate and iron. The presence of larger pyritic framboids indicates that the pore waters in the sediment column were at least episodically sulfidic, and the alignment of small pyrite grains along lamina indicate that there was only minimal to moderate physical reworking of the anoxic/dysoxic sediment column at the site of Skyline 16. The presence of ferroan dolomite crusts on many of the dolomite grains also indicates minimal reworking of the sediment column. The preservation of small fibrous forms of marcasite with a narrow size distribution among the grains indicates

that the mineral formed directly in the euxinic water column (c.f., Berner, 1969; Wignall and Newton, 1998; Schieber, 2007). Algal blooms decrease the pH locally in the water column, and sufficiently large blooms would allow fibrous marcasite to form instead of pyrite in the sulfidic water column. Furthermore, large algal bloom events may have led to episodic sulfur production, resulting in abundant pyrite-rich laminations in very small disseminated framboids. Pyrite particles may have also been introduced from airborne sources or the distal plumes of turbidites, and then settled to the lake floor.

Interestingly, saline minerals such as shortite and nahcolite are not commonly found in Skyline 16, despite hypersaline phases occurring synchronously with the upper R-6 (the organic-rich interval beneath the focus interval of this study) and the Mahogany Zone (Vanden Berg and Birgenheier, 2017).

Abiogenic calcium carbonate deposition is attributed to precipitation events during warmer months, when carbon dioxide sequestration from the water column by planktonic photosynthesis lowered the pH of surface waters and precipitated calcium carbonate (Eugster and Hardie, 1978). Detrital carbonate could also be derived from dust storms, which vary in intensity over decadal time-scales (Ripepe et al., 1991). However, inorganic proxies in this study demonstrate low levels of aeolian input, suggesting this mechanism is unlikely to account for the observed amounts of carbonate. Micritic carbonate is commonly dispersed at the finer scale as part of the groundmass and dolomite at the coarser scale (Figure 4-c) similar to previous work in the northern Uinta Basin (Johnson et al., 2019).

2.4.3 Transported material

Ankerite, a calcium-iron-magnesium-manganese carbonate mineral closely related to dolomite and formed in iron-rich hydrothermal veins and metamorphic rocks, is

generally observed in thin section as very weathered grains with irregular boundaries. Albitic feldspar is common in the neighbouring Piceance Basin and considered to be authigenic in origin, due to subhedral to euhedral crystal habits and a maximum size of ~20 μm (Desborough, 1975; Birdwell et al., 2019). Large clast sizes (>100 μm; Figure 4-c) of anhedral albite suggests a detrital origin (produced from granitic detritus) from sources that are not proximal to the lake. The more frequent small clasts (<20 μm) of subhedral albite are likely formed authigenically, similar to the albite observed in the Piceance Basin. Previous studies suggested clastic input was sourced from the south of Lake Uinta, with large fluvial systems transporting texturally mature sediments to the lacustrine system during the EECO hyperthermals (Gall et al., 2017; Birgenheier et al., 2019). This resulted in the ephemeral deposition of large sandstone sheets before the waning of the EECO at the base of the Mahogany Zone. However, the textural immaturity of sedimentary grains observed in this study suggest that a different source provided material to Lake Uinta. The infrequent presence of highly subhedral ankerite and anhedral albite may support a provenance located toward the north, from the volcanic centres of the granitic Absaroka Mountains (Wyoming), or the volcanic fields of the Challis Arc (Idaho) which were delivering detritus to the Greater Green River Basin (Figure 4-c; Moye et al., 1988; Hiza, 1999) during deposition of the Mahogany Zone (Smith et al., 2008). Volcaniclastic material deposited in the Piceance Basin during this interval has been petrographically linked to the Absaroka volcanic field, indicating a hydrologically linked Lake Gosiute and Lake Uinta and a transport direction towards the south (Johnson et al., 2019).

Paleo-reconstructions for the Mahogany Zone support the transport of water and sediment from Lake Gosiute of the Greater Green River Basin (which was coevally infilling with material from the Idaho River during the development of the Mahogany

Zone), into the Piceance Basin, and then over the flooded Douglas Creek Arch, and into the Uinta Basin. Thus, simultaneous north-south filling of Lake Gosiute delivered water and sediment into Lake Uinta via the connected basins, carrying sediments over a protracted transport route, and likely contributing to increased water depth (Smith et al., 2008; Chetel and Carroll, 2010). Other sources than the Absaroka or Challis fields could include the Wind River Mountains, which also provided volcanic material to the Uinta Basin (Johnson et al., 2019; Smith et al., 2010).

Although the decline of the EECO is known to have had a profound effect on the basin in terms of large-scale changes in sedimentary expression (i.e., from an ephemeral fluvial system to a deep, highly productive lake; Birgenheier et al., 2019; Plink-Björklund, 2015), it also resulted in a change to a more northerly sedimentary provenance. Much of the transported detritus would have been delivered by lateral transport in bed load or dense suspension.

2.5 Conclusions

The behaviour of the terrestrial carbon cycle is a key uncertainty in the warm world projected for our future. Understanding dominant sources and variations of organic matter in large terrestrial CO_2 sinks, such as the Green River Formation during the deposition of the Mahogany Zone, is crucial for better forecasting of terrestrial responses to climate perturbations.

Organic matter types and distribution vary widely within the Mahogany Zone, but amorphous organic matter derived from algal blooms is dominant throughout. Highly changeable amounts of terrestrial input were transported to the basin, with periods of lower relative inputs of organic matter sourced from terrestrial ecosystems correlating to highs of TOC. This suggests that the primary productivity of the

lacustrine algal community, preserved as AOM, is the principal contributor to the extremely high TOC in the Mahogany Zone.

Details of the form and distribution of the organic matter provide important clues into the controls on primary productivity and deposition. Longer-term sub-orbital cycle fluctuations such as ENSO or sunspot variation resulted in accumulation of organic matter in millimeter-scale laminations, with lighter carbonate- and siliciclastic-rich laminae interspersed at the microscale in the darker high-TOC laminations observed at the core scale. This decadal-scale pacing of conditions favourable to high-TOC deposition in a Cenozoic warm world is an important consideration for carbon drawdown by large lakes in models of terrestrial carbon cycles of the past, present and future. Indeed, large organic-matter fluxes and associated carbon drawdown over decadal periodicities suggest that large, highly productive lakes may act as important terrestrial CO_2 sinks and play a moderating role in a warming world.

2.6 Acknowledgements

This contribution represents a portion of A. Elson's doctoral dissertation at the University of Southampton, funded by the Natural Environment Research Council Centre for Doctoral Training in Oil & Gas. Oliver Bench assisted with field work and sample collection. P. Sargent Bray is acknowledged for help with organic geochemistry, Richard Pearce is appreciated for assistance with SEM, and Dan E. Doran and Matt Beverly-Smith are thanked for making the polished thin sections. Thanks is given to Justin Birdwell and Mike Vanden Berg for their Skyline 16 SEM data, and for four reviewers who's comments and suggestions improved the writing and figures in the manuscript. Discussions with Michael Vanden Berg, Mike Smith, and Clara Chang contributed to the development of this manuscript. Funding was provided by CASP and the NSF for fieldwork and workshop attendance for A. Elson,

and the Donors to the Petroleum Research Fund of the American Chemical Society

to J. H. Whiteside.

Chapter 3 Tectonically driven brine input controls on primary productivity in an organic-rich Eocene lake

Authors: Amy L. Elson[1], John E. A. Marshall[1], Jessica H. Whiteside[1]

[1] Ocean and Earth Science, National Oceanography Centre Southampton, UK

This chapter is modified from a research article under review in Geochimica et Cosmochimica Acta: Elson, A, L., Marshall, J, E.A., and Whiteside, J. H. Tectonically driven brine input controls on primary productivity in an organic-rich Eocene lake. (In review). A. Elson prepared and ran the samples for lipid biomarker analysis, analysed the results and wrote the manuscript. All the co-authors provided editing and feedback.

Highlights:

- Biomarkers record variable water column conditions at peak oil-shale deposition
- Highly variable salinity and hypersalinity persisted during lower TOC intervals
- Salinity changes acted as a key ecological stressor on biota in the water column
- This led to a cessation of conditions favouring prodigious organic C accumulation

Abstract

The long-lived Eocene lakes of the Green River Formation host a sedimentary archive of terrestrial response to the Early Eocene Climatic Optimum (EECO, 53.26 to 49.14 Ma) and include the Mahogany Zone of the palaeo-Lake Uinta, which spans the less understood decline and termination of the EECO and represents the optimum preservation of organic matter (~45% TOC). The molecular geochemistry of three Mahogany Zone cores is investigated. Two of the studied cores (P-4 and Skyline 16) sample the basin-margin while Utah State 1 recovered basin-centre conditions. Molecular fossils from the Mahogany Zone display high gammacerane indices (>0.87) and Pr/Ph values, indicative of anoxic stratified conditions and

hypersalinity development. The lowermost and uppermost parts of the Mahogany Zone indicate strong but highly variable hypersalinity and stratification coupled with lower productivity. A broad peak in productivity observed in the middle section of each record, indicated by generally higher TOC accumulation, is characterised by low to moderate stable salinity stratification. This suggests that highly variable salinity and hypersalinity acted as key stressors to ecological development. When lake conditions experienced highly variable salinity conditions suboptimal for algal productivity, episodes of hypersalinity in the water column created conditions that were too extreme to support a biodiverse community, resulting in intervals of low TOC preservation. The spatial and temporal variations in salinity conditions reflect long-term tectonic controls on riverine and lake water distribution among the sub-basins of the regional Uinta Basin, modulated by climatically-driven evaporitic cycles expressed in the Greater Green River Basin. Understanding the key tectonic and climatic controls that led to high-TOC and saline mineral-rich deposits such as the Mahogany Zone provides insights into the response of large super-productive lakes to environmental perturbations and their role in organic carbon sequestration during periods of high atmospheric CO_2.

3.1 Introduction

3.1.1 Climatic warming in the early Eocene

The onset of the Eocene is marked by a negative $\delta^{13}C$ excursion associated with transient warming at the Paleocene-Eocene Thermal Maximum (PETM), followed by ~six million years of gradual warming that culminated in the Early Eocene Climatic Optimum (53.26 to 49.14 Ma) and then gradual cooling leading to Antarctic ice-sheet expansion and the development of icehouse conditions close to the Eocene-Oligocene boundary (Pagani et al., 2005; Zachos et al., 2001, 2008; Foster

et al., 2017; Inglis et al., 2020; Westerhold et al., 2020). The EECO witnessed the highest atmospheric CO_2 concentrations and global temperatures in the last 65 million years (i.e., ~10-16°C warmer than pre-industrial values; Kirtland Turner et al., 2014; Lauretano et al., 2018; Westerhold et al., 2018a; Zachos et al., 2001, 2008) with peak warming from 51.5-50.9 Ma. Superimposed on this longer-term Eocene warming are periodic isotopic excursions in $\delta^{13}C$ and $\delta^{18}O$ records (Westerhold et al., 2020) that are recognized as short-lived episodes of drastically elevated temperatures (>5°C) associated with the release of light carbon and $\delta^{13}C$ excursions of ~-1 to -6‰, varying widely between different sites and substrates (e.g., the PETM, ~56 Ma; ETM2, ~53.7 Ma; and ETM3, ~52.8 Ma; Nicolo et al., 2007; Zachos et al., 2008, 2010; Stap et al., 2009; Dunkley Jones et al., 2010; Sluijs and Dickens, 2012). These hyperthermals are paced by the 100-kyr and 405-kyr eccentricity cycles (Zachos et al., 2010; Littler et al., 2014; Westerhold et al., 2017). The PETM and ETM2 have been much more extensively studied than the declining limb of the EECO, which is characterised by less extreme hyperthermals and appears to be driven by astronomically paced changes in ocean ventilation of dissolved organic carbon (Sexton et al., 2011). In a broader context, the early Eocene witnessed large-scale ecosystem responses to these climatic-oceanic changes that were recorded in the terrestrial and marine record through extinction events and evolutionary turnovers (McKenna, 1983; Wolfe, 1985; Huber and Caballero, 2011), at a time when much of the globe was comparable to today in terms of plate geometry including the positioning of ridges and subduction zones (Hyland and Sheldon 2013; Müller et al. 2016; West et al., 2020; Stein et al., 2021).

3.1.2 Continental vs. marine contexts for palaeoclimate studies

Marine records used in palaeoclimate studies are typically more continuous and have lower sedimentation rates (~cm kyr^{-1}) compared to terrestrial records (~m

kyr^{-1}) due to susceptibility to erosion and hiatus (Westerhold et al., 2018b). Continental interior basins infilled with fluvial and lacustrine strata are highly sensitive to climatic and tectonic controls (Carroll and Bohacs, 1999; 2001; Pietras and Carroll, 2006) and often comprise important but understudied records of palaeoclimate change (Inglis et al., 2017; van Dijk et al., 2020).

Recent studies of early Eocene continental records from North America (e.g. Bighorn Basin; Abels et al., 2016; Wang et al., 2017; Westerhold et al., 2018b) identified eccentricity-paced carbon isotope excursions that allow for comparison to key marine EECO records (e.g. Ocean Drilling Program (ODP) Site 1262 and Site 1263, Walvis Ridge, Atlantic Ocean; Zachos et al., 2010; Littler et al., 2014; Lauretano et al., 2015). Much of North America (up to latitudes of 65 °N) was warm and humid during the early Eocene (Dilhoff et al., 2013), resulting in expansive temperate to sub-tropical forests (Greenwood and Wing 1995; Smith et al., 2012; Breedlovestrout et al., 2013; Greenwood et al., 2016; West et al., 2020). Lignite-derived MAAT estimates for continental temperatures in the mid-latitudes range from 20 to 26 °C (Inglis et al., 2017).

3.1.3 Climatic and tectonic influences on Green River Formation deposition

The lacustrine and fluvial deposition of the Green River Formation represents the peak hyperthermal regime of the EECO through the more stable post-EECO climate state. The sequence spans north eastern Utah, north western Colorado and south western Wyoming, occupying several Laramide-related intermontane fault-bounded basins. The large ancestral lakes Uinta and Gosiute occupied the southern and northern basins, respectively (Figure 1) and produced one of the largest oil shale

deposits in North America, containing thermally immature hydrocarbon resources estimated at 1.32 trillion barrels (Johnson et al., 2010).

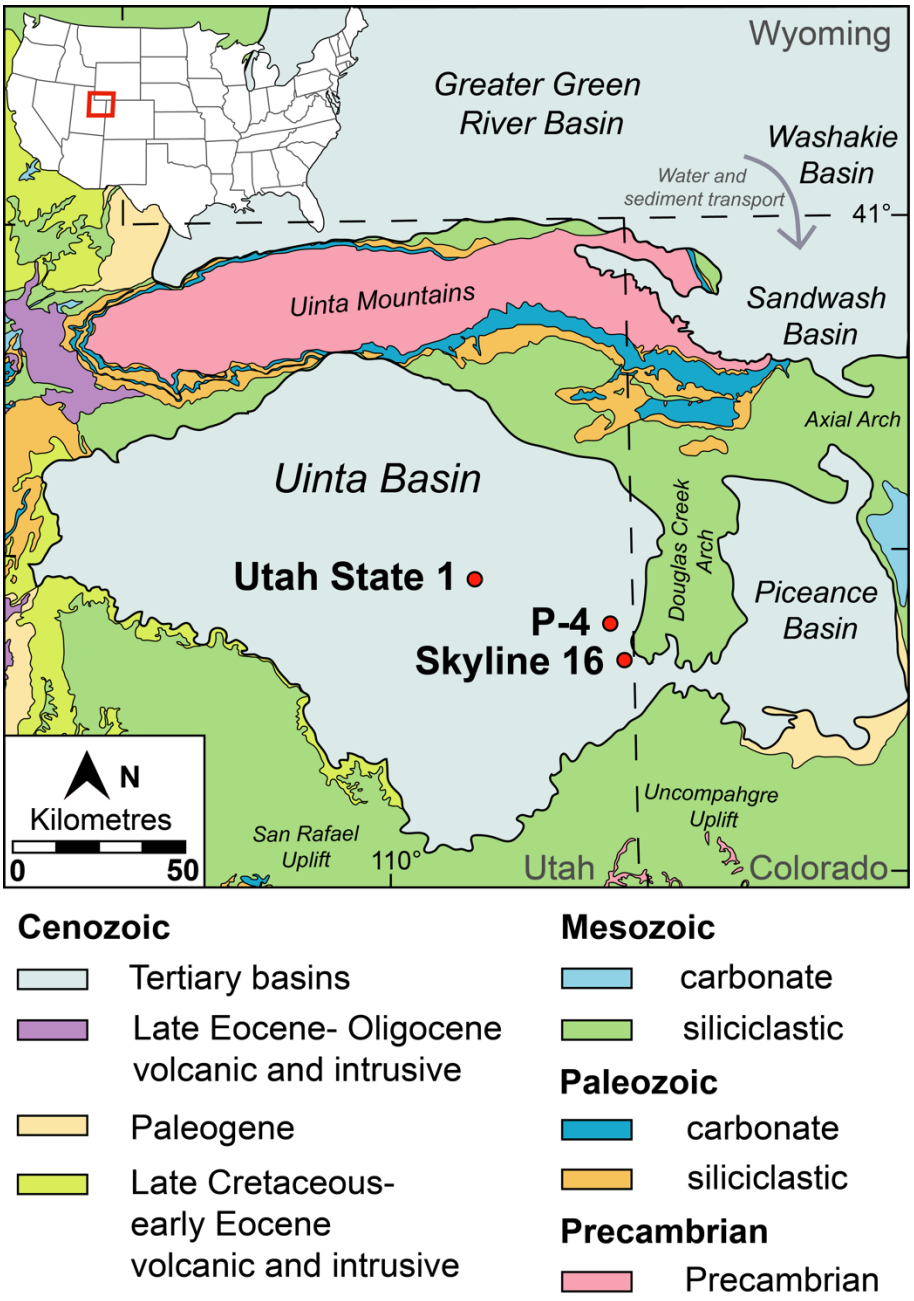

Figure 1: Locations of the three cores in this study, Utah State 1, P-4 and Skyline 16. Lake Uinta was at highstand during deposition of the Mahogany Zone, submerging the Douglas Creek Arch and hydrologically linking the Uinta and Piceance basins (Modified from Pietras et al., 2020).

In the Uinta Basin, the Green River Formation was deposited in a series of cyclically alternating organic-rich and organic-lean intervals, culminating in the deposition of

the prolific Mahogany Zone, when the lake was at its deepest (Cashion, 1967; Johnson et al., 2010). The sedimentary cycles have been attributed to tectonic controls (Pietras et al., 2003a, 2003b; Smith et al., 2003; 2010) and orbital pacing, with the 405-kyr eccentricity cycle resulting in a greater seasonal contrast during eccentricity maxima and appearing to correspond to cyclic drier phases in the Uinta Basin (Bradley, 1929; Fischer and Roberts, 1991; Whiteside and Van Keuren, 2009; Kocken et al., 2019). The Mahogany Zone is primarily composed of kerogen-rich dark brown oil shales and lighter brown-grey carbonaceous mudstone, ranging from ~1–45% total organic content (TOC). Organic geochemical and detailed core analyses indicate a persistently stratified water column throughout deposition of the Mahogany Zone (Tissot et al., 1978; Vanden Berg and Birgenheier, 2017), yet high TOC variability indicates an overarching control distinct from redox conditions alone.

In addition to the dominant carbonate and organic-rich mudstones, the Green River Formation contains clastic and saline sediments deposited during major fluvial incursions and evaporitic phases associated with key climatic and tectonic events, including the EECO (Dyni, 2006; Gall et al., 2017; Birgenheier et al., 2019). The hydrological regime underwent profound reorganisation in this climate transition (Carmichael et al., 2017), with thick fluvial sandstone deposits forming in an ephemeral flash-flood environment in the Uinta Basin during the hyperthermals of the EECO. Finer-grained sediments marking a lower-energy precipitation regime and decreased sediment supply developed during the stable post-EECO climate state, when the lake deepened (Gall et al., 2017; Birgenheier et al., 2019). Contemporaneous fluvial and floodplain deposition adjacent to the Lake Gosiute in present-day Wyoming, represented by the volcaniclastic Bridger Formation, yields geochemical and floral data recording mild temperatures and little to no frost during

the termination of the EECO (~49.14 Ma; Westerhold et al., 2018a; Chetel et al., 2011; Stein et al., 2021).

Previous geochemical and geophysical studies have revealed that generally, the oil-shale-rich intervals of the Green River Formation, including the prolific Mahogany Zone, represent the wetter peaks of the 405-kyr cycle. Dry phases of the 405-kyr cycle appear to correspond with saline intervals and significant evaporite deposition in the centre of the Uinta Basin (Dyni, 1974a, 1974b; Whiteside and Van Keuren, 2009; Vanden Berg and Birgenheier, 2017). However, large thickness variations at both high and low frequencies and lateral variation in the terrestrial basin compounds the orbital signal (e.g., Olsen and Kent, 1999; Machlus et al., 2008). The hypersaline nature of the Piceance Basin has been well documented (Johnson, 1985; Tänavsuu-Milkeviciene and Sarg 2012) and details of the hypersaline phase in the Mahogany Zone have been recently reported (Vanden Berg and Birgenheier, 2017), but their wider climatic and tectonic contexts await further studies.

Valuable insights into climatic and regional tectonic influences can be obtained through the study of organic biomarkers. There is a long history of pioneering organic geochemical research in the Green River Formation, and several key biomarkers were discovered here, including; steranes and triterpanes, perhydro-beta-carotene, and gammacerane (Hills et al., 1966; Tissot et al., 1978; Dyni, 1987). As a closed lacustrine system, the Green River Formation was extremely sensitive to basin and climatic changes, and the ~400 kyr depositional cycle (Smith et al., 2008b; Whiteside and Van Keuren, 2009) of the markedly TOC-rich Mahogany Zone is ideally suited for high-resolution geochemical studies to disentangle the complex controls on the duration and extent of this large organic-carbon sequestration event. High-resolution continental records over the termination of the EECO (~49.14 Ma) are rare and the eccentricity-paced cyclicity observed in the oil-yield values and C/N

ratios (Whiteside and Van Keuren, 2009) in the Green River Formation mirrors the beat of the early Eocene hyperthermals found in both the marine and continental realms (Machlus et al., 2008; Zachos et al., 2010; Sexton et al., 2011; Littler et al., 2014; Lauretano et al., 2015; Stein et al., 2021).

3.2 Materials and Methods

3.2.1 Site description

A plethora of industry cores have been commissioned because of the economic significance of the lower and middle Green River Formation's prolific hydrocarbon potential. Three cores, varying in proximity to the paleo-shoreline, were sampled through the organic rich Mahogany Zone across the Uinta Basin. Utah State 1, drilled by TOSCO (The Oil Shale Corporation), captures a deeper, basin-centre position during deposition of the Mahogany Zone (UTM 12T 627029 4429992). The P-4 Chevron White Shale Project core (hereafter referred to as P-4) was drilled in the eastern Uinta Basin, closer to the basin-margin and edge lacustrine environment of the Mahogany Zone (UTM 12T 659426 4421812). The most proximal core, Skyline 16, represents a basin-margin, lacustrine setting, containing a shallower and marginally thinner section of the Mahogany Zone (UTM 12T 661444 4415107). It was drilled by the Utah Geological Survey.

3.2.2 Age model

The Green River Formation is punctuated by numerous tuff layers from the north-eastern Absaroka and Challis Volcanic provinces. Two dated tuff horizons (Smith et al., 2008) in close vicinity of the Mahogany Zone of the P-4 drill core have been used to develop an age model. Detailed sedimentological analysis supports a linear sedimentation rate and the main facies present is profundal laminated mudstone

(Walters et al., 2020; Whiteside and Van Keuren, 2009; Smith et al., 2008). The Curly and Wavy tuffs are dated with $^{40}Ar/^{39}Ar$ stepwise degassing on euhedral biotite crystals to 49.32 ±0.33 Ma and 48.66 ± 0.27 Ma respectively.

3.2.3 Organic geochemistry

3.2.3.1 Biomarker Methods

Gammacerane, a saturated triterpenoid hydrocarbon derived from tetrahymanol, has been widely utilised as a biomarker for salinity stratification and hypersalinity. Bacterivorous ciliates (such as Tetrahymena) residing at or below the chemocline biosynthesize tetrahymanol (gammacer-3β-ol) during intervals when their diet is deprived of sterols. Upon diagenesis and early catagenesis, gammacerane is released and its ratio to the C_{30} hopane is therefore useful as an indicator of hypersalinity and water column stratification (Venkatesen, 1989; Sinninghe Damsté et al., 1995; Peters et al., 2005). Pristane (C_{19}) and phytane (C_{20}) are isoprenoid alkanes derived from algae and photosynthetic bacteria, higher plants, and archaebacteria (ten Haven et al., 1987; Didyk et al., 1978). The ratio (Pr/Ph) between these compounds has been used to understand redox conditions in sub-aqueous environments, with values <0.8 indicating anoxic conditions and values between 0.8–3.0 suggesting a sub-oxic environment (ten Haven et al., 1987; Amane and Hideki, 1997; Sarmiento and Rangel, 2004).

The primary source of organic matter in lacustrine environments is chiefly composed of phytoplankton, although large contributions may be sourced from decaying terrestrial higher plant matter depending on the surrounding terrigenous vegetation and fluvial controls (Dyni, 2006). *N*-alkane average chain length distributions can be used to identify ecological shifts in the vegetation such as those associated with

varying inputs of longer-chain terrestrial plant material (Ficken et al., 2000; Jansen et al., 2010).

3.2.3.2 Organic Geochemistry Methods

Rock plugs through the Mahogany Zone from Utah State 1, P-4 (2274–2376 ft; 683–785 ft respectively; sub-sampled at the Lamont-Doherty Earth Observatory of Columbia University) and Skyline 16 (430–513 ft; sub-sampled at the Utah Geological Association, at depths with known total organic carbon measurements), were removed with a water-cooled drill press (Delta DP300L), and powdered by agate mortar and pestle. Samples retrieved from the Mahogany Zone drill cores are typically comprised of light brown to black, laminated mudstones with TOC values ranging from 0.35 to 44.6 wt. %, averaging 11.2 wt. % (Whiteside and Van Keuren, 2009). Samples are subdivided into the upper, middle and lower Mahogany Zone in the Results and Discussion for ease of comparison (Tables 1, 2 and 3). Molecular extraction and fractionation were conducted at the National Oceanography Centre Southampton. Total lipid extracts (TLE) were isolated from powdered rock using a Thermo 350 Accelerated Solvent Extractor with the following program: preheat = 5 min; heat = 5 min; static = 5 min; pressure = 1500 psi; flush = 70%, purge = 300 s.; cycles = 3; solvent = dichloromethane:methanol (9:1, *v*/v). Solvent extracts were reduced to dry with a Genevac EZ-2 vacuum centrifuge, transferred to small vials, evaporated under a stream of nitrogen, and then gravimetrically quantified. The TLEs were fractionated using small silica gel columns and fractions were eluted with hexane, hexane: dichloromethane (DCM) (4:1, *v*/*v*), and DCM: methanol (MeOH) (1:1, *v*/*v*), yielding the aliphatic, aromatic and polar fractions, respectively. Activated copper was added to each fraction to remove elemental sulphur. Biomarker identification was performed using a Thermo Trace 1310 gas chromatograph (GC) coupled to a Thermo TSQ8000 triple quadrupole mass spectrometer (MS). The GC

used a DB-5 column (30 m ×0.25 mm i.d, 0.25-μm film thickness) with the following oven program: 40°C (held for 2 min), increased at a rate of 6°C/min to 310°C, and then held for 20 minutes. Compound identification of *n*-alkanes and pristane/phytane was made using mass spectra and comparison with an in-house reference oil (North Sea Oil-1).

The gammacerane indices for the Utah State 1, P-4 and Skyline 16 cores were calculated as: (Gammacerane/(Gammacerane*C30αβ)*10). Average chain length (ACL) and the degree of 'waxiness' can characterise the *n*-alkane distribution of samples and reveal variations in paleoecology. ACL values incorporate the weighted averages of carbon chain lengths and has been calculated as follows (Ficken et al., 2000):

$$\text{ACL} = \frac{((25\times C_{25})+(27\times C_{27})+(29\times C_{29})+(31\times C_{31})+(33\times C_{33}))}{C_{25}+C_{27}+C_{29}+C_{31}+C_{33}}$$

The waxiness ratio, an environmental source parameter that evaluates the input of waxy terrestrially-derived material to aquatic organic matter (Connan and Cassou, 1980), is calculated as:

Waxiness= Σ *n*-C_{21}-C_{31}/Σ *n*-C_{15}-C_{20}

3.3 Results

3.3.1 Gammacerane Indices

In Utah State 1, the gammacerane indices range from 0.16–0.53, with relatively moderate values in the lower Mahogany Zone (0.25–0.53; 2338.5–2380.6 ft) remaining low (0.16–0.20) between 2316.3 and 2330.25 ft, and after this increasing up through the section to values of 0.46 (2296.2 ft). In the basin margin core P-4, gammacerane index values vary from 0.07–0.87 with the peak oil shale of the

Mahogany Bed deposited at a time with a moderate gammacerane index (Figure 2; 0.28). Several peaks with high (>0.7) gammacerane indices are identified and values increase slightly upwards through the Mahogany Zone.

In Skyline 16, the gammacerane index values vary from 0.034–0.84 indicating heterogeneous conditions and salinity stratification through the Mahogany Zone. Values are more variable towards the top and base of the section, and also generally higher, suggesting intervals of hypersalinity are captured in these samples (Figure 4). In the middle of the section around the Mahogany Bed (460 ft), gammacerane index values remain low, but above zero, indicating some degree of salinity stratification is present through the Mahogany Zone at the most proximal core location. The gammacerane indices show that the water column had robust salinity stratification through the Mahogany Zone of the sampled cores.

Table 1: Depth in feet with total organic content, gammacerane indices, pristane/phytane, carbon preference index, and waxiness values for Utah State 1.

Depth (ft)	Mahogany Zone Subdivision	TOC	GI	Pr/Ph	CPI	Waxiness
2272.3	Upper	2.08	0.35	0.75	28.90	4.31
2275.2	Upper	15.39	0.34	1.04	27.94	0.78
2279.2	Upper	4.03	0.45	0.85	28.95	2.97
2280.3	Upper	16.49	0.29	0.94	28.25	2.15
2283.6	Upper	13.34	0.27	0.94	27.86	2.05
2284.2	Upper	11.26	0.30	1.00	28.15	1.74
2286.3	Upper	15.08	*	*	*	*
2290.3	Upper	11.13	0.37	1.07	28.32	1.84
2292.1	Upper	8.48	0.40	1.00	28.47	2.16

2296.2	Upper	4.93	0.46	0.94	28.59	3.43
2301.2	Upper	3.32	0.39	0.70	29.01	7.19
2302.07	Upper	*	0.29	0.77	28.53	3.17
2303.1	Upper	5.3	*	*	*	*
2304.7	Upper	*	0.35	0.83	28.57	1.42
2308.3	Middle	16.05	0.24	0.80	28.69	2.03
2311.5	Middle	11.56	0.21	0.75	28.87	3.12
2314.1	Middle	44.55	0.19	0.77	28.36	1.81
2316.3	Middle	20.36	0.21	0.80	28.76	2.44
2317.4	Middle	29.21	0.20	0.77	28.86	2.78
2318.2	Middle	18.16	0.18	0.78	28.92	2.79
2319.4	Middle	7.73	0.18	0.68	28.87	3.38
2322.7	Middle	23.46	0.17	0.80	28.76	2.07
2327.6	Middle	11.03	0.18	0.64	29.24	5.84
2330.3	Middle	10.58	0.16	0.75	28.83	2.82
2332.4	Middle	0.35	*	*	*	*
2333.9	Middle	9.18	0.24	0.71	28.78	3.22
2335.1	Middle	4.73	0.22	0.74	28.80	2.95
2337.2	Middle	19.08	0.22	0.61	29.36	6.10
2338.5	Middle	16.91	0.28	0.75	28.69	2.65
2341.2	Middle	20.31	0.28	0.77	28.74	2.50
2344.3	Middle	8.24	0.30	0.73	29.25	4.10
2348.5	Lower	7.98	0.36	0.91	28.59	2.11
2351.1	Lower	1.24	0.49	0.35	29.00	12.18
2353.1	Lower	6.99	*	*	*	*
2355.1	Lower	1.48	*	*	*	*
2357.3	Lower	12.17	0.45	1.20	27.68	0.71

2359.3	Lower	3.77	0.39	0.88	28.74	1.78
2362.6	Lower	26.02	0.53	1.19	28.21	0.57
2365.2	Lower	4.71	0.25	0.81	29.26	4.19
2368.1	Lower	2.73	0.42	1.06	29.06	1.55
2371.5	Lower	11.2	0.37	0.81	28.63	1.15
2374.7	Lower	7.57	0.46	0.97	28.39	1.27
2377.2	Lower	2.95	0.33	0.84	29.49	2.47
2378.9	Lower	3.33	0.50	0.73	29.98	4.62
2380.6	Lower	0.42	0.54	0.88	29.70	1.48

*Blank values due to an earlier TOC sampling strategy then analysis followed by biomarker analyses on samples retrieved at a later date

Table 2: Depth in feet with total organic content, gammacerane indices, pristane/phytane, carbon preference index, and waxiness values for P-4.

Depth (ft)	**Mahogany Zone Subdivision**	**TOC**	**GI**	**Pr/Ph**	**CPI**	**Waxiness**
685.3	Upper	5.65	0.43	0.59	1.36	2.07
686.2	Upper	9.4	*	*	*	*
687.4	Upper	2.83	*	*	*	*
690.8	Upper	8.47	*	*	*	*
691.6	Upper	7.86	*	*	*	*
692.3	Upper	11.86	*	*	*	*
693.5	Upper	*	0.25	0.61	1.30	0.87
694.2	Upper	24.89	*	*	*	*
695.5	Upper	12.51	*	*	*	*
696.3	Upper	9.04	0.27	0.61	1.99	1.15

697.3	Upper	4.16	0.47	0.53	2.41	4.14
699.0	Upper	10.18	0.55	0.49	2.26	1.78
699.7	Upper	8.6	0.73	0.52	2.42	2.10
700.4	Upper	4.08	0.64	0.49	2.57	5.45
702.1	Upper	4.32	0.30	0.52	2.46	4.00
704.5	Upper	5.33	0.21	0.46	2.62	5.12
705.1	Upper	*	**	0.21	3.48	18.61
705.9	Upper	5.16	0.07	0.40	2.52	6.46
705.9	Upper	5.24	*	*	*	*
707.0	Upper	6.31	0.18	0.49	2.52	5.70
708.4	Upper	28.55	0.24	0.41	1.48	2.88
708.4	Upper	28.58	*	*	*	*
708.7	Upper	15.27	0.73	0.53	1.69	0.83
709.8	Upper	9.24	0.27	0.41	1.92	2.64
709.8	Upper	9.39	*	*	*	*
711.6	Upper	12.84	0.23	0.47	1.21	4.15
712.9	Upper	6.91	0.19	0.45	2.07	2.71
712.9	Upper	7.53	*	*	*	*
713.9	Upper	10.71	0.21	0.44	1.71	3.07
714.5	Middle	9.79	0.15	0.45	1.87	1.55
714.5	Middle	10.91	*	*	*	*
715.8	Middle	15.24	0.29	0.43	1.69	2.31
716.7	Middle	43.06	0.16	0.45	1.73	1.92
716.7	Middle	35.66	*	*	*	*
718.6	Middle	29.55	0.11	0.42	1.97	1.96
719.9	Middle	11.5	0.28	0.37	2.04	2.75
719.9	Middle	12.24	*	*	*	*

720.5	Middle	21.74	0.08	0.39	1.58	3.29
722.2	Middle	*	0.30	0.36	2.49	4.71
722.7	Middle	7.29	0.07	0.35	2.35	4.59
722.7	Middle	8.8	*	*	*	*
724.9	Middle	9.04	0.09	0.40	1.78	1.48
725.6	Middle	25.72	*	*	*	*
727.2	Middle	7.65	0.09	0.39	2.42	3.90
728.5	Middle	*	0.16	0.38	1.99	4.11
729.8	Middle	25.65	0.10	0.38	2.32	1.97
731.9	Middle	*	0.10	0.42	2.05	1.32
733.8	Middle	10.56	0.22	0.36	2.34	4.12
735.4	Middle	6.26	0.16	0.09	3.01	6.12
737.4	Middle	5.39	0.15	0.39	1.98	3.89
738.7	Middle	*	0.20	0.39	2.12	3.60
740.6	Middle	16.08	*	*	*	*
742.5	Middle	3.27	0.23	0.39	1.41	5.05
744.4	Middle	4.06	0.27	0.45	1.25	3.89
745.4	Middle	16.42	0.22	0.43	2.54	1.87
746.7	Middle	10.66	*	*	*	*
748.5	Middle	*	0.13	0.42	2.05	4.08
750.6	Lower	10.68	0.23	0.45	2.18	4.17
752.7	Lower	7.63	*	*	*	*
755.1	Lower	3.4	0.37	0.52	1.50	3.94
757.2	Lower	10.94	0.87	0.50	1.92	2.13
759.1	Lower	9.87	*	*	*	*
760.9	Lower	1.62	0.48	0.35	1.42	7.46
761.9	Lower	1.88	0.30	0.26	1.55	33.21

763.2	Lower	7.92	0.43	0.53	0.86	3.86
765.0	Lower	2.15	0.45	1.42	1.00	16.81
766.4	Lower	9.39	0.45	0.48	1.16	2.91
767.5	Lower	15.81	*	*	*	*
768.3	Lower	2.48	*	*	*	*
768.9	Lower	3.49	*	*	*	*
769.5	Lower	2.5	0.27	0.30	1.73	2.90
770.4	Lower	8.39	*	*	*	*
771.6	Lower	18.35	*	*	*	*
772.8	Lower	1.77	*	*	*	*
773.8	Lower	2.61	0.32	0.35	2.33	2.90
774.8	Lower	1.1	*	*	*	*
775.6	Lower	*	0.38	0.59	1.60	3.73
776.1	Lower	2.9	**	0.54	2.91	3.82
777.1	Lower	7.23	*	*	*	*
778.5	Lower	5.23	0.14	0.97	0.67	2.89
781.7	Lower	*	0.28	0.93	0.84	1.91
782.2	Lower	2.58	*	*	*	*
783.5	Lower	5.81	*	*	*	*
784.5	Lower	2.17	**	0.82	3.21	2.90

*Blank values due to an earlier TOC sampling strategy then analysis followed by biomarker analyses on samples retrieved at a later date

** Missing gammacerane indices values due to inability to isolate gammacerane with the close overlapping C_{31R} homohopane in the chromatograph

Table 3: Depth in feet with total organic content, gammacerane indices, pristane/phytane, carbon preference index, and waxiness values for Skyline 16.

Depth (ft)	Mahogany Zone Subdivision	TOC	GI	Pr/Ph	CPI	Waxiness
420.0	Upper	3.32	0.50	0.49	4.13	1.71
422.1	Upper	2.33	0.54	0.51	4.17	1.31
425.2	Upper	2.14	0.84	0.51	4.30	1.08
429.5	Upper	2.74	0.53	0.53	3.45	2.81
431.5	Upper	5.02	0.42	0.59	3.45	2.04
437.9	Upper	13.18	0.11	0.60	1.85	0.96
444.9	Upper	11.04	0.61	0.58	2.85	2.04
453.9	Middle	7.54	0.22	0.36	3.82	3.63
463.9	Middle	26.57	0.03	0.35	3.34	2.09
468.1	Middle	8.14	0.08	0.35	2.84	1.97
472.1	Middle	29.18	0.13	0.38	2.52	1.62
477.9	Middle	4.44	0.11	0.37	3.52	3.71
485.8	Middle	13.71	0.17	0.48	2.89	2.49
493.7	Lower	23.76	0.22	0.56	2.52	0.79
496.3	Lower	2.38	0.54	0.49	3.17	2.28
503.8	Lower	3.01	0.72	0.47	3.17	3.17
508.1	Lower	1.12	0.36	0.50	3.22	3.03
510.6	Lower	8.99	0.26	0.52	2.32	1.49
515.7	Lower	1.61	0.66	0.70	4.48	1.10

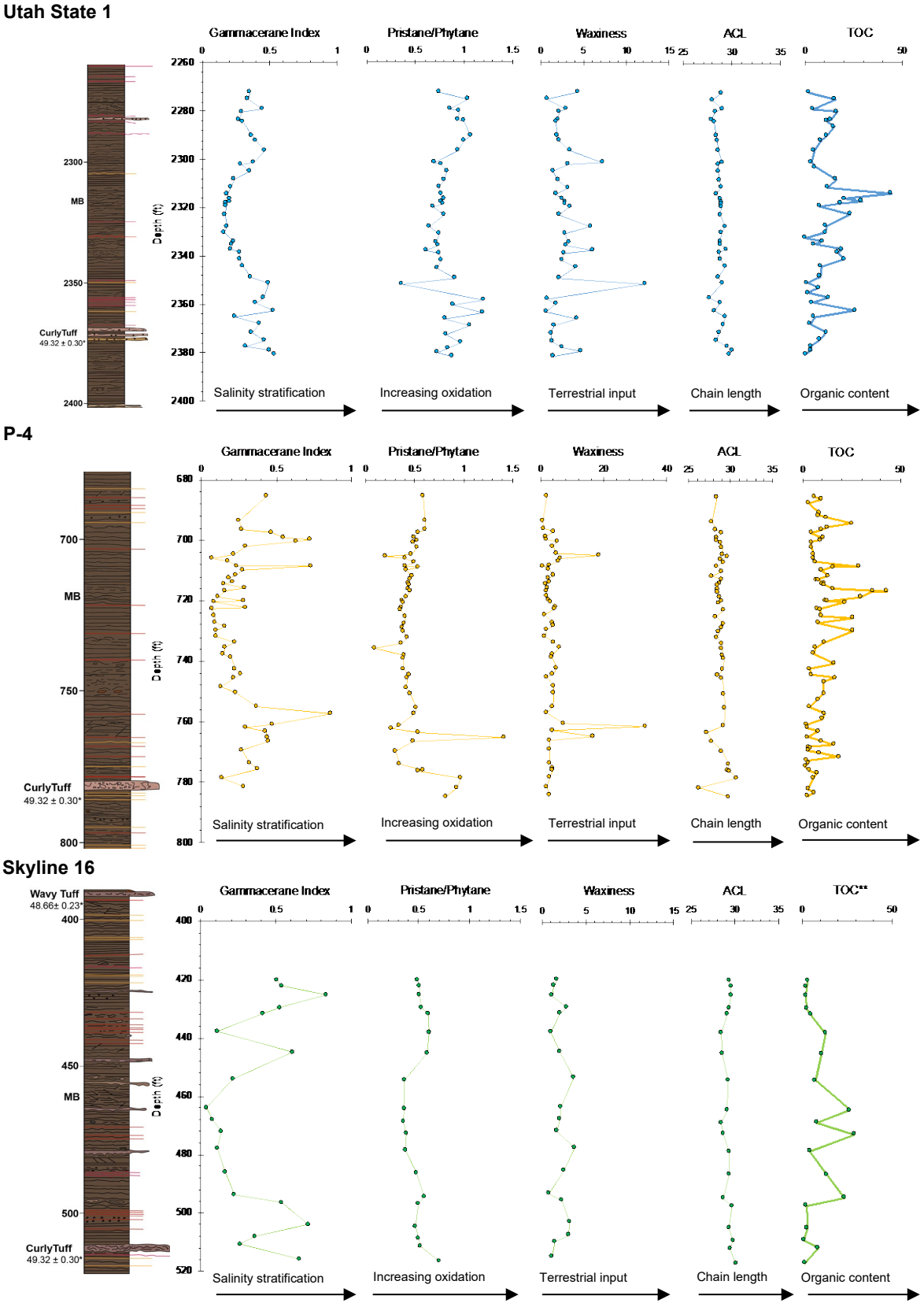

Figure 2: (Top) Utah State 1 core results: Stratigraphic column through the Mahogany Zone, Utah State 1. From left: gammacerane indices show variations in salinity stratification ((gammacerane/gammacerane + C_{30}αβ)*10); pristane/phytane ratio indicating anoxic to sub-oxic water column conditions; 'waxiness', which evaluates terrestrial material input

(Σ *n*-C_{21}-C_{31}/Σ *n*-C_{15}-C_{20}); ACL is average chain length of analysed organics and characterises the *n*-alkane distribution of samples, allowing for identification of ecological shifts; total organic carbon (TOC) reveals variation of oil shale richness. (Middle) P-4 core results: Stratigraphic column through the Mahogany Zone, P-4. Gammacerane indices of analysed hydrocarbons, with high values suggesting hypersalinity. (Bottom) Skyline 16 core results: Stratigraphic column through the Mahogany Zone, Skyline 16. Gammacerane indices, with high values indicating hypersaline intervals. **TOC values for Skyline 16 generated by M. Vanden Berg and J. Birdwell at the USGS, Denver. MB= Mahogany Bed Marker. (*Radioisotopic dates from Smith et al., 2008).

3.3.2 Pristane/phytane

The pristane/phytane ratio is a paleo-redox proxy of water column conditions. In Utah State 1, pristane/phytane values are elevated (0.35–1.20; Figure 2) compared to the other cores analysed, indicating reducing to sub-oxic conditions through the Mahogany Zone in the lake depocentre. In the P-4 lake margin core, values range from 0.09–1.42 becoming variable towards the base of the core, reducing through the Mahogany Zone and appearing to become oxic (Pr/Ph = 1.42) at an interval that correlates to a tuffaceous debris flow (see appendix B; P-4 core log). Pristane/phytane values remain below 1 in Skyline 16 throughout the section (0.35–0.7), indicating strongly reducing conditions for the duration of the Mahogany Zone in this core.

3.3.3 Pristane/*n*-C_{17} vs. phytane/*n*-C_{18}

Pristane/*n*-C_{17} vs. phytane/*n*-C_{18} provides insight into redox conditions and the degree of thermal maturation of a sample (Figure 3; Peters et al., 2007). Utah State 1, P-4 and Skyline 16 plot in distinct groups, with the two proximal cores overlapping the most, indicating the most similar water column conditions. Utah State 1, the most basinal of the lacustrine sites, predominately plots in the sub-reducing zone with 12 samples indicating fully reducing conditions. Tuffaceous debris flows transport in organic matter from shallower oxic environments, resulting in rare values indicating

oxygenated water conditions in P-4, which aside from three samples that indicate sub-reducing conditions, is found to be reducing through the section. Skyline 16 values indicate reducing water column conditions through the Mahogany Zone, and none of the three cores underwent maturation to a strong degree, indicating a thermal immaturity that is ideal for organic geochemical studies.

3.3.4 Gammacerane indices vs pristane/phytane

Gammacerane indices vs pristane/phytane provides the relationship between salinity stratification and water column anoxia, and the variation of this with proximity to the Douglas Creek Arch. Utah State 1, P-4 and Skyline 16 have been subdivided into the upper, middle and lower Mahogany Zone (Figure 4; Table 1, 2, 3). An increasingly reducing environment is observed as the cores become more proximal, and more reducing values are generally found in the middle ('peak') Mahogany Zone compared to the upper and lower sections of the cores. Highly variable salinity stratification values are found in the upper and lower sections of the Mahogany Zone in all three cores, whereas only moderate values of salinity stratification, coupled with a reducing water column, are seen during the peak Mahogany Zone. Box and whisker plots for the sub-divided cores demonstrate increased variability of salinity stratification in the upper and lower Mahogany Zone, with least variable values consistently found during the peak Mahogany Zone (Figure 4). Utah State 1, the basin-centre core, has generally elevated salinity stratification values compared to the P-4 and Skyline 16 cores. However, less variation is observed in the salinity stratification and values indicative of extreme hypersalinity are not present, whereas hypersalinity is likely to have existed during the upper and lower sections of P-4 and Skyline 16. P-4 has the highest variability of gammacerane indices values through the upper, middle and lower Mahogany Zone. Skyline 16 shows a similar variability in the upper and lower core, but variation in values is very minor during the mid-

Mahogany Zone. This is reflected in both of the other sites, which also show the least variability in salinity stratification and chemocline fluctuation during the mid-Mahogany Zone.

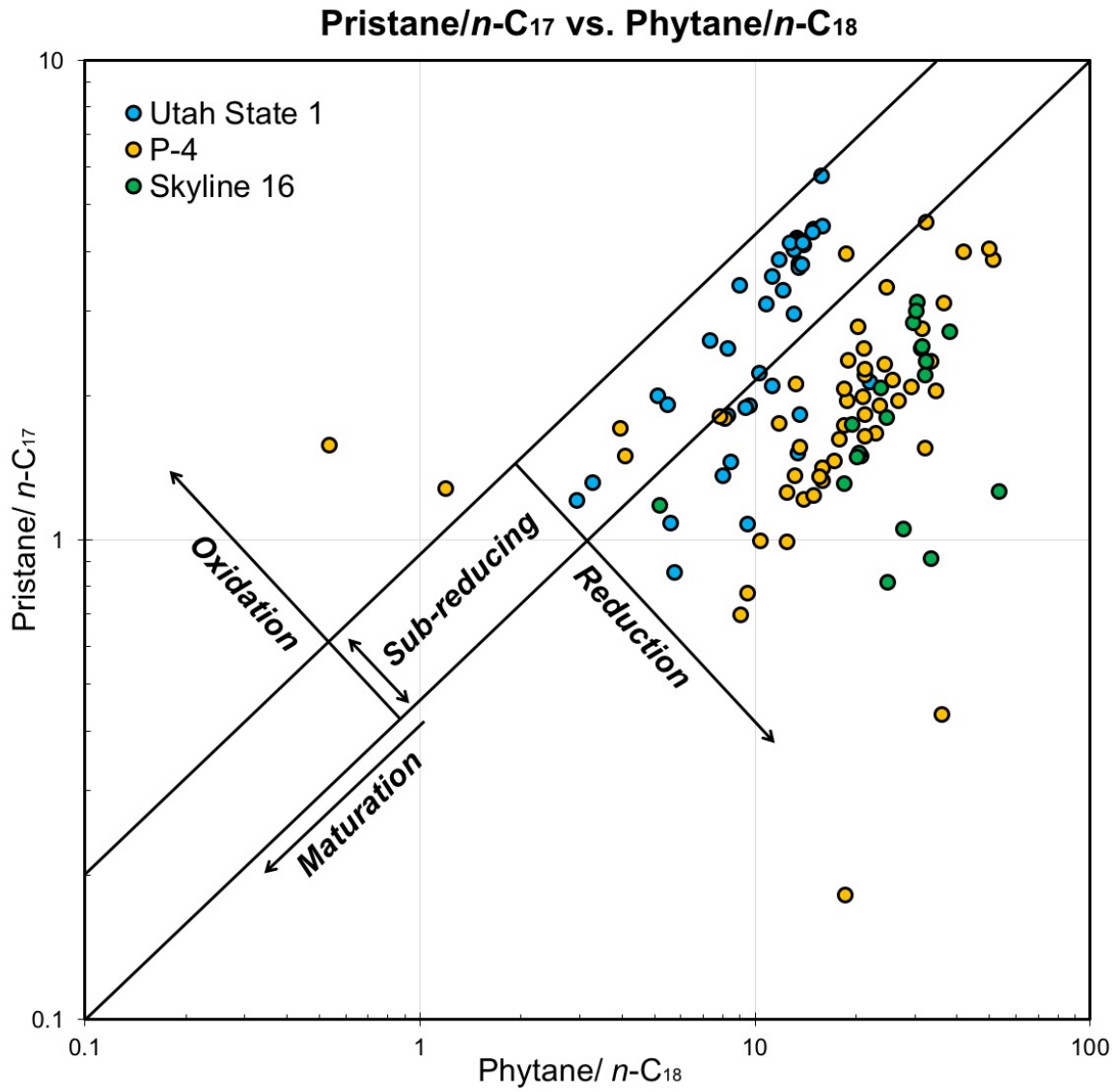

Figure 3: Cross plot of Pristane/*n*-C_{17} vs. Phytane/*n*-C_{18}, for Utah State 1, P-4 and Skyline 16. Utah State 1, the most basinal of the lacustrine sites, predominately plots in the sub-reducing zone, whereas the more proximal sites P-4 and Skyline 16 group in the reducing zone. Tuffaceous debris flows result in rare values indicating oxygenated water conditions.

3.3.5 Average Chain Length

The average chain length through the basin centre core ranges from 27.7–23.0 and has some greater variation towards the base and top of the section (Figure 2). In P-4, average chain length values are homogenous through the section, with more

variation observed in the deepest samples (781.7–763.15 ft) and values ranging between 26.3–29.7. Average chain length values in Skyline 16 range from 28.5–30.2, with values slightly higher than Utah State 1 and P-4. Minor variability is present up through the Mahogany Zone, representing changes in different proportions of various compounds being preserved.

3.3.6 Waxiness

The degree of waxiness in Utah State 1 range from 0.2–11.6. Several peaks of increased terrigenous material are present through the section, with large events present at 2301.2 and 2351.1 ft (Figure 2). In the basin-margin P-4 core, waxiness values range from 0.8–33.2, with far higher terrestrial material present here than observed in the Utah State 1 waxiness proxy record. Very large peaks representing high proportions of leaf waxes in comparison to aquatic organic matter are present at 705.1 and 761.9 ft, which are similar horizons where the same perturbations are observed in the Utah State 1 core. The degree of waxiness in the Skyline 16 core varies between 0.8–3.7, representing variable amounts of longer chain *n*-alkane input from leaf waxes. These values are low in comparison to the large peaks seen in Utah State 1 and especially P-4, which may be a result of a lower resolution record in Skyline 16 and a sampling bias missing these infrequent large leaf wax-contributing run-off events, where lacustrine turbidites and hypopycnal flows gradually deposit the suspended clay fraction (Boggs, 1995).

3.3.7 Total Organic Carbon

TOC values are highly elevated and vary through the three cores, with highest values recorded in the basin-centre (Figure 2). In Utah State 1, TOC ranges from 0.4–44.6% and varies between high and low values rapidly, peaking at the laterally extensive Mahogany Bed Marker (2314 ft; Figure 2). P-4, located adjacent to the

basin-margin during the Mahogany Zone, has TOC values ranging from 1.1–43.1%. The proximal core of Skyline 16 is located on the basin-margin and contains the lowest TOC values of the three cores, varying from 1.1–29.8%.

3.4 Discussion

3.4.1 Fidelity of the biomarker ratios

3.4.1.1 Other sources of organic matter

Pristane (Pr) and phytane (Ph) are primarily derived from the phytol side chain of chlorophyll-*a* in the phytoplankton community (Witkowski et al., 2018), with phytane preferentially preserved in reducing conditions and pristane preferentially preserved during oxic conditions. The Pr/Ph ratio has long been used as an indicator of reducing and oxic conditions in the water column (Didyk et al., 1978; Hughes et al., 1995), however, these compounds can be produced by multiple sources (e.g. methanogens and halophiles; Risatti et al., 1984, ten Haven et al., 1987). Phytane can also be derived from bis-phytanyl ethers found in archaebacteria, and pristane from tocopherols (Philp, 1994), which in sufficient amounts may lead to a decoupling of Pr/Ph from redox conditions. We argue that inputs from alternative sources contribute minimally to the pristane/phytane record, due to being vastly outweighed by the extreme productivity of the algal community within the photic zone during the Mahogany Zone. Methanogenesis can be inhibited by highly sulphidic conditions in lacustrine environments, and evidence for high levels of iron sulphides in the Green River Formation decreases the likelihood of large methanogen inputs (Tuttle and Goldhaber, 1993).

Gammacerane, a pentacyclic triterpenoid first discovered in the Green River Formation (Hills et al., 1966) is only known to derive from tetrahymanol (Venkatesen, 1989; ten Haven et al., 1987; Sinninghe Damste et al., 1995; Peters

et al., 2005), where an increase of the ratio of the concentration of gammacerane to that of the C_{30} hopane is linked to increases in salinity and water column stratification. Other sources of tetrahymanol have been identified in the natural world, and include cultures of an anaerobic rumen fungus (*Piromonas communis*) (Kemp et al., 1984), as well as ferns (Zander et al., 1969) however, the pathway to gammacerane generation is during stressed environmental conditions, where the precursor molecule is forced to accept tetrahymonol in lieu of sterols, make it highly unlikely that significant alternate sources of tetrahymanol, not reflective of the saline environment, existed either in the water column or from external transport. The gammacerane indices are thus truly reflecting lake water column salinity conditions.

3.4.1.2 Mass transport deposits

As well as being produced by multiple sources, pristane and phytane can be transported by mass transport deposits, and so may not faithfully record redox conditions at the time of deposition (ten Haven et al., 1987). Debris flows and lower energy distal turbidites are identified in the Mahogany Zone and often related to ash-flow deposits (Birgenheier and Vanden Berg, 2011). This may go some way in explaining the apparent presence of oxic conditions in the basin-centre during periods of oil shale deposition (Figure 3). Skyline 16, which has minimal debris flow facies represented during the Mahogany Zone, may better represent true redox conditions in the basin than P-4 and Utah State 1. Minimal thermal maturation to the signal is supported by the high pristane/C_{17} to phytane/C_{18} values and moderate average chain length values, indicating no major alteration.

3.4.1.3 Terrestrial input to the basin

The large variations of leaf wax (0.2–11.6; Figure 2) reflected in the waxiness ratio may be the result of multiple controls, including variations in the minor amounts of

n-alkanes produced in the lake. A change in basin drainage capture or vegetation amount could influence the amount of leaf wax being transported into the lake system or high levels of run off from the mountains and shorelines surrounding the lake could increase the levels of terrestrial input (Eglinton and Eglinton 2008; Sachse et al., 2004; 2012). This may also be expressed in subtle changes of the sedimentology, with occasional laminae of clastic grains in the laminated calcareous mudstones of the P-4 and Utah State 1 cores and rare higher energy siltstone and sandstones representing the distal plumes of turbidites, which may indicate a change or avulsion in fluvial style (Gall et al., 2017). Subtle variations in the sedimentology, with occasional siltier laminations do not indicate a significant change in local fluvial systems and may represent an increase in runoff due to local weather changes or an intense short-lived storm, accounting for these rare spikes seen in both the P-4 and Utah State 1 cores. Leaf wax transport and increased runoff of freshwater into the lake would be higher under these conditions (Diefendorf and Freimuth, 2017), with decreasing volumes of terrestrial material towards the basin centre as observed between Utah State 1 and P-4. These multi-core events which deliver spikes of leaf wax into the basin may be related to the eccentricity pacing at the ~100 kyr and ~400 kyr scale observed in this formation (Fischer and Roberts, 1991; Whiteside and Van Keuren, 2009) and are not clearly reflected in the more sparsely sampled Skyline-16 core, likely an effect of the sampling density.

3.4.2 Inter-site variation in redox values

The spatial variation in Pr/Ph values from algal lipids from Skyline 16 to Utah State 1 may have been affected by several processes, including inputs from multiple fluvial systems, mass transport deposits, and the mixing of lake layers during seasonal overturning (Sachse et al., 2004), the latter potentially resulting in the remineralisation of organic matter. Less reducing Pr/Ph values observed in Utah

State 1 may be a result of the increased fetch the basin-centre core received, in an open lake setting. A more significant fetch would lower the seasonal thermocline and overturn the upper water column during windier periods, resulting in remineralisation of organic matter. Seasonal overturning may be less severe at the more sheltered proximal sites, presenting less opportunity for remineralisation (Kelts and Talbot, 1990). Volcanic material can strongly influence redox conditions, and high amounts of transported tuffaceous material, such as the Curly and Wavy tuffs, and numerous thinner unnamed ash beds, is present in the centre and eastern Uinta Basin (Birgenheier and Vanden Berg, 2011). Ash-flows transported from the Challis and Absaroka volcanic provinces (Smith et al., 2008; 2010) via the Piceance Basin may have supported strongly reducing conditions in the basin-margin cores, located proximal to volcanic material input, as well as providing more nutrients to the photic zone, driving further water column stratification in comparison to the basin-centre core.

3.4.3 Spatial and temporal variations in salinity stratification and hypersalinity

At all three locations, higher gammacerane index values are in the upper and lower Mahogany Zone with minor-moderate values in the mid-Mahogany Zone (Figure 4). Converse to expected trends, severity of hypersalinity decreases with distance from the Douglas Creek Arch and is stronger in the shallower cores. Although hypersalinity is weakest in the depo-centre, higher gammacerane indices over the entire section (see Figure 4-b) indicate a more stable salinity stratification in the basin-centre compared to a less stable, hypersaline-prone environment in the basin-margin cores.

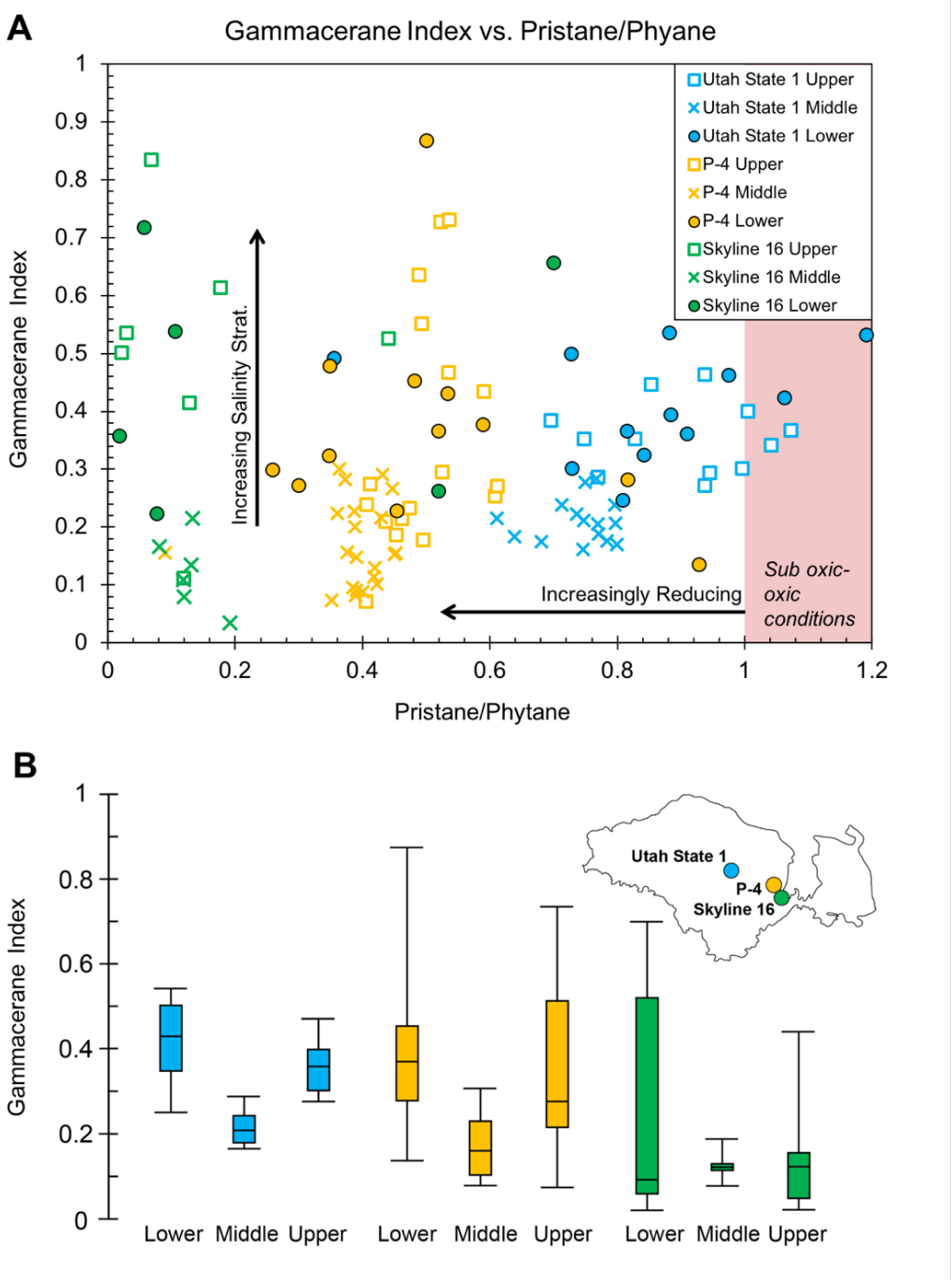

Figure 4: (A) Gammacerane Indices vs Pristane/Phytane, for the Mahogany Zone in the Utah State 1, P-4 and Skyline 16 cores, subdivided into upper, middle and lower sections. (B) Box and whisker plots for the sub-divided cores, revealing increased variability of salinity stratification in the upper and lower Mahogany Zone of the three cores, with least variable values always found during the middle (peak) Mahogany Zone. Salinity stratification values extend to lower values in the P-4 and Skyline 16 cores, and these cores generally show greater variability in salinity conditions than the basal Utah State 1 core. Whiskers represent highest and lowest values, and the box indicates the position of the upper quartile, mean and lower quartile for each set of results.

3.4.3.1 Precipitation/evaporation controls

Drivers of salinity stratification in lacustrine basins are often attributed to enhanced evaporation in the region, concentrating saline minerals in the residual lake water. Closed lacustrine basins, like the Uinta Basin, are particularly vulnerable to this process. The Mahogany Zone was deposited at a global onset of Eocene cooling (~48-49 Ma; Inglis et al., 2015; Smith et al., 2010; Gall et al., 2017), with temperatures slowly decreasing from the EECO. On the backdrop of global cooling, Lake Uinta was at a highstand, indicating that levels of evaporation strong enough to decrease lake level and/or concentrate saline minerals in this basin were unlikely.

3.4.3.2 Water balance-driven variations in brine input

Regionally, the Green River Formation basins of Utah, Colorado and Wyoming were interconnected through the highstand period of the Mahogany Zone. The northern Greater Green River Basin was far shallower and flatter in relief than its southern counterpart and experienced high evaporation as a result (Bohacs et al., 2003; Smith et al., 2010). Contemporaneous to oil-shale deposition in Lake Uinta, the Greater Green River Basin experienced infilling from sediment and water capture of the Idaho River. This forced displacement of evaporitic-mineral rich water and volcaniclastic sediments from the Lake Gosiute down to the Piceance Basin of Colorado and then into the connected highstand Lake Uinta (Figure 1; Johnson, 1985; Smith et al., 2008). The Skyline 16 and P-4 cores are located closer to the Douglas Creek Arch and as a result, would have been very sensitive to intermittent brine input associated with the transported Greater Green River Basin material (Figure 5). This is reflected in the high variability seen in the gammacerane indices for both P-4 and Skyline 16 (Figure 3, 4). Lower variability is seen at Utah State 1, but stronger salinity stratification of the water column persisted in the centre of the lake, where dense saline waters collected in the depo-centre, resulting in a brine

pool occupying the deepest part of the lake floor. The presence of large nahcolite nodules in Utah State 1, which would have precipitated in such stratified hypersaline lake bottom waters in the depocenter, (Vanden Berg and Birgenheier, 2017) and absence of these in Skyline 16 and P-4, which contain smaller crystals of shortite, supports this. Increasing inputs of volcaniclastic sediments have been proven to have played a role in organic carbon sequestration during the PETM, and so Tuffaceous layers in the Mahogany Zone may have precipitated authigenic carbonate and sequestered carbon (Longman et al., 2021). However, the richest TOC intervals are typically found in the laminated brown mudstone samples, with tuff layers relatively depleted in TOC (Whiteside and Van Keuren, 2009).

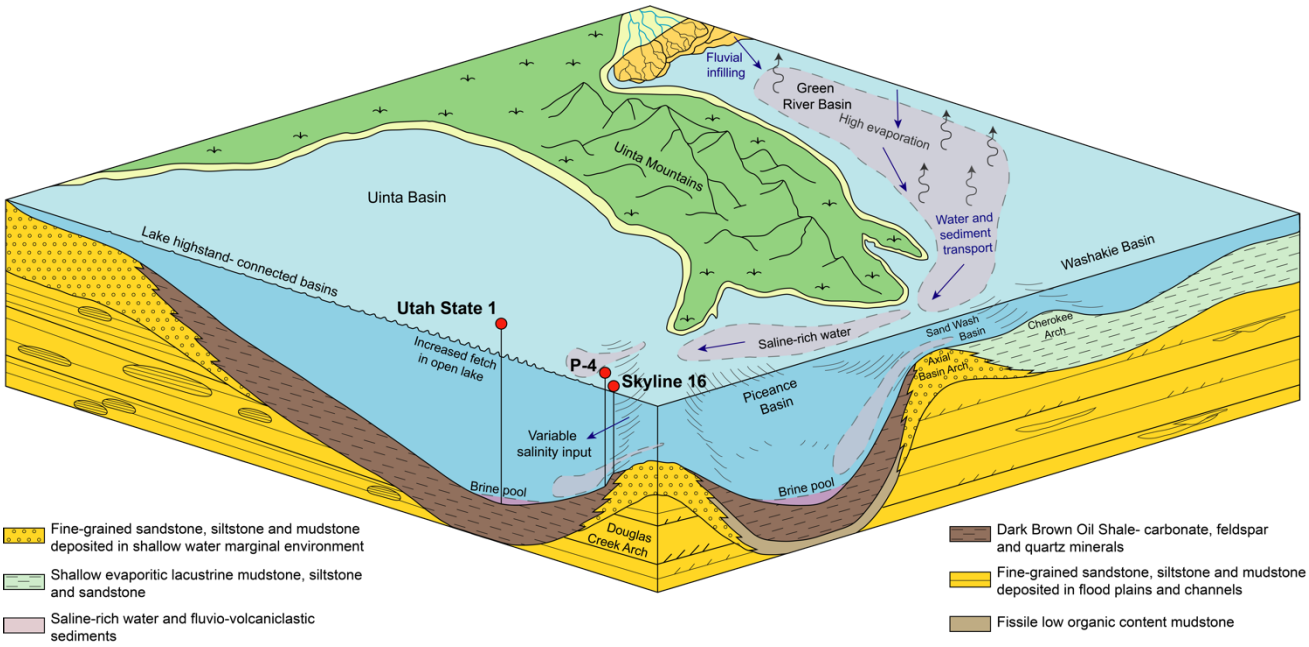

Figure 5: Illustrative model of the Uinta Basin during Mahogany Zone deposition, showing connected basins of the Green River Formation. Basin infilling in the northern Greater Green River Basin, coupled with high evaporation in the shallower-relief basin there, forced evaporitic saline waters and volcaniclastic sediments (delivered from capture of the Idaho River system) into the Piceance and Uinta basins. Due to a location nearer Douglas Creek Arch, sediments in the Skyline 16 and P-4 cores experienced large salinity changes as a result of intermittent brine input (associated with transported material), which is reflected in the variability of their gammacerane indices (see Fig. 4). Dense saline waters collected in the deepest parts of the basin, resulting in brine pool at the lake floor and less variable but stronger salinity stratification of the water column at Utah State 1.

3.4.3.3 Salinity stratification stymying primary productivity

In contrast to expectations, intervals with the strongest salinity stratification are not associated with highest TOC. Instead, elevated gammacerane indices correlate with relatively low values in TOC (Figure 2). During the peak Mahogany Zone and deposition of the Mahogany Bed Marker (~45% TOC; Whiteside and Van Keuren, 2009), salinity stratification is moderate and variability is low in all three cores (Figure 4), indicating that stability of the environment supported high primary productivity rates and the richest oil shale of the Green River Formation. In the upper and lower sections of the Mahogany Zone, where TOC values are lower, both higher variation in salinity stratification and additional hypersaline phases may have impacted the photosynthetic community, likely through stressing ecological conditions and hampering primary productivity in the basin. This may have restricted the photosynthetic organisms to species which are more halophilic and tolerant of the extreme conditions as accumulation of brine in the eastern palaeo-center resulted in the growth of large nodules of nahcolite similar to the adjacent Piceance Basin (Brownfield et al., 2010a; Johnson and Brownfield, 2015). Additional minor inputs of evaporite brine may have been mobilised at the shallow lake margin to the lake depocenter before precipitation of shortite and nahcolite in saline pore waters (Vanden Berg and Birgenheier, 2017; Jagniecki et al., 2013).

As intervals with high TOC appear to be linked to a lower intensity of salinity stratification, fluxes in primary productivity may be the most important control of the highly variable TOC through the Mahogany Zone (<1-45 wt.%; Figure 2) and the resultant organic carbon drawdown to the terrestrial realm. This is estimated for the Mahogany Zone as ~76.07 Gt of organic carbon over the ~400 kyr cycle of peak oil shale deposition in Lake Uinta (214.5 billion barrels of Mahogany zone oil in-place for the Uinta Basin based on Fischer Assay oil yield; Birdwell et al., 2015). Low

sedimentation rates persisted in the highstand lake (Birgenheier et al., 2019; Walters et al., 2020) and most of the sediments are sourced from suspension settling, unlike earlier in the basin history, when large fluvial systems developed in the EECO and large deltaic systems prograded into the Uinta Basin (Gall et al., 2017; Birgenheier et al., 2019). It is unlikely that variation in sediment supply and the subsequent clouding of the water column and dilution of organic matter exerted the major control on TOC, as much of the Mahogany Zone comprises carbonate or organic-dominated mudstones (Whiteside and Van Keuren, 2009). Similarly, a continually reducing environment through the Mahogany Zone, as evidenced by low pristane/phytane ratios and the presence of gammacerane, as well as supporting evidence from prior studies (Dyni, 1987; Vanden Berg and Birgenheier, 2017), indicate that variation in preservation conditions would not have been a major driver for the TOC trends. Spatial and temporal variations in salinity conditions were the result of water balance-driven variations of brine input into the terminal Uinta Basin (Figure 5), before the transition into an organic-lean environment. Dual tectonic and climate influences in the Green River Formation are reflected in the terminal Uinta Basin, at sub-orbital and orbital scales (Fischer and Roberts, 1991; Roehler, 1993; Whiteside and Van Keuren, 2009). Although tectonically driven drainage changes exerted a strong control on the variation in fresher and saline material transported to the Piceance and Uinta basins, climatically driven precipitation/evaporation cycles would have strongly affected the shallower Greater Green River Basin and concentrated the resultant transported material. Deteriorating ecological conditions in the lake, through increasing salinity stratification and large volumes of dense saline waters collecting, coupled with the increasing input of volcaniclastics, may have been a driver in the cessation of the orbitally paced organic rich and lean

intervals that culminated in this large organic carbon drawdown event and the extraordinarily organic-rich Mahogany Zone (Whiteside and Van Keuren, 2009).

3.5 Conclusions

The long-term tectonic and climatic evolution of the Lake Uinta region and consequent variations in environmental conditions have had profound control on the organic matter in the Green River Formation. Density stratification of the water column persisted through the Mahogany Zone and periods of hypersalinity developed. Closer to the source of saline material, such as the proximal locations in the east of the Uinta Basin, were more sensitive to changes in salinity stratification, which is reflected in the high variability of salinity conditions in the P-4 and Skyline 16 lake margin cores. The changeability of salinity stratification and hypersalinity was a key stressor of ecological conditions in the Mahogany Zone. The sediments with high TOC from the basin-centre core, which is subject to less variable, more moderate salinity stratification, and from the mid-Mahogany Zone, which hosts peak oil shale accumulations, consistently exhibit the least variability in salinity stratification. Pristane/phytane values indicate that the sediments sampled by the basin-centre core accumulated under the least reducing conditions, suggesting a decoupling of the pristane/phytane proxy from redox conditions.

Spatial and temporal variations in salinity conditions were the result of long-term tectonic controls driving the water balance between fresher and brine-rich inputs to the terminal Uinta Basin. The locus of evaporitic mineral formation was in the neighbouring Lake Gosiute of the Greater Green River Basin. Tectonically induced landform changes in the connected Greater Green River Basin caused large volumes of dense saline waters to flow across the Douglas Creek Arch during lake highstands and collect in the bathymetric lows in the Uinta Basin during periods of

increased evaporite precipitation. The resulting increased ecological stress on biota living in the water column, coupled with the increased supply of clastic material, may have been an important driver leading to the cessation of conditions favouring prodigious organic accumulation in the Mahogany Zone. The Mahogany Zone represents the last of the eccentricity-scale organic-rich cycles of this long-lived lake, and acted as a large carbon sink (~76.07 Gt) following the peak hothouse climate of the Cenozoic.

3.6 Acknowledgements

This contribution represents a portion of A. Elson's doctoral dissertation at the University of Southampton, funded by the Natural Environment Research Council Centre for Doctoral Training in Oil & Gas (Student number: 28882555). Oliver Bench assisted with field work and sample collection and P. Sargent Bray is acknowledged for help with organic geochemistry. Discussions with Margot Cramwinckel and Max Holmström contributed to the development of this manuscript. Funding was provided by CASP and the NSF for fieldwork and workshop attendance for A. Elson, and the Donors to the Petroleum Research Fund of the American Chemical Society to J. H. Whiteside.

Chapter 4 Stable hydrological cycle in the United States continental interior during the Early Eocene Climatic Optimum

Amy L. Elson[1], Megan Rohrssen[2], John Marshall[1], Gordon N. Inglis[1], Jessica H. Whiteside[1]

[1] School of Ocean and Earth Science, University of Southampton, National Oceanography Centre Southampton, UK

[2] Geology and Environmental Sciences, Central Michigan University, USA

This chapter is modified from a research article under review in Palaeogeography, Palaeoclimatology, Palaeoecology: Elson, A. L., Inglis, G. I., Marshall, J, E.A, and Whiteside, J. H. Stable hydrological cycle in the United States continental interior during the early Eocene Climatic Optimum. (In review). A. Elson prepared and ran samples for compound characterisation and then compound-specific hydrogen isotope analysis, and wrote the manuscript. G. I. Inglis plotted co-variation of compounds and performed a Demming regression on the data. All the co-authors provided editing and feedback.

Highlights:

- Leaf wax and algal lipid δ^2H reconstruct the hydrological cycle in the early Eocene
- Leaf wax and algal δ^2H values exhibit large lake inter-site variability (up to 100‰)
- Gradual variations in δ^2H values indicate a stable hydrological cycle in the EECO
- Stable hydroclimate may have promoted organic matter burial within the lake system
- High C_{org} burial may have acted as an important negative climate feedback

Keywords: Eocene; Green River Formation; EECO; hydrogen cycle; compound-specific hydrogen isotope analysis; lacustrine

Abstract

The early Eocene was characterized by a series of transient episodes of rapid global warming superimposed on the long-term early Cenozoic warming trend, culminating in the Early Eocene Climatic Optimum (~53.3 to 49.1 million years ago). Details of the hydroclimate regime operating during the EECO are poorly constrained, especially for continental interior sites. The Green River Formation (GRF) of Utah and Colorado was deposited in a suite of large, unusually productive lakes that offers an ideal opportunity to study the hydrological response to warming. Here we report on the hydrogen isotopic composition (δ^2H) of leaf wax (long-chain *n*-alkanes) and algal (phytane) lipids preserved in the organic-rich Mahogany Zone (49.3 to 48.7 Ma) and use these data to reconstruct precipitation and lake water δ^2H records, respectively. Algal lipid and leaf wax δ^2H values exhibit a strong linear relationship ($R^2 = 0.78$), suggesting that algae and higher plants are utilising the same hydrogen sources for biosynthesis. We observe large variations in algal and leaf wax δ^2H values (~50 to 75‰) in the basin as a whole, suggesting that locally variable water sources also influenced lake water δ^2H. However, leaf wax and algal lipid δ^2H values show little variation through the Mahogany Zone, suggesting a uniform hydrological regime. This contrasts with the more variable hydrological regime that prevailed during early Eocene hyperthermals. The early Eocene hyperthermals in the Uinta region do not coincide with the deposition of similarly organic-rich sediments, suggesting that a stable hydrological regime may promote conditions that enable the preservation of organic matter within continental-interior lake systems, potentially leading to an important negative climate feedback during the early Eocene and other greenhouse climates.

4.1 Introduction

The early Eocene (56.0 to 47.8 million years ago; Ma) Green River Formation provides a 15 Myr sedimentary record of intermittently interconnected terminal continental-interior basins that extended across north eastern Utah, north western Colorado and south western Wyoming (Bradley, 1929; Tissot et al., 1978; Dyni, 1987; Smith et al., 2008, 2010) (Figure 1). In the GRF of the Uinta Basin, Utah, Lake Uinta varied from freshwater to saline, with at least three hypersaline intervals identified (Vanden Berg and Birgenheier, 2017). The first of these coincides with the interval richest of organic content in the GRF, the Mahogany Zone. Deposited over ~400 thousand-years (kyr), the lacustrine strata comprise of sediments deposited in the deepest part of the paleo-lake (Tissot et al., 1978). This unusually organic-rich section is found throughout the basin and contains a thin (0.5m) marker bed of peak total organic carbon (TOC; 43 wt.%; Whiteside and Van Keuren, 2009), referred to as the Mahogany Bed marker. The Mahogany Zone is constrained by radioisotopic dating (49.32 ± 0.30 to 48.66± 0.23 Ma; Smith et al., 2008; 2010), and has the potential to provide important constraints on continental climate during the early Eocene, as Early Eocene-aged terrestrial sections with good age constraints are relatively sparse.

The Mahogany Zone was deposited during the end stages of an interval of peak warming known as the Early Eocene Climatic Optimum (EECO; 53.3 to 49.1 Ma). The EECO was the most intense and prolonged period of climatic warming in the past 66 million years, with global surface temperatures reaching ~10-16°C above pre-industrial levels during peak EECO conditions (Zachos et al., 2001; Inglis et al., 2020). The EECO is also characterised by an intensified hydrological cycle (Carmichael et al., 2017) with evidence for enhanced rainfall in high-latitudes (Inglis et al., 2020). However, the hydrological response within the low to mid-latitude

continental interiors has been only assessed in a few studies (Hyland and Sheldon, 2013; Carmichael et al., 2017). A better understanding of hydrological cycle perturbations during the early Eocene could provide important insights into a range of biogeochemical processes, including soil erosion rates, methane cycling and organic carbon burial (Carmichael et al., 2017 and references therein). These processes could have acted as either positive or negative climate feedbacks, helping to increase or decrease global temperatures, respectively. However, this requires better constraints on the hydrological cycle of these large early Eocene lakes.

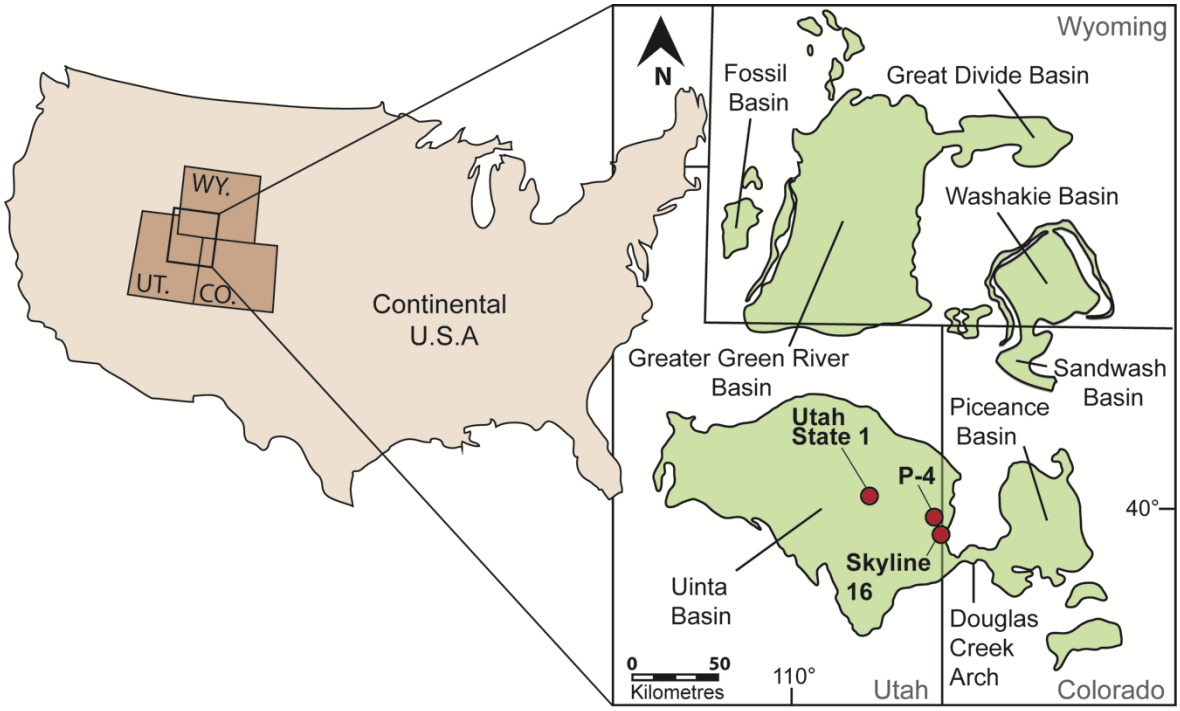

Figure 1: The lateral extent of the Green River Formation spanning north-east Utah, north-west Colorado and southern Wyoming (Grande, 1984). This study focused on the southern Uinta Basin in Utah, through three Mahogany Zone sections varying in proximity to the paleoshore. Utah State 1 is in the basin-centre during the deposition of the Mahogany Zone, whereas P-4 and Skyline 16 represent the basin-margin during this time. Locations of the cores are indicated in red circles.

Here we determine compound-specific hydrogen isotope (δ^2H) values in leaf waxes and algal lipids to reconstruct precipitation changes and interrogate hydrological change over the mid-latitudes during the deposition of this key interval. Leaf waxes

record the δ^2H of the source water from the surrounding vegetative environment, whereas phytane is commonly derived from autotrophic aquatic microorganisms and provides insights into the δ^2H value of lake water (Volkman et al., 1998; Eglinton and Eglinton 2008; Sachse et al., 2004; 2012). We use lipid δ^2H values to infer changes in the δ^2H value of precipitation during the latest EECO (~49.1 Ma) and assess the stability of the hydrological cycle during this event. We also explore the role of the hydrological cycle in the deposition of the organic-rich Mahogany Zone during the termination of the EECO.

4.2 Background and methods

4.2.1 Site description

Continual industry interest in the oil shales of the GRF has resulted in numerous boreholes, particularly in the Uinta Basin. We sampled a centre to margin transect of the profundal zone through three Mahogany Zone sections (Figure 1). The main facies present is continuous parallel- to minorly undulose laminated mudstone with little bioturbation. Drilled by the TOSCO corporation, the Utah State 1 core represents a deeper, basinal zone of the Uinta Basin (reported as longitude/latitude in decimal degrees: 40.010576, -109.511638). The P-4 Chevron White Shale Project core (P-4) was drilled in the eastern section of the Uinta basin, targeting a basin-margin, lacustrine environment (39.931419, -109.134227). Drilled by the Utah Geological Survey, the Skyline 16 core represents a more proximal basin-margin, lacustrine setting and contains a more condensed section of the Mahogany Zone (39.870658, -109.112281).

4.2.2 Age model

The Green River Formation is punctuated by numerous tuff layers from the north eastern Absaroka Volcanic Province. Two dated tuff horizons, named the Wavy and Curly tuffs, are located above and immediately below the Mahogany Zone of the P-4 drill core (Smith et al., 2008) and have been used to develop an age model for the P-4, Skyline 16 and Utah State 1 Mahogany Zone sections. Detailed sedimentological analysis supports a near-linear accumulation rate of 100-200 μm/yr (Smith et al., 2008; Whiteside and Van Keuren, 2009; Walters et al., 2020). The tuffs are dated with $^{40}Ar/^{39}Ar$, measured on single crystal analysis of biotite, to 49.32 ±0.33 Ma (Curly Tuff) and 48.66 ± 0.27 Ma (Wavy Tuff).

4.2.3 Organic geochemistry

Rock plugs through the Mahogany Zone from Utah State 1, P-4 and Skyline 16 (2274-2376 ft, 683- 785 ft and 430-513 ft respectively) were removed with a water-cooled drill press (Delta DP300L), and powdered by agate mortar and pestle. Molecular extraction and fractionation were conducted at the University of Southampton. Total lipid extracts (TLE) were isolated from powdered rock using a Thermo 350 Accelerated Solvent Extractor with the following program: preheat = 5 min; heat = 5 min; static = 5 min; pressure = 1500 psi; flush = 70%, purge = 300 s.; cycles = 3; solvent = dichloromethane:methanol (9:1, *v*/*v*). Solvent extracts were evaporated using a Genevac EZ-2 vacuum centrifuge and subsequently fractionated using silica gel columns. The TLE was eluted with hexane, hexane:dichloromethane (DCM) (4:1, *v*/*v*), and DCM:methanol (MeOH) (1:1, *v*/*v*), yielding the aliphatic, aromatic and polar fractions, respectively. Activated copper was added to each fraction to remove elemental sulphur.

Biomarker identification was performed using a Thermo Trace 1310 gas chromatograph (GC) coupled to a Thermo TSQ8000 triple quadrupole mass spectrometer (MS). The GC used a DB-5 column (30 m ×0.25 mm i.d, 0.25-μm film thickness) with the following oven program: 40°C (held for 2 min), increased at a rate of 6°C/min to 310°C, and then held for 20 minutes. Compound identification of *n*-alkanes and pristane/phytane was made using mass spectra and comparison with an in-house reference oil (North Sea Oil-1).

Compound-specific isotope analysis was conducted using a Thermo Scientific Trace 1310 GC with a DB-5 column (30 m x 0.25 i.d.25- μm film thickness) coupled to a Delta V plus isotope ratio–Mass Spectrometer via a Thermo GC Isolink and Conflo IV. Samples were injected splitless and the GC program was as follows: 40° for 2 minutes then 6°C/minute to 310°C, and then held for 15 minutes. Results are reported in per mil notation (‰), implying a factor of 1000 and were corrected using a mixture of *n*-alkanes, several with known isotopic values (*n*-C_{16} to *n*-C_{30}), the A-7 standard reference material obtained from Arndt Schimmelmann (Schimmelmann et al., 1999). Triplicates of the standards were run before and after the analysis of every five samples and a blank sample of sand (typical standard deviations as follows; Utah State 1: 4.28‰; P-4: 1.25‰; Skyline 16: 4.84‰), with results rejected when the standard deviation for standards ran in triplicate exceeded 5‰. Error bars in Figure 2 represent the standard deviation of the *n*-alkane A-7 mix run in concert with samples, and the H_3^+ factor calculated prior to each sample sequence was consistently below 4 ppm V^{-1}. Hydrogen isotopes are expressed relative to Vienna Standard Mean Ocean Water (VSMOW) with a precision of ±1.5‰ and an average error of 3.27 ‰.

Several methods for characterising the *n*-alkane distribution of a sample have been developed, including the carbon preference index (CPI), average chain length (ACL)

and OEP (odd over even predominance). The carbon preference index (CPI) was calculated through each core location (Marzi et al., 1993) to determine variation in *n*-alkane chain length and sources:

$$\text{CPI}= \frac{(2\times(C_{23}+C_{25}+C_{27}+C_{29}))}{(C_{22}+2\times(C_{24}+C_{26}+C_{28})+C_{30})}$$

ACL represents the weighted averages of carbon chain lengths and can be calculated as (Ficken et al., 2000):

$$\text{ACL}= \frac{((25\times C_{25})+(27\times C_{27})+(29\times C_{29})+(31\times C_{31})+(33\times C_{33}))}{C_{25}+C_{27}+C_{29}+C_{31}+C_{33}}$$

Vascular plants synthesise hydrocarbons with a strong predominance of odd over even numbered *n*-alkanes, so OEP can be used to evaluate terrestrial organic matter input. The formula used here (Scalan and Smith, 1970) to determine OEP is:

$$\text{OEP}= \frac{(C_{27}+(6\times C_{29})+C_{31})}{((4\times C_{28})+(4\times C_{30}))}$$

4.3 Results

4.3.1 Lipid distributions

We found slight site-specific variations in *n*-alkane abundance, with moderate CPI values (<5.0) indicating the presence of relatively immature organic matter input throughout the three sections (Figure 2). In the distal Utah State 1 core, CPI values are low and range from 1.4 and 2.4 and little variation is observed, with slight fluctuation observed towards the base and top of the Mahogany Zone. In comparison, the proximal P-4 core contains higher but more variable CPI values ranging from 0.7– 3.5 with larger variations towards the base and top of the section. The most proximal core, Skyline 16, exhibits the highest CPI values from 1.9– 4.5 with a similar pattern of highest variation towards the base and top. Abundance of δ^2H_{lipids} were too low in the deeper sections of P-4 and Skyline 16, however, the

basin margin cores appear to vary in terrestrial input more than the basin centre core, despite generally having higher CPI values.

Table 1: Depth in feet with odd-over-even carbon number predominance (OEP), average chain length (ACL), carbon preference index (CPI), leaf wax δ^2H and phytane δ^2H values for core Utah State 1 samples.

Depth (ft)	OEP	ACL	CPI	Leaf wax δ^2H	Phytane δ^2H
2272.25	3.48	28.90	2.42	-158.86	-266.94
2275.15	3.06	27.94	1.88	*	-279.25
2279.15	3.86	28.95	2.37	-161.13	-274.62
2280.3	2.56	28.25	1.72	*	-281.65
2283.6	1.87	27.86	1.37	*	-250.76
2284.2	2.94	28.15	2.04	*	*
2290.15	3.39	28.32	2.14	-169.38	-274.86
2292.12	3.09	28.47	2.11	-157.17	-271.51
2296.22	3.51	28.59	2.28	-153.80	-281.41
2301.17	2.83	29.01	2.01	-156.34	-268.47
2302.07	3.11	28.53	1.94	-139.56	-260.36
2304.7	2.61	28.57	1.70	-162.97	-284.25
2308.3	2.52	28.69	1.69	*	-291.45
2311.45	2.64	28.87	1.76	-166.79	-277.75
2314.1	2.47	28.36	1.69	-165.19	-289.57
2316.3	2.37	28.76	1.76	*	-265.28
2317.4	1.96	28.86	1.66	-149.64	-265.58
2318.15	2.35	28.92	1.84	-151.41	-260.90
2319.4	2.51	28.87	1.72	*	*
2322.7	2.33	28.76	1.74	-148.76	-256.54

2327.6	2.59	29.24	1.89	-150.37	-283.00
2330.25	2.80	28.83	1.89	-156.75	-264.58
2333.85	2.69	28.78	1.80	-144.86	-273.10
2335.1	2.28	28.80	1.84	-153.14	-269.69
2337.2	2.99	29.36	2.04	*	*
2338.5	2.57	28.69	1.75	*	*
2341.15	2.95	28.74	1.85	-157.73	-292.42
2344.3	3.08	29.25	2.05	*	*
2348.5	2.75	28.59	1.80	*	*
2351.1	2.70	29.002	1.88	-150.64	-281.19
2357.3	2.52	27.68	1.49	*	*
2359.3	3.00	28.74	1.76	-145.59	-254.77
2362.6	2.51	28.21	1.44	*	*
2365.15	3.22	29.26	1.97	-142.08	-249.74
2368.07	2.59	29.06	1.54	*	-262.38
2371.5	2.80	28.63	1.69	-111.20	-259.37
2374.7	2.31	28.39	1.46	*	-268.12
2377.15	3.27	29.47	2.15	-155.83	-256.20
2378.9	2.68	29.98	1.88	*	-245.78
2380.6	1.53	29.70	1.35	*	*

* Abundance of H isotopes too low for measurement

Table 2: Depth in feet with odd-over-even carbon number predominance (OEP), average chain length (ACL), carbon preference index (CPI), leaf wax δ^2H and phytane δ^2H values for core P-4 samples.

Depth (ft)	**OEP**	**ACL**	**CPI**	**Leaf wax δ^2H**	**Phytane δ^2H**
685.3	2.35	28.40	1.36	*	*

693.45	1.34	27.78	1.30	-96.79	*
696.3	2.56	28.27	1.99	*	*
697.3	5.13	29.03	2.41	*	*
698.95	4.13	28.39	2.26	*	*
699.7	4.68	28.47	2.42	-95.02	-237.87
700.4	4.14	28.84	2.57	*	*
702.1	3.63	29.06	2.46	-101.82	-238.77
704.5	4.12	29.16	2.62	*	*
705.1	5.91	29.67	3.48	*	*
705.9	4.48	28.87	2.52	-103.27	-238.40
706.95	3.87	29.18	2.52	*	*
708.4	3.02	28.42	1.48	*	*
708.7	1.88	**	1.69	-89.91	-240.88
709.8	3.41	29.04	1.92	*	*
711.6	2.19	27.80	1.21	*	-236.47
712.6	4.14	29.00	2.07	*	*
713.9	3.39	28.77	1.71	*	*
714.45	3.37	28.48	1.87	-102.15	-242.26
715.8	3.27	28.55	1.69	*	*
716.7	3.31	28.58	1.73	-109.12	-245.82
718.6	3.66	28.81	1.97	*	*
719.9	4.04	29.02	2.04	-102.37	-237.94
720.5	3.04	28.61	1.58	-110.15	-243.57
722.15	3.94	**	2.49	*	*
722.65	4.91	29.28	2.35	-100.64	-240.80
724.9	3.64	28.31	1.78	*	*
727.2	3.99	29.30	2.42	-107.94	-244.47

728.5	3.08	28.98	1.99	*	*
729.8	4.21	28.62	2.32	*	*
731.85	4.22	28.42	2.05	-143.04	-247.00
733.8	3.28	29.01	2.34	-104.32	-239.77
735.4	5.76	28.99	3.01	*	*
737.7	4.47	29.15	1.98	-89.45	-224.65
738.7	3.81	29.22	2.12	-100.10	-232.91
742.5	3.57	29.16	1.41	-95.84	-225.45
744.4	5.46	28.57	1.25	*	*
745.4	5.30	28.96	2.54	*	*
748.5	3.49	**	2.05	-108.07	-232.87
750.6	4.16	29.24	2.18	*	*
755.1	4.19	29.35	1.50	*	*
757.2	4.83	**	1.92	*	*
760.9	5.24	29.22	1.42	*	*
761.9	3.00	**	1.55	*	*
763.15	0.70	27.25	0.86	*	*
765.1	1.09	**	1.00	*	*
766.4	1.48	27.87	1.16	*	*
769.5	2.99	29.05	1.73	*	*
773.8	5.17	29.80	2.33	*	*
775.6	6.13	29.74	1.60	*	*
776.1	7.41	29.94	2.91	*	*
778.5	1.65	30.81	0.67	*	*
781.7	0.49	26.27	0.84	*	*
784.5	10.60	29.82	3.21	*	*

* Abundance of H isotopes too low for measurement

**Missing ACL index values due to too low abundances of the *n*-C_{35} alkane

Table 3: Depth in feet with odd-over-even carbon number predominance (OEP), average chain length (ACL), carbon preference index (CPI), leaf wax δ^2H and phytane δ^2H values for core Skyline 16 samples.

Depth (ft)	OEP	ACL	CPI	Leaf wax δ^2H	Phytane δ^2H
420	8.74	29.28	4.13	-197.38	*
422.1	9.09	29.55	4.17	*	*
425.2	10.12	29.59	4.30	*	-276.02
429.5	7.14	29.30	3.45	-169.47	-278.80
431.5	7.93	29.05	3.45	-166.34	-265.36
437.9	4.14	28.47	1.85	-208.51	-290.34
444.9	5.34	28.55	2.85	-184.52	-287.90
453.9	8.33	29.22	3.82	-178.59	-295.60
463.9	6.96	29.13	3.34	-174.46	-295.37
468.1	5.82	28.45	2.84	-168.23	-295.52
472.1	5.29	28.64	2.52	-164.06	-292.93
477.9	7.78	29.29	3.52	-157.56	-292.34
485.8	5.43	29.28	2.89	*	*
493.7	6.32	28.65	2.52	*	*
496.3	7.61	29.65	3.17	*	*
503.8	7.88	29.33	3.17	*	*
508.1	8.76	29.77	3.22	*	*
510.6	5.99	29.44	2.32	*	*
515.7	10.43	30.16	4.48	*	*

* Abundance of H isotopes too low for measurement.

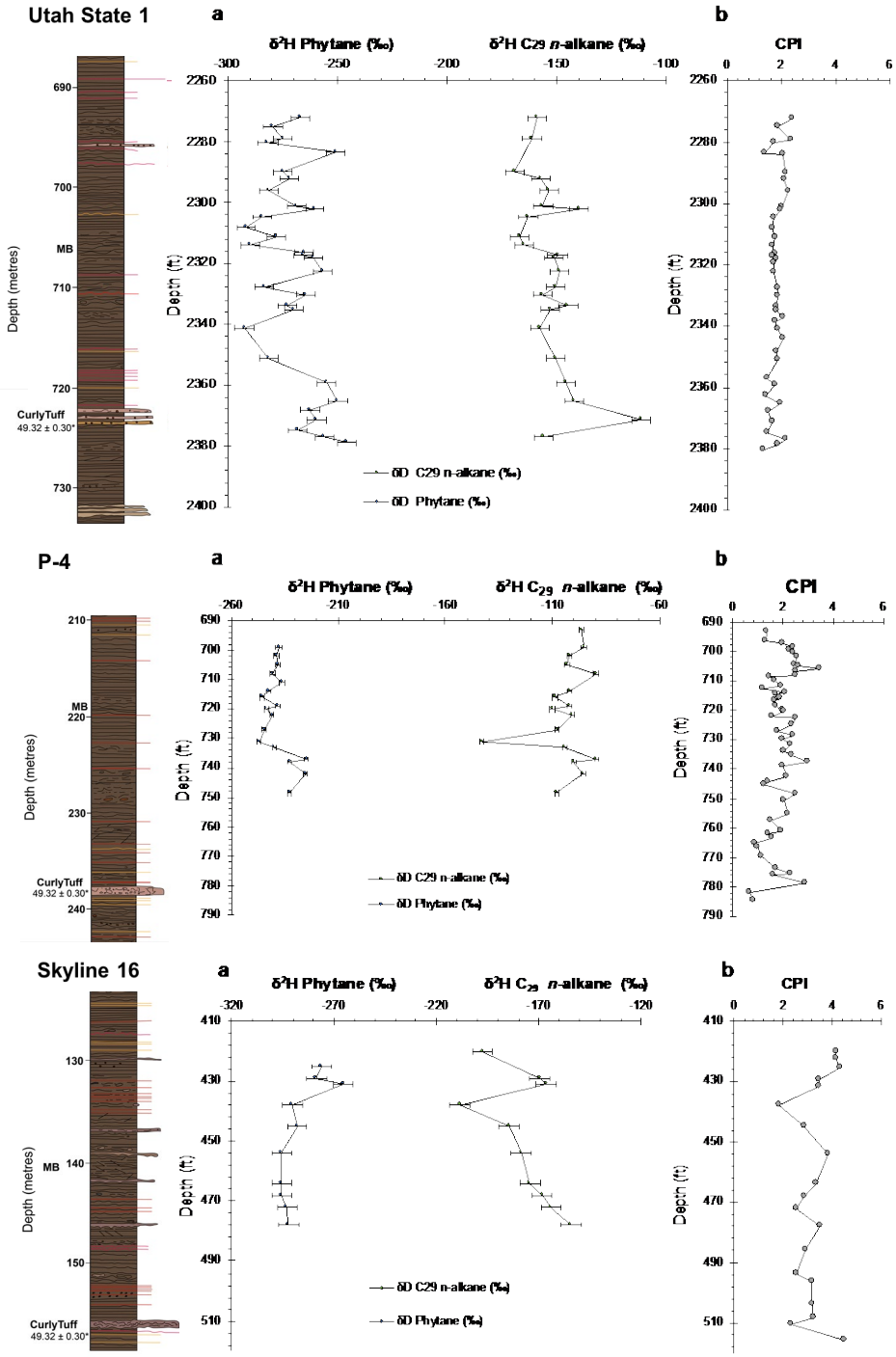

Figure 2: (Top) Utah State 1 core results: Stratigraphic column through the Mahogany Zone, Utah State 1 (a) Left: δ^2H of phytane values. Right: δ^2H of C_{29} *n*-alkane through the basin centre. (b) CPI measurements with higher values indicating an increased input of vascular plant material (calculated from Marzi, 1993.) (Middle) P-4 core results: Stratigraphic column through the Mahogany Zone, P-4 (a) Left: δ^2H of phytane and C_{29} *n*-alkane. Right: δ^2H through the basin margin. (b) CPI measurements. (Bottom) Skyline 16 core results: Stratigraphic column through the Mahogany Zone, Skyline 16 (a) Left: δ^2H of phytane. Right: δ^2H of C_{29} *n*-alkane through the basin margin. (b) CPI measurements. MB= Mahogany Bed Marker. (*Smith et al., 2008). Error bars represent 1σ uncertainties.

In the lake centre setting of Utah State 1, OEP values range between 1.5– 3.9, varying more in the lower and upper section of the Mahogany Zone. The OEP ratio in the lake margin setting of P-4 varies from 0.5 to 10.6, displaying a high amount of variation of *n*-alkanes at the top and towards the base. OEP values in Skyline 16 fluctuate from 4.1 up to 10.2, with higher values observed towards the upper and the lower portions of the Mahogany Zone. Utah State 1 samples generally have lower OEP values than those in the P-4 and Skyline 16 cores indicating less leaf wax material (tables 1–3).

In the basinal Utah State 1 core, ACL is characterised by very similar values through the section (27.7 to 30.0), with stronger variation in values towards the base and top of the section. ACL values in P-4 range from 26.3– 30.8, with more variation observed in the deepest samples (781.7– 763.15 ft). In Skyline 16, ACL values vary from 28.5 to 30.2, showing minor variability with values slightly higher than Utah State 1 and P-4 (tables 1-3).

The hydrocarbon fraction also contained a range of C_{29}–C_{35} hopanes that occur as αβ- and βα- isomers. Due to the low abundance of ββ- isomers, the degree of hopanoid isomerisation was assessed using the C_{31} hopane 22S/(22S + 22R) index. In the Utah State 1 core, values range from 0.1– 0.7, whereas in the P-4 core, values range from 0.1– 0.2. C_{31} hopane 22S/(22S + 22R) values for Skyline 16 are very low and range from 0– 0.1.

4.3.2 Compound-specific hydrogen isotope values

4.3.2.1 Utah State 1

δ^2H values of the C_{29} long chain *n*-alkane range from -111.2 to -169.4‰ (Figure 2). The highest δ^2H value (-111.2‰) is found at 2371.5 ft (correlating to the Curly Tuff bed, an ash layer deposited in a tuffaceous debris flow; Smith et al., 2008) and the

lowest δ^2H value (-169.4‰) is found at 2290.15 ft. Low δ^2H values at 2314.1 and 2311.45 ft (-165.2 and -166.8 ‰ respectively) represent beds that are rich in organic matter, including the Mahogany Bed at 2314 ft.

δ^2H values of phytane are very low, ranging from -245.7 to -292.4‰, with the highest δ^2H values observed at the base of the section. δ^2H phytane values in the Mahogany Zone become progressively lower upwards through the section. Values are more variable in comparison to C_{29} *n*-alkane δ^2H values. Extremely low values are observed at 2314.1 and 2308.3 ft (-289.6 and -291.4‰ respectively) and coincides with low δ^2H C_{29} *n*-alkane values.

4.3.2.2 P-4

C_{29} *n*-alkane δ^2H values from the more proximal P-4 core range from -89.4 to -143.0‰, which are higher than values in Utah State 1 and Skyline 16. Less variability is observed in this proximal core (typically ±10‰) and no clear trend is observed upwards through the section. The most negative δ^2H value is seen at 731 ft (-143.0‰) and the second lowest recorded is -110.1‰, immediately below the deposition of the Mahogany Bed.

In the proximal P-4 core, $\delta^2H_{phytane}$ values are very low and vary from -247.0 to -224.6‰. Larger amounts of variation are seen in this section compared to the P-4 C_{29} *n*-alkane δ^2H profile, however they are similar to the variation in isotopic values seen in the basin centre Utah State 1 δ^2H phytane section. We observe an upwards trend of increasingly negative δ^2H values in the middle and upper sections with more positive δ^2H values towards the base (748.5– 738.0 ft).

4.3.2.3 Skyline 16

δ^2H values in the Skyline 16 core for C_{29} *n*-alkane vary from -164.1 to -208.5‰ (472.1 ft and 437.9 ft respectively). Upwards through the Mahogany Zone, δ^2H

values become increasingly lighter aside from an isotopically heavy set of data points, which are also observed in Skyline 16 phytane δ^2H data (429 ft and 431 ft). Despite these isotopically heavier δ^2H points, the data suggest an upwards trend in lighter δ^2H values through the Mahogany Zone samples in Skyline 16.

Basin margin δ^2H phytane values in the Skyline 16 core vary from -295.6 to -265.4‰. Much of the section, however, shows much more limited variation. For example, within the upper Mahogany zone there is only a 2‰ difference over the sampled interval. In the more sparsely sampled upper core, basin margin values become more positive and variable than in the rest of the section.

4.4 Discussion

4.4.1 Controls on phytane δ^2H values within the Uinta Basin

4.4.1.1 Non-algal sources

The hydrogen isotopic value of phytane is affected by multiple controls, including but not limited to: variations in environmental water sources, changes in phytane source, and contributions of snow melt, which need to be properly considered when interpreting the isotopic record. Phytane is mostly derived from the phytl side chain of chlorophyll-*a* and averages the input from the whole phytoplankton community (Witkowski et al., 2018). However, phytane can have multiple sources (e.g. methanogens and halophiles; ten Haven et al., 1987), which may influence phytane δ^2H values. We argue that inputs from methanogens and halophiles are relatively minor, due to the extreme productivity of the lake autotrophs within the photic zone and evidence for predominantly microbial organic matter found in petrographical studies (Elson et al., 2021). These lake autotrophs would have likely vastly outweighed the potential input from these alternate sources.

4.4.1.2 Changes in water source

Early Paleogene topography reconstructed for the Uinta Mountains reached at least 3000 metres high with a basin floor paleoelevation of, at most, 1000 metres high (Sewall and Sloan, 2006; Gao and Fan, 2018) and may have supplied snowmelt to the surrounding lake basins potentially affecting surface water δ^2H values (Norris et al., 1996). The input of highly depleted deuterium snowmelt into the lake basin may affect growth water δ^2H values. However, proxy estimates from the basin have placed mean annual air temperature (MAAT; Wing, 1998) and warm month mean temperature (WMMT) estimates at ~16°C and ~40°C (Snell et al., 2013), respectively. Combined with floral and faunal studies, this suggests that temperatures would rarely drop below zero (Wing, 1998). Well- preserved palm trees (e.g. *Phoenix windmillis;* Snell et al., 2013), have also been found through the Green River Formation, indicating CMMT > 5°C and MAT > 10°C around the basins. This suggests it is unlikely that temperatures were low enough for sustained input of isotopically light snowmelt into the Uinta Basin locally.

4.4.2 Controls on leaf wax δ^2H values within the Uinta Basin

The hydrogen isotopic composition (δ^2H) of leaf wax biomarkers (δ^2H_{wax}) primarily reflects plant source water and – by extension – the hydrogen isotopic composition of precipitation ($\delta^2H_{precipitation;}$ Sachse et al., 2012). However, a fractionation factor ($\varepsilon_{precipitation}$) is required to estimate $\delta^2H_{precipitation}$. Here we employ a net fractionation factor of 110 ± 20 ‰ as this captures the variability in modern C_3 gymnosperms and angiosperms (Sachse et al., 2012; Pedentchouk et al., 2008), which results in $\delta^2H_{precipitation}$ values of -43‰ (Utah State 1), +7‰ (P-4) and -67‰ (Skyline 16). These values are isotopically heavy in ^2H (-53‰, -103‰ and -23‰ respectively, relative to modern values of -96‰, -99‰ and -100‰; Bowen and Revenaugh, 2003), which

may be the result of several factors. Warmer source waters will yield more ^{2}H-enriched water vapour and additionally, under warmer climates, decreased rainout at the low-latitudes result in high $\delta^{2}H$ precipitation at the mid-to-high latitudes. However, there are large (~75‰) inter-site variations that suggest additional controls on $\delta^{2}H_{precipitation}$ values (see below).

4.4.2.1 Diagenesis

Hydrogen exchange processes can alter $\delta^{2}H_{lipid}$ values slowly over time and overprint the original environmental signature (Sessions et al., 2004). The most common way to assess hydrogen exchange is to compare long-chain *n*-alkane and isoprenoid (e.g. phytane) $\delta^{2}H$ values (Pedentchouk et al., 2006). In immature sediment samples, isoprenoids (e.g. phytol) are ^{2}H-poor (ca. -150 to -200‰) relative to long-chain *n*-alkanes. However, with increasing maturation, the offset between isoprenoids and long-chain *n*-alkanes diminishes to zero. In the Uinta Basin, the offset between isoprenoids (phytane) and *n*-alkanes is consistent and large (~100 to 140‰; Figure 3), suggesting minimal hydrogen exchange. The Green River Formation is also known for the thermal immaturity of its vast oil shale resources (Birgenheier and Vanden Berg, 2011). Relatively low thermal maturity is supported by high OEP (4.1 to 10.4) and lower CPI values (<5) recorded through the Mahogany Zone. Overall, this suggests that the impact of diagenesis on $\delta^{2}H$ values is minimal. Higher CPI values may indicate that $\delta^{2}H$ data has been influenced by hydrogen exchange, however there is no systematic relationship with measured *n*-alkane $\delta^{2}H$ and CPI, suggesting no evidence for post-depositional alteration of the $\delta^{2}H$ values.

Low C_{31} hopane 22S/(22S + 22R) values (< 0.1) are characteristic of relatively low thermal maturity, whereas high values (~0.5) suggest high thermal maturation (Mackenzie et al., 1980). Low and stable C_{31} hopane 22S/(22S + 22R) indices are

observed at Skyline 16 (average: 0.06, n = 18, σ = 0.04; see appendix D) and P-4 (average: 0.08, n = 31, σ = 0.06), indicating low thermal maturity. Although higher values are observed at Utah State 1 (average: 0.20, n = 40, σ = 0.17), the presence of long-chain *n*-alkanes with an odd-over-predominance (1.3– 4.5) and high *n*-C_{17}/pristane and *n*-C_{18}/phytane values (>1; see chapter 3) suggest relatively low overall thermal maturation.

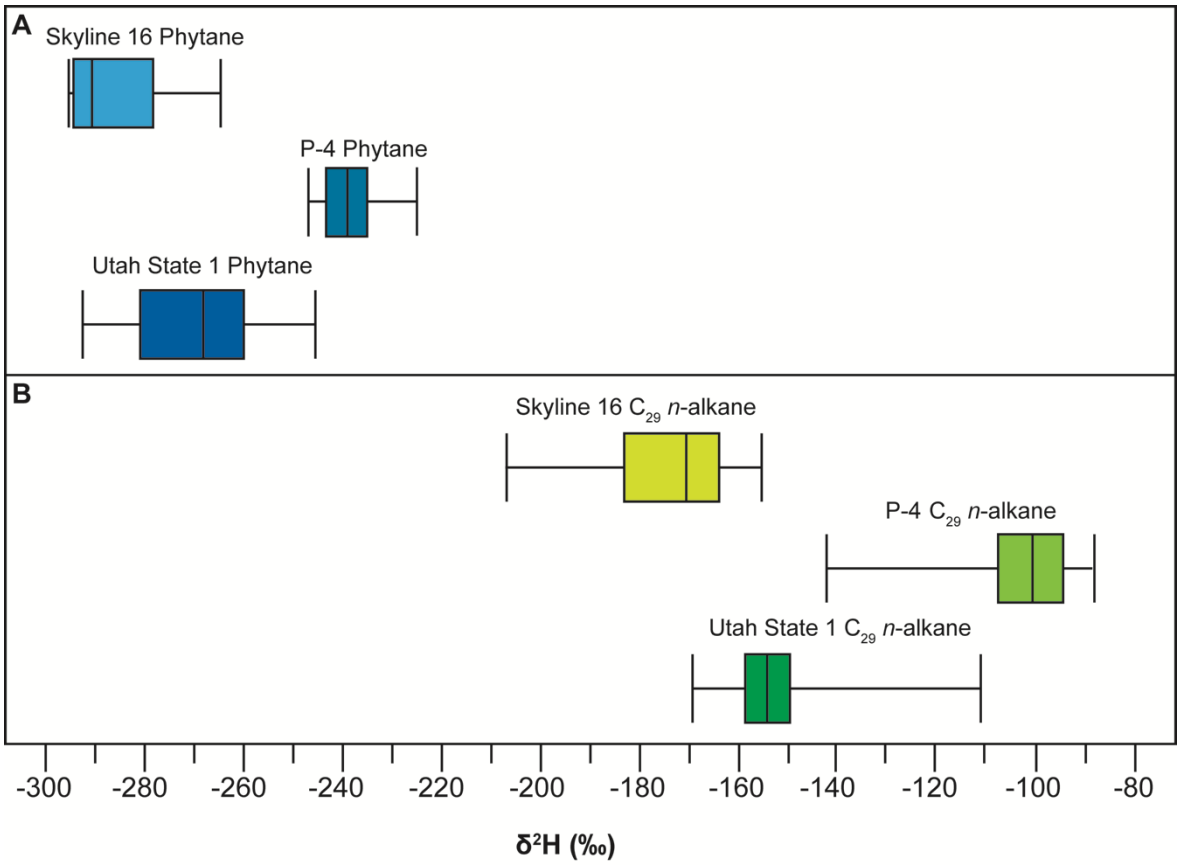

Figure 3: Hydrogen isotope distributions of (A) phytane and (B) *n*-alkanes generated from three different sites in the Uinta Basin. Phytane δ^2H values are consistently ^2H-depleted relative to long-chain *n*-alkanes, primarily due to the different biosynthetic pathways. Large inter-site variations in phytane and *n*-alkanes are the result of strong δ^2H controls via local processes. Whiskers represent highest and lowest values, and the box indicates the position of the upper quartile, mean and lower quartile for each set of results.

4.4.2.2 Plant type

Changes in the plant community can influence the apparent fractionation between δ^2H_{wax} and $\delta^2H_{precipitation}$ values (ε_{precip}). In modern C3 plants, $\varepsilon_{precipitation}$ values range

between ca. -80 to -150‰ (Sachse et al., 2012 and references therein). However, accounting for changes in plant community in ancient settings is challenging (Feakins, 2013). Recent work has used the pollen assemblage to calculate plant-specific fractionation factors (e.g. Feakins 2013; Inglis et al., 2020). However, this was not possible here because of the very high content of amorphous organic matter (AOM) in the samples. By volume this comprises the bulk of the samples so that any attempt to dissolve the sample in hydrochloric acid (HCl) or hydrofluoric acid (HF) is near impossible. The AOM both shields the mineral content which is also not sufficiently abundant that removing it disaggregates the sample to release the palynomorphs. An attempt was made to disaggregate the AOM with a tunable ultrasonic probe after the HF treatment but this had little effect. Alternatively, a shift in the average chain length (ACL) could potentially reveal a change in the higher plant community, as shown during the PETM (e.g. Schouten et al., 2007). Although modern plant surveys cast doubt as to whether the ACL can discriminate between key plant types (with the exception of mosses; Bush and McInerney, 2013), invariant ACL values in the Uinta Basin sediments imply no significant change in vegetation during the EECO.

4.4.2.3 Changes in source water δ^2H

In modern sediments, leaf wax δ^2H values are correlated with source water δ^2H (i.e., precipitation). However, evaporative ^2H-enrichment of soil and/or leaf water can modify leaf δ^2H to more positive values, especially in (semi-)arid settings (Kahmen et al., 2012) (Figure 4). The isotopic difference between terrestrial and aquatic biomarkers has previously been used to constrain soil and/or leaf water evaporative enrichment ($\varepsilon_{terr\text{-}aq}$ following Rach et al., 2017) and is typically calculated using long-chain *n*-alkanes (C_{29}–$C_{33;}$ i.e. higher plants) and mid-chain *n*-alkanes (C_{21}–C_{25}; i.e. submerged macrophytes). However, other algal biomarkers can be used for the later

(Rach et al., 2017). Here we use long-chain *n*-alkanes (C_{29}–C_{33}) and phytane (a general phytoplankton biomarker derived mainly from chlorophyll-*a*) to constrain soil and/or leaf water evaporation and the input of more positive δ^2H values in the Uinta Basin.

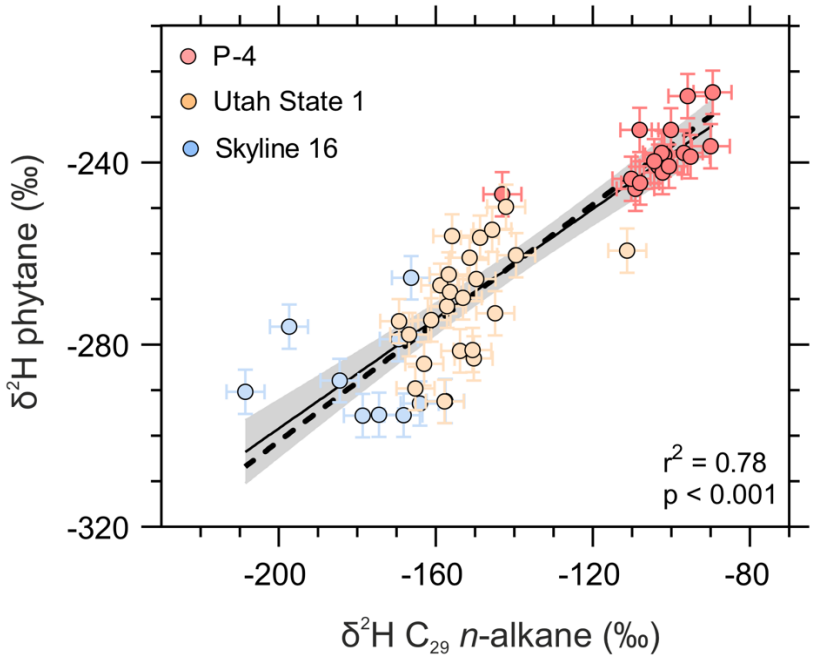

Figure 4: Co-variation of phytane- and C_{29} *n*-alkane δ^2H values within early Eocene Uinta Basin sediments together with a Deming regression (dashed line) and simple linear regression (solid line). Also shown are the 95% confidence interval for the simple linear regression.

We find that phytane δ^2H values are consistently more negative relative to long-chain *n*-alkanes. This yields low $\varepsilon_{terr\text{-}aq}$ values (ca. -100 to -140‰) across all three sites. This large offset is primarily due to the different biosynthetic pathways; leaf wax lipids are produced via the acetogenic pathway (relatively high ^2H) whereas phytol (and by extension, phytane) is produced via the DOXP/MEP pathway (relatively light in ^2H) (Rontani and Volkman, 2003). The significant positive linear relationship between δ^2H_{terr} and δ^2H_{aq} (r^2 = 0.78; $p < 0.001$) suggests minimal evaporative ^2H-enrichment of soil and/or leaf water within the Uinta Basin (Figure 4). It also implies that leaf wax δ^2H values reflect lake water δ^2H values, rather than

precipitation δ^2H values. This has been observed in modern evaporative lake systems (Garcin et al., 2012) and is consistent with evidence for evaporative conditions in the Eocene-aged Uinta Basin (Vanden Berg and Birgenheier, 2017). It is likely that the salinity of the Uinta Basin was also highly variable and explains the wide variability in leaf wax and phytane δ^2H within the basin (Vanden Berg and Birgenheier, 2017).

The δ^2H signature of the lake surface water incorporated in the lipids of photosynthetic algae would have been particularly sensitive to water balance changes in the basin, either through precipitation/evaporation or the addition of isotopically distinct water from other sources. Previous work in the Uinta Basin has identified three hypersaline zones within the upper GRF (Vanden Berg and Birgenheier, 2017). The first of these hypersaline phases coincides with deposition of the Mahogany Zone and is restricted to the eastern side of the basin, where the depocentre of the lake was located. Drivers of hypersalinity have been attributed to the input of Lake Gosiute water and associated high-density brines from the Greater Green River Basin to the north, which was far more evaporitic in nature and was undergoing north-south infilling (Smith et al., 2008). Water delivered from the shallower, evaporitic basin would have been isotopically heavier relative to $\delta^2H_{precipitation}$ and transported to Lake Uinta, where it would be incorporated in the source water of autotrophs in the water column during episodic intervals related to the closure of Lake Gosiute (Figure 5). Further to the south-east and shallower than the other locations, Skyline 16 may have received less input from this source of high δ^2H water in comparison to Utah State 1 or P-4. The avulsion of river channels and adjustment of regional fluvial systems to a decreasingly energetic hydrological regime may have also resulted in different water sources being delivered to P-4 and Skyline 16, despite their relative proximity (Gall et al., 2017; Birgenheier et al., 2019).

The response of $\delta^2H_{phytane}$ to basinal changes reveal a competing signal of original source water δ^2H and post-rainout alterations related to basin-closure to the north and contemporaneous input of ^2H-rich, saline water.

4.4.3 Orogenic effects

Intercontinental basins are particularly sensitive to tectonic controls that can have numerous consequences for basin accommodation, sediment supply and lake stratification (Carroll and Bohacs, 1999). Changes in tectonic upheaval may cause increased airmass rainout, resulting in an 'amount effect' response of the mid-latitude hydroclimate delivering ^2H-light precipitation to the basin (Dansgaard, 1964; Sachse et al., 2012).

During deposition of the GRF, steady subsidence of the Uinta Basin increased accommodation space, while the sediment supply fluctuated, often paced by the Eocene hyperthermals (Gall et al., 2017). At the time of deposition of the Mahogany Zone, this long-term tectonic subsidence continued as a result of flexure from Laramide related uplifts, including the Uinta Mountains towards the north and the Uncompaghre Uplift and San Rafael Swell towards the south. Paleocurrent data suggests the Douglas Creek Arch, a key structural high controlling connectivity between the Uinta and Piceance Creek basins, was uplifted during the Sunnyside Delta interval of the middle GRF and prior to Mahogany Zone deposition (Birgenheier et al, 2019). In addition to the relatively short time span studied and the presence of several topographic highs surrounding the Uinta Basin, it is unlikely that changes in tectonic upheaval, resulting in a potential amount effect (Dansgaard, 1964) was a driver for the minor upwards depletion of δ^2H observed in this section.

4.4.4 Early Eocene GCM comparisons

Comparisons of general circulation models (GCM) and geological proxy data is increasingly being utilised to understand hydrological change during the early Eocene climate. Recent studies have attempted to simulate the amount of precipitation in the western US during the early Cenozoic, with varying boundary conditions (e.g. 6x pre-industrial CO_2, high or low orbital forcing) (Carmichael et al., 2016; Kiehl et al., 2018).

Carmichael et al., (2016) compare GCM-derived precipitation from the extended EoMIP ensemble (Eocene Modelling Intercomparison Project; Lunt et al., 2012) under a range of CO_2 simulations. Elevated CO_2 is simulated to cause a near- global increase in modelled palaeo-temperature, but the warming in regions is accompanied by variable precipitation patterns, with increases and decreases in precipitation reported in climate models. In the western US, mean annual precipitation (MAP) change in response to increasing CO_2 is varied amongst models. Precipitation is stable with up to 6x CO_2 relative to pre-industrial (~900–1200 mm/yr MAP) in HadCM3L whereas increased precipitation (~900–2900 mm/yr MAP) is produced in CCSM3 with higher CO_2 simulations of 4x CO_2, 8x CO_2, 16x CO_2 (Lunt et al., 2010; Liu et al., 2009; Huber and Caballero, 2011; Carmichael et al., 2016). This range in precipitation change for increasing CO_2 highlights the importance of efforts to link proxy records with modelling outputs, as the impact of the Mahogany Zone as an organic carbon sink, along with other organic-rich events (e.g. Azolla event; Brinkhuis et al., 2006), will vary under different CO_2 conditions.

Changes in orbital parameters investigated in Kiehl et al., (2018) reveal a decrease in precipitation in the North American continental interior with the addition of maximum orbital forcing parameters and maximum insolation in Northern Hemisphere summers. This has been attributed to a weakening of moisture

transport from the Pacific resulting in enhanced seasonality of the regional water hydroclimate and a drier North America. Hyperthermal events identified in the Greater Green River Basin of Wyoming are agued to occur at eccentricity minima (Smith et al., 2014), which may have hosted wetter conditions in the region according to GCM simulations (Kiehl et al., 2018). This is supported by recent work in the Uinta Basin where hyperthermals are identified as ephemeral deposits in the Sunnyside Delta interval of the GRF, during intervals of enhanced precipitation (Gall et al., 2017; Birgenheier et al., 2019).

4.4.5 Stable hydrological cycle promoted OC burial during the EECO

For the US continental interior, our leaf wax and phytane δ^2H data indicate only gradual changes in source water δ^2H in the Uinta Basin during deposition of the Mahogany Zone. This could indicate a stable hydrological cycle during the termination of the EECO, which differs from the more variable and dynamic hydrologic response observed during transient climatic events in the region, i.e., the PETM and EECO hyperthermals (Hyland et al, 2018).

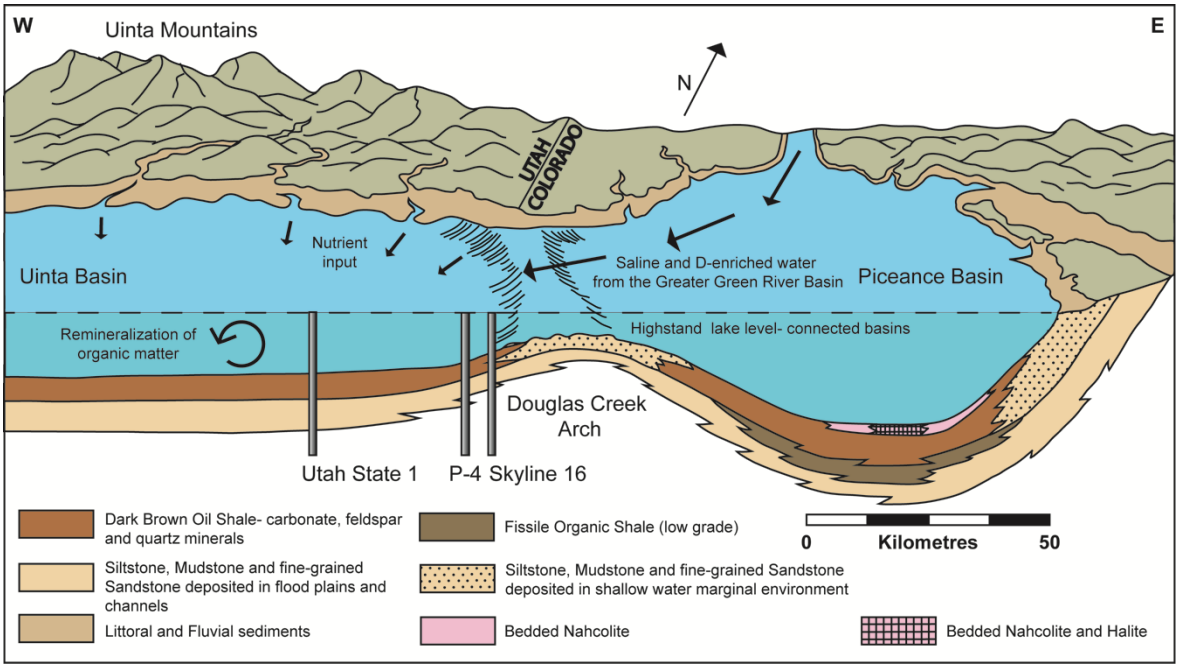

Figure 5: The Uinta and Piceance basins connected by Lake Uinta at highstand, with locations of the basinal Utah State 1, proximally-located P-4 and the shallowest core,

Skyline 16. Saline-rich and isotopically enriched water originating in the Greater Green River Basin (Figure 1) was transported into the connected Piceance Basin and over the submerged Douglas Creek Arch, into the Uinta Basin, spatially affecting source water for the algal lipids in the paleolake Uinta (Adapted from Dyni, 1987).

Increasingly negative δ^2H values for the C_{29} *n*-alkane and phytane in the basin-centre Utah State 1 core may be the result of increased precipitation locally, as the hydrological cycle readjusts from the transient warming events in the early Eocene to the prolonged peak warmth of the EECO and subsequent cooling into the mid Eocene (Hyland et al., 2017; Gall et al., 2017). An increased perennial rainout upwards through the section may have driven enhanced productivity in the lake basin, as the high and episodic sediment supply (and associated clouding of the water column) waned from an ephemeral hydrologic system during the Eocene hyperthermals (Gall et al., 2017; Birgenheier et al., 2019), towards a limited sediment supply, lower energy highstand lake.

A stable hydrological cycle is also reflected in the low siliciclastic input observed through the interval, with reduced seasonality and perennial fluvial discharge providing a steady nutrient supply during the post-hyperthermal EECO (Birgenheier et al., 2019). Reduced siliciclastic input during the post-hyperthermal EECO would have also limited dilution from inorganic (clastic) sediments and thus promoted rich organic matter accumulation within the lake. In contrast, the Eocene hyperthermals are associated with high seasonality and ephemeral fluvial discharge, leading to large siliciclastic inputs (Gall et al., 2017; Birgenheier et al., 2019). The hyperthermal phase also lacks evidence for OC-rich deposits (Birgenheier et al., 2019). Collectively, this suggests that during the termination of the EECO, the development of a stable hydrological cycle may have been critical to the development of the OC-rich (>35%) Mahogany Zone (~48-49 Ma). The gradual change in δ^2H of the aquatic and terrestrial compounds also indicates that stability following an episodic

hydrological cycle during the earlier Eocene hyperthermals was a driver for the development of the Mahogany Zone. These large highly productive saline lakes possibly acted as carbon sinks, providing a negative climate feedback mechanism during intervals between hyperthermals (Birgenheier et al., 2019).

Intriguingly, the deposition of the Mahogany Zone is coincident with the onset of long-term Eocene cooling (~48-49 Ma; Inglis et al., 2015; Smith et al., 2010; Gall et al., 2017). Large amounts of organic carbon would have been sequestered in Lake Uinta (~76 Gt; Elson et al., 2021), similar to the OC-rich (>5%) deposition observed in deposits from the same time period in the High Arctic (Brinkhuis et al., 2006) and Nordic Seas (Brinkhuis et al., 2006; Barke et al., 2012). This suggests a link between carbon cycling and global climate evolution. Unlike the Uinta Basin, the high Arctic is characterised by low salinity conditions. However, both are strongly stratified, largely anoxic basins (Brinkhuis et al., 2006; Vanden Berg and Birgenheier, 2017) characterised by limited siliciclastic input (Birgenheier et al., 2019). Both suggest a stable hydrological cycle during the EECO and imply a causal relationship between the hydrological cycle, organic matter burial and carbon cycling during the early Eocene.

4.5 Conclusions

Leaf wax and algal lipid δ^2H analysis reveal that a stable hydrological regime existed in the mid-latitude continental interior during the latest EECO (~49.1 Ma). Leaf wax and algal lipid δ^2H exhibit a linear relationship indicating they capture the original source water δ^2H signal. However, large inter-site variation implies that the δ^2H values of source waters varied locally, which may have arisen from the input of ^2H-rich, saline water from Lake Gosiute. Consequently, we urge caution in the use of

long-chain *n*-alkanes as a proxy for poleward moisture transport without proper consideration effects arising from multiple local water sources.

Unlike the more variable hydrological regime of the early Eocene hyperthermals, the limited variations in δ^2H values from base to top of the Mahogany Zone suggests a relatively stable hydrological cycle during the latest EECO. We interpret this to indicate that the hydrologic cycle responds differently during rapid vs. gradual climatic perturbations. A stable hydrological regime appears to provide conditions that promote organic matter productivity and preservation within large lacustrine systems and may serve as an important negative climatic feedback during intervals of sustained global warmth.

Acknowledgements

This contribution represents a portion of A. Elson's doctoral dissertation at the University of Southampton, funded by the Natural Environment Research Council Centre for Doctoral Training in Oil & Gas. Oliver Bench assisted with field work and sample collection and P. Sargent Bray is acknowledged for help with organic geochemistry. Discussions with Mike Vanden Berg contributed to the development of this manuscript. Funding was provided by CASP and the NSF for fieldwork and workshop attendance for A. Elson, and the Donors to the Petroleum Research Fund of the American Chemical Society to J. H. Whiteside. G.N.I was funded by a GCRF Royal Society Dorothy Hodgkin Fellowship (DHF\R1\191178).

Chapter 5 Conclusions

The aims of this dissertation were to determine three aspects of paleo-reconstructions of the hydrological cycle during the EECO: the role of large, extremely organic-rich lakes in regulating greenhouse climate; competing drivers of the development, peak and waning of large organic carbon depositional systems; and multiple co-located sites for a single event. Specifically, this thesis has three main objectives:

1) An evaluation of the sedimentary character and organic petrography of extremely rich lacustrine strata to reconstruct the controls on vertical- and micro-scale variation in terrestrial organic carbon (Chapter 2).
2) The recovery of lipid biomarkers from multiple terrestrial sites to constrain productivity controls and burial indications during accumulation of a section exhibiting highly variable organic content (Chapter 3).
3) The recovery of compound-specific hydrogen isotopes from multiple terrestrial sites in the mid-to-low latitudes to constrain the hydroclimate regime operative during the terminal phase of the EECO (Chapter 4).

5.1 Micro-scale heterogeneity of organic matter distribution and type

In Chapter 2, I detailed the highly heterogeneous lacustrine deposits in the prolifically organic-rich Mahogany Zone to assess the vertical- and micro-scale variation in sources of organic matter. I integrated organic petrography and geochemistry with sedimentary observations to show wide variation in organic matter types and distribution in these Eocene lakes. I observed that amorphous organic matter derived from microbial blooms is the dominant form of organic matter throughout the Mahogany Zone. Longer term sub-orbital cycle controls on the accumulation of organic matter occurs at a lamination scale, suggesting decadal periodicities in organic-matter fluxes and associated carbon drawdown. Intervals with high proportions of terrestrially derived organic matter correspond to less TOC-rich intervals (Chapter 1; $\mathbf{H_1}$). The decadal pacing of conditions favourable to high algal productivity and prolific-TOC deposition in a Cenozoic warm world is an

important consideration for carbon burial by large lakes in carbon cycle models for the past, present and future.

5.2 5.2 Salinity controls on primary productivity

In Chapter 3, I generated biomarker records from three drill cores to evaluate intra-basinal variability in molecular fossils extracted from the Mahogany Zone and the response to regional drainage changes and exposure to a prolonged hothouse climate and subsequent extreme biotic stress in a lacustrine basin. My lipid biomarker records reconstructed palaeo-lake salinity conditions that were previously limited to the upper hypersaline phases of the Lake Uinta, confounding earlier attempts to fully understand how basin changes drove variation in organic carbon drawdown.

I demonstrated that variability in salinity stratification and hypersalinity in the lake basin was a key stressor of ecological conditions in the Mahogany Zone and the result of water balance-driven variations of brine input transported from the connected northern Green River Formation basins into Lake Uinta. (**H_2**). The resulting increased ecological stress on biota living in the water column, coupled with the increased supply of clastic material, may have been an important driver leading to the cessation of conditions favouring prodigious organic accumulation in the Mahogany Zone.

5.3 Reconstruction of the mid-latitude terrestrial hydroclimate

In Chapter 4, I generated compound specific hydrogen isotopic records (δ^2H) of leaf waxes (*n*-alkanes) for precipitation δ^2H reconstruction and algal (phytane) lipids to provide insight into lake water δ^2H values in the photic zone. Algal lipid and leaf wax δ^2H values exhibited a strong linear relationship ($R^2 = 0.8$), indicating that algae and higher plants are utilising the same hydrogen sources for biosynthesis (**H_3**). Local processes, such as locally variable water sources and precipitation/evaporation cycles, influenced isotopic values resulting in inter-site variation of algal and leaf wax δ^2H (~50 to 75‰), however Chapter 4 also demonstrated relatively invariant hydrogen isotopic records throughout the deposition of the Mahogany Zone, suggesting a uniform hydrological regime during the EECO. Chapter 4 demonstrated that the hydrological cycle operated differently during gradual vs.

transient warming events, and that a stable hydrological regime promoted organic matter preservation within these large lake systems. The results from Chapter 4 suggest that these organic-rich, long-lived large lakes acted as an important negative feedback mechanism by providing a ~76.06 Gt carbon sink during the post-hyperthermal EECO.

The isotopic investigations from algal lipids and leaf waxes addressed the response of the mid-latitude, North American continental interior hydrological cycle during the declining limb and termination of the Early Eocene Climatic Optimum. My records provide a time series of changing microbial communities and their biomarker signatures, complementing a wealth of scientific enquiry into the prolifically organic-rich Green River Formation.

5.4 5.4 Future work

Recent advances in the use of phytane as a pCO_2 tracer in the ancient marine realm might prove useful for continental sections. This proxy is predicated on the stable carbon isotopic fractionation associated with photosynthesis (Ɛp) in phytane increasing as pCO_2 increases (Witkowski et al., 2018). This proxy has been employed in marine sediments as the environment is likely homogenous and stable, avoiding potential decoupling that may occur in local carbon cycles of terrestrial and lacustrine settings (identified and discussed in Chapter 3). The Mahogany Zone of the Uinta Basin may be an ideal location to adopt a terrestrial-derived phytane-derived Ɛp study, due to the immaturity of the organic material, the high amounts of phytane and the tightly constrained geochemical and sedimentological nature of the succession. This would provide a novel insight to the atmospheric concentration of carbon dioxide recorded in the continental interior and may support future studies on terrestrial records that are not as prolifically TOC-rich as the Mahogany Zone.

Furthermore, carbon isotopes of highly-depleted hopanoids in the Green River Formation may provide insight into the methane cycling of large organic-rich lakes in hothouse worlds supporting understanding of the dual carbon source/sink nature that can exist in lacustrine basins.

While this investigation benefited from access to multiple cores across the Uinta Basin, the most distal basin to the locus of salinity (Chapter 3), questions remain

about the control of local processes on hydrogen isotopes. Future studies should, therefore, attempt to recover compound specific hydrogen isotopes across the various basins of the Green River Formation to understand and map the strong local processes of evaporation-driven salinity on hydrogen isotopes, and the usefulness of hydrogen isotopes as a palaeo-salinity indicator in terrestrial basins.

Appendix A Utah State 1 Core Log- Mahogany Zone

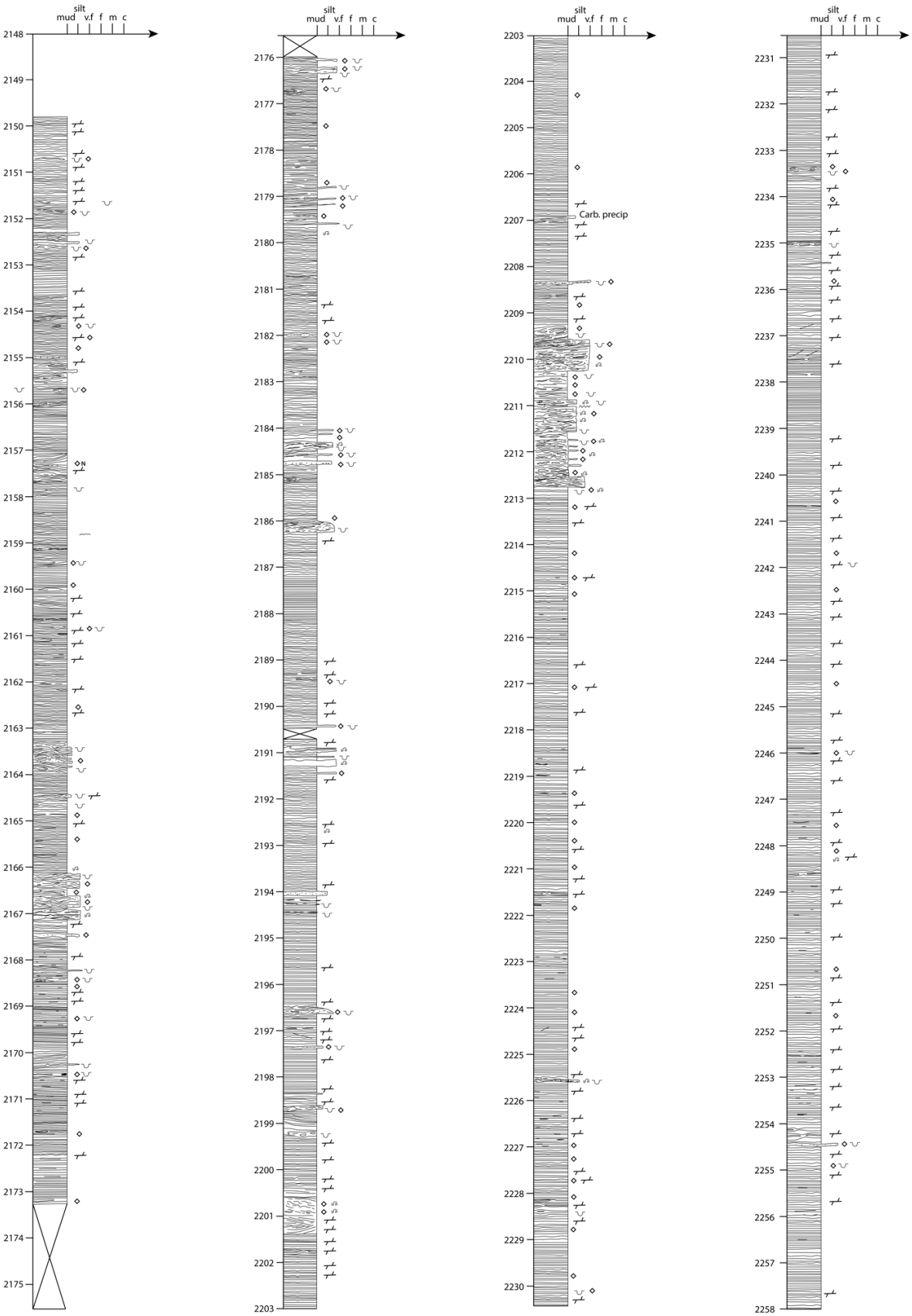

Appendix A

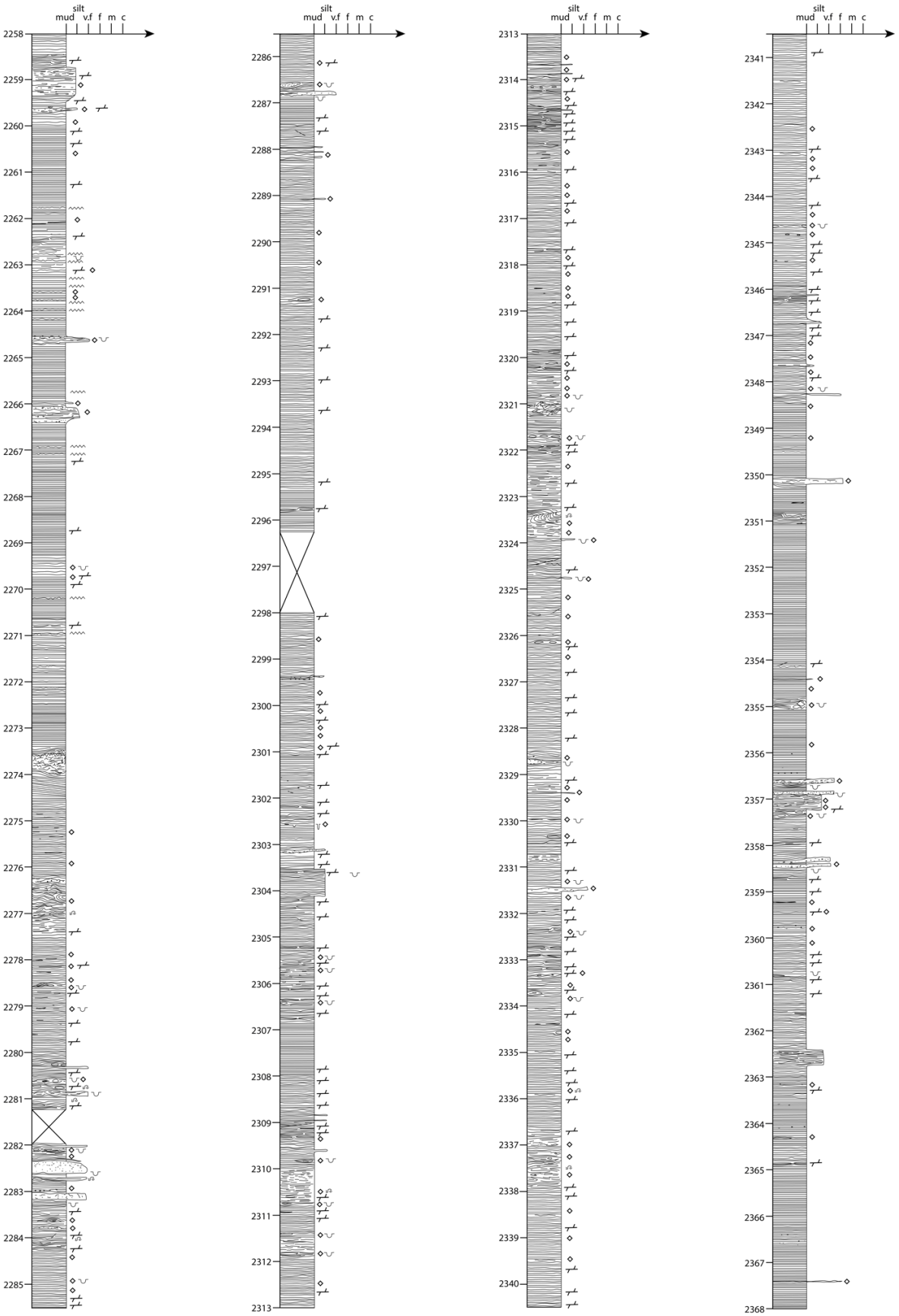
silt
mud v.f f m c
2258
2259
2260
2261
2262
2263
2264
2265
2266
2267
2268
2269
2270
2271
2272
2273
2274
2275
2276
2277
2278
2279
2280
2281
2282
2283
2284
2285
silt
mud v.f f m c
2286
2287
2288
2289
2290
2291
2292
2293
2294
2295
2296
2297
2298
2299
2300
2301
2302
2303
2304
2305
2306
2307
2308
2309
2310
2311
2312
2313
silt
mud v.f f m c
2313
2314
2315
2316
2317
2318
2319
2320
2321
2322
2323
2324
2325
2326
2327
2328
2329
2330
2331
2332
2333
2334
2335
2336
2337
2338
2339
2340
silt
mud v.f f m c
2341
2342
2343
2344
2345
2346
2347
2348
2349
2350
2351
2352
2353
2354
2355
2356
2357
2358
2359
2360
2361
2362
2363
2364
2365
2366
2367
2368

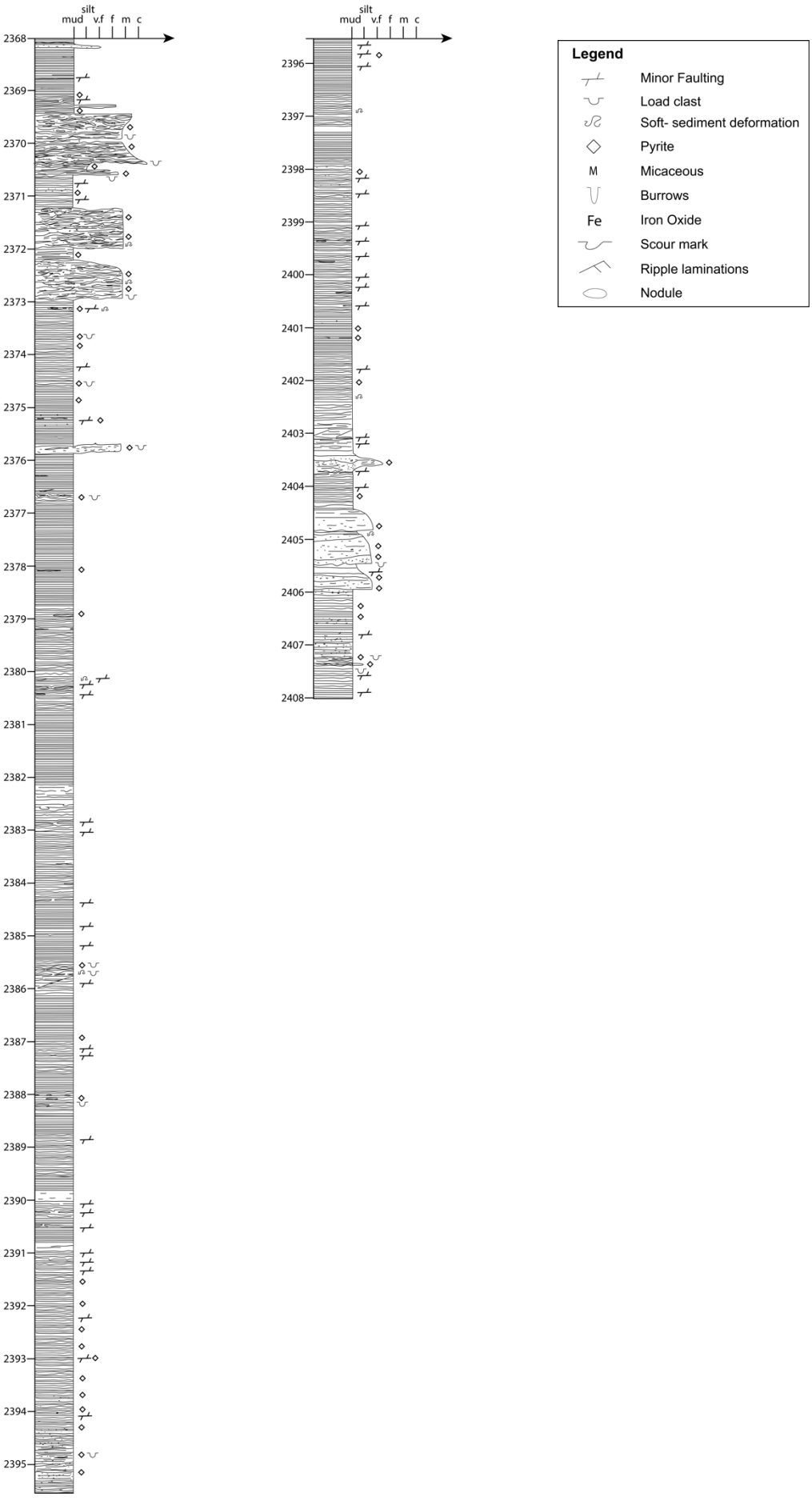
silt
mud v.f f m c
2368
2369
2370
2371
2372
2373
2374
2375
2376
2377
2378
2379
2380
2381
2382
2383
2384
2385
2386
2387
2388
2389
2390
2391
2392
2393
2394
2395
silt
mud v.f f m c
2396
2397
2398
2399
2400
2401
2402
2403
2404
2405
2406
2407
2408
Legend
Minor Faulting
Load clast
Soft- sediment deformation
Pyrite
M Micaceous
Burrows
Fe Iron Oxide
Scour mark
Ripple laminations
Nodule

Appendix B P-4 Core Log- Mahogany Zone

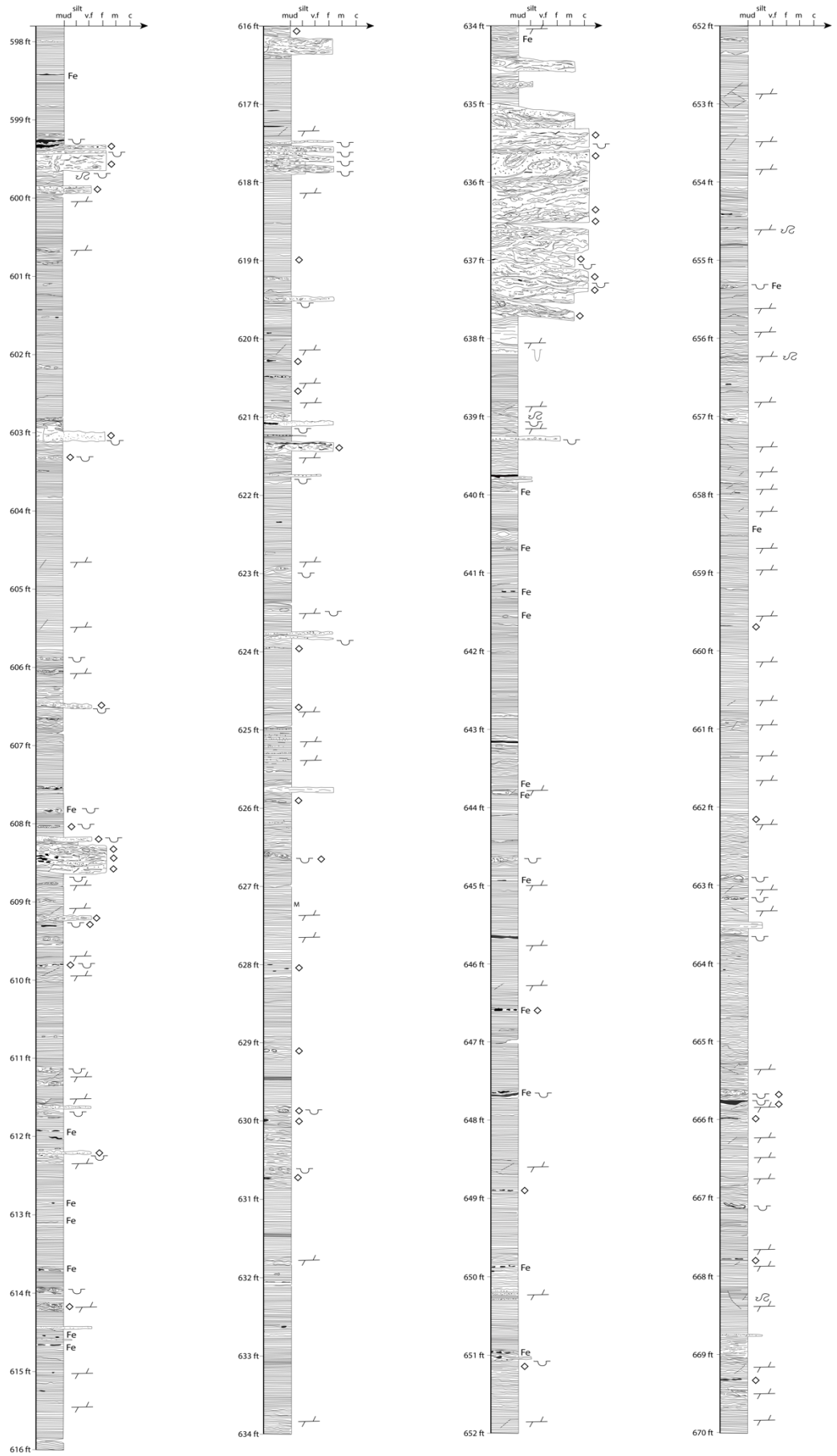

Appendix B

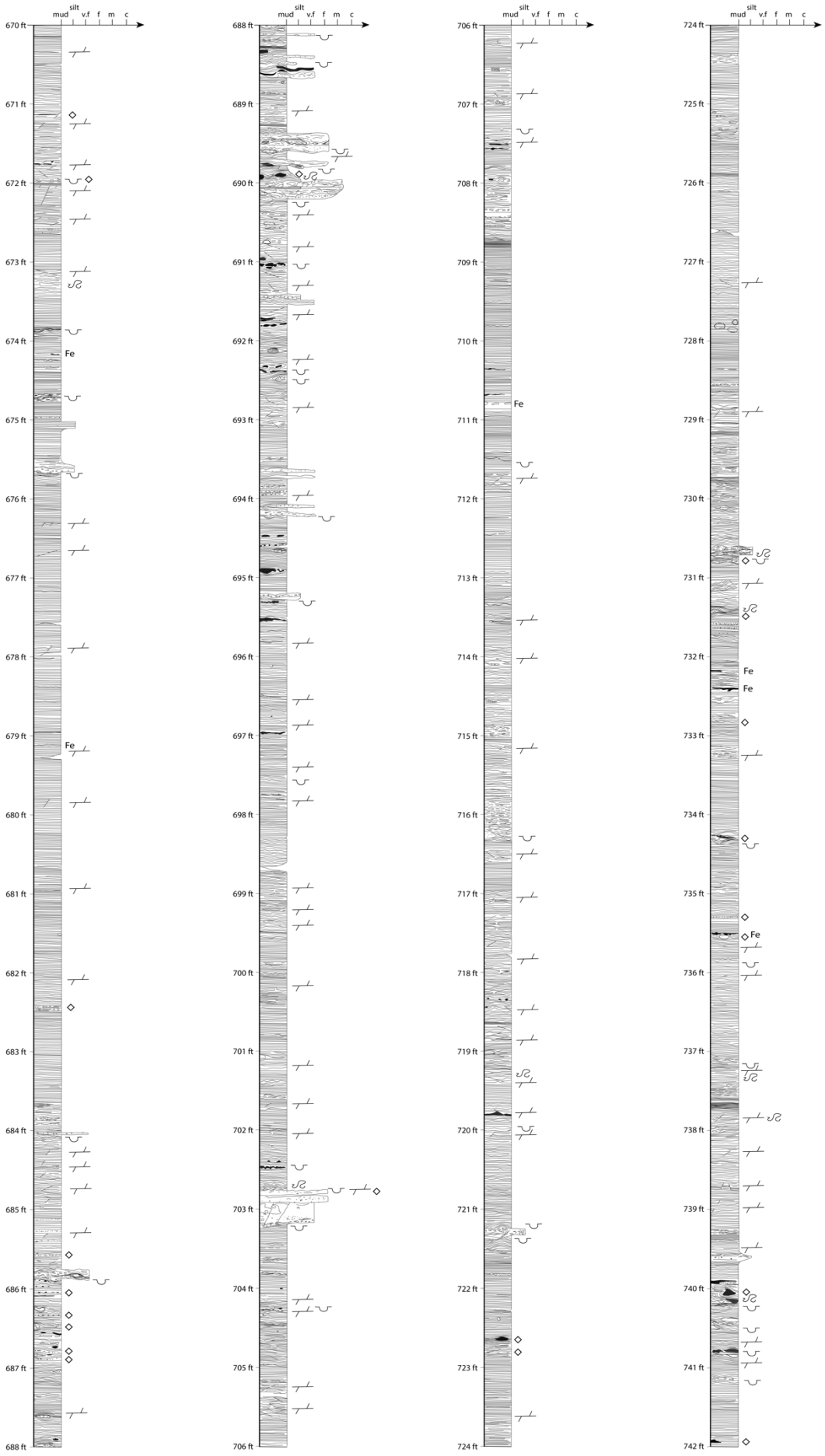
mud
silt
v.f
f
m
c
670 ft
671 ft
672 ft
673 ft
674 ft
675 ft
676 ft
677 ft
678 ft
679 ft
680 ft
681 ft
682 ft
683 ft
684 ft
685 ft
686 ft
687 ft
688 ft
Fe
Fe
688 ft
689 ft
690 ft
691 ft
692 ft
693 ft
694 ft
695 ft
696 ft
697 ft
698 ft
699 ft
700 ft
701 ft
702 ft
703 ft
704 ft
705 ft
706 ft
706 ft
707 ft
708 ft
709 ft
710 ft
711 ft
712 ft
713 ft
714 ft
715 ft
716 ft
717 ft
718 ft
719 ft
720 ft
721 ft
722 ft
723 ft
724 ft
Fe
724 ft
725 ft
726 ft
727 ft
728 ft
729 ft
730 ft
731 ft
732 ft
733 ft
734 ft
735 ft
736 ft
737 ft
738 ft
739 ft
740 ft
741 ft
742 ft
Fe
Fe
Fe

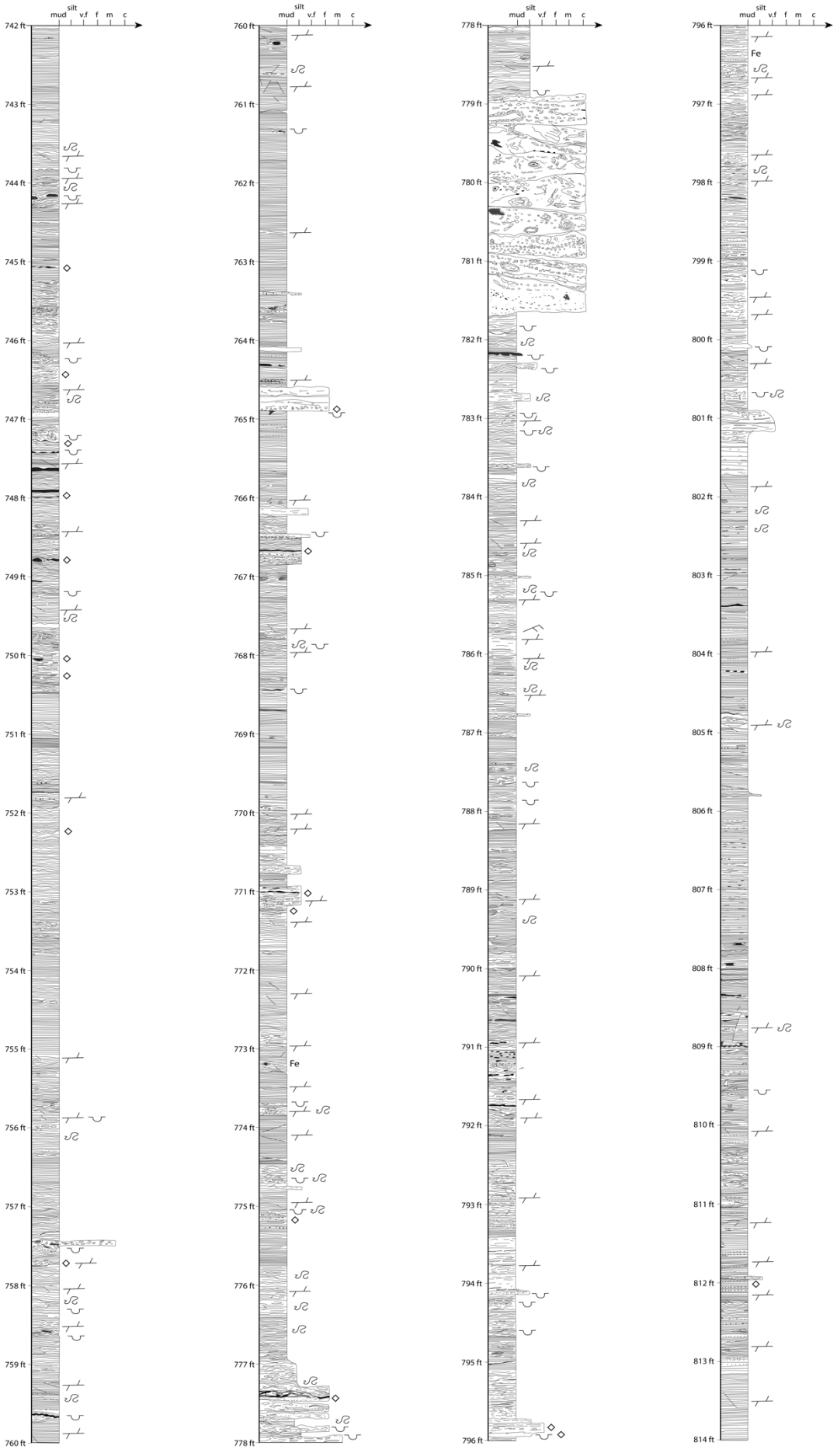
silt
mud v.f f m c
742 ft
743 ft
744 ft
745 ft
746 ft
747 ft
748 ft
749 ft
750 ft
751 ft
752 ft
753 ft
754 ft
755 ft
756 ft
757 ft
758 ft
759 ft
760 ft
760 ft
761 ft
762 ft
763 ft
764 ft
765 ft
766 ft
767 ft
768 ft
769 ft
770 ft
771 ft
772 ft
773 ft
Fe
774 ft
775 ft
776 ft
777 ft
778 ft
778 ft
779 ft
780 ft
781 ft
782 ft
783 ft
784 ft
785 ft
786 ft
787 ft
788 ft
789 ft
790 ft
791 ft
792 ft
793 ft
794 ft
795 ft
796 ft
796 ft
Fe
797 ft
798 ft
799 ft
800 ft
801 ft
802 ft
803 ft
804 ft
805 ft
806 ft
807 ft
808 ft
809 ft
810 ft
811 ft
812 ft
813 ft
814 ft

Appendix B

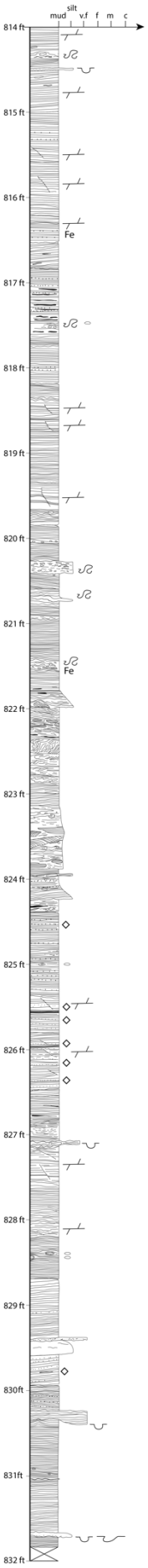

Legend

- Minor Faulting
- Load clast
- Soft- sediment deformation
- Pyrite
- M — Micaceous
- Burrows
- Fe — Iron Oxide
- Scour mark
- Ripple laminations
- Nodule

Appendix C Skyline 16 Core Log- Mahogany Zone

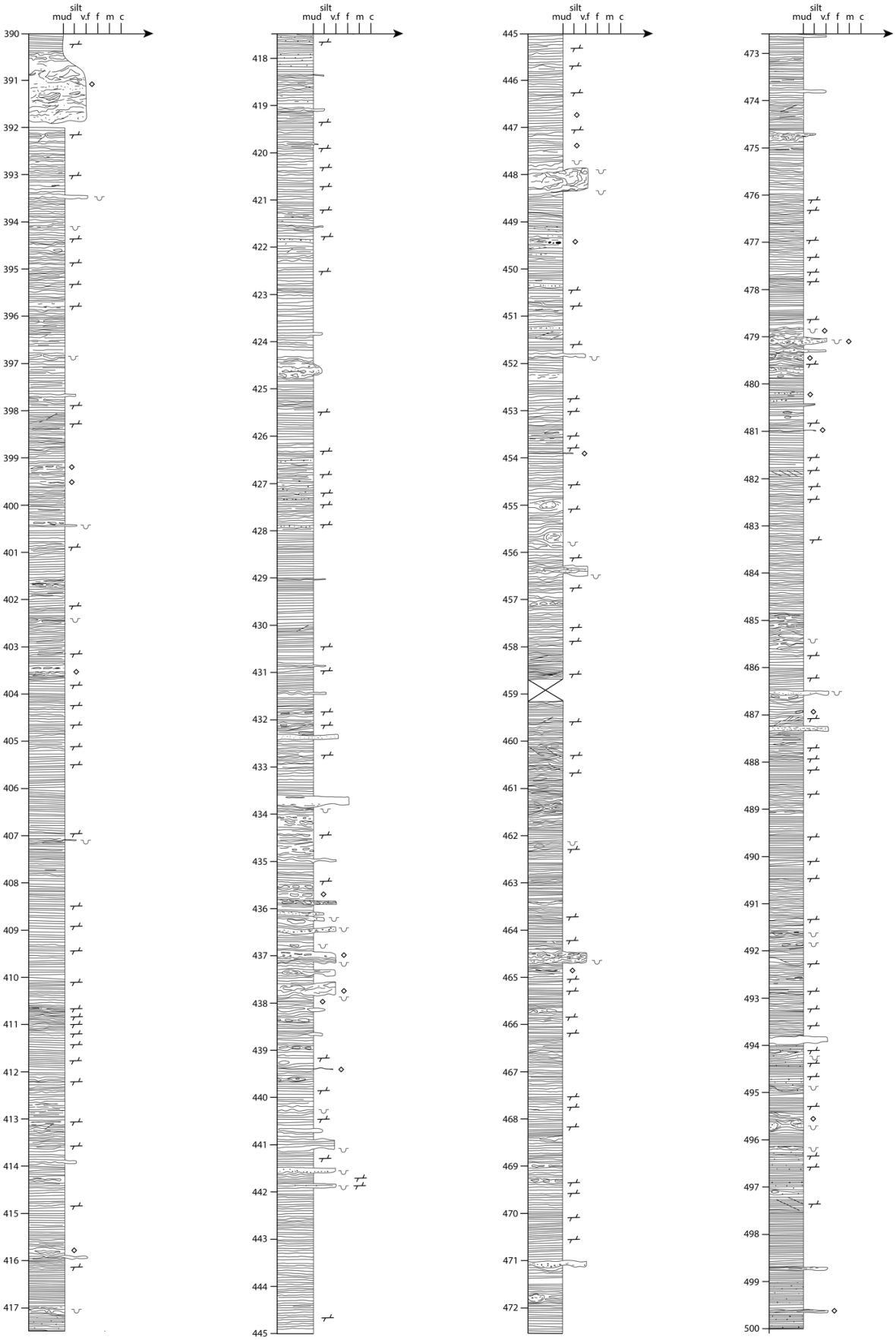

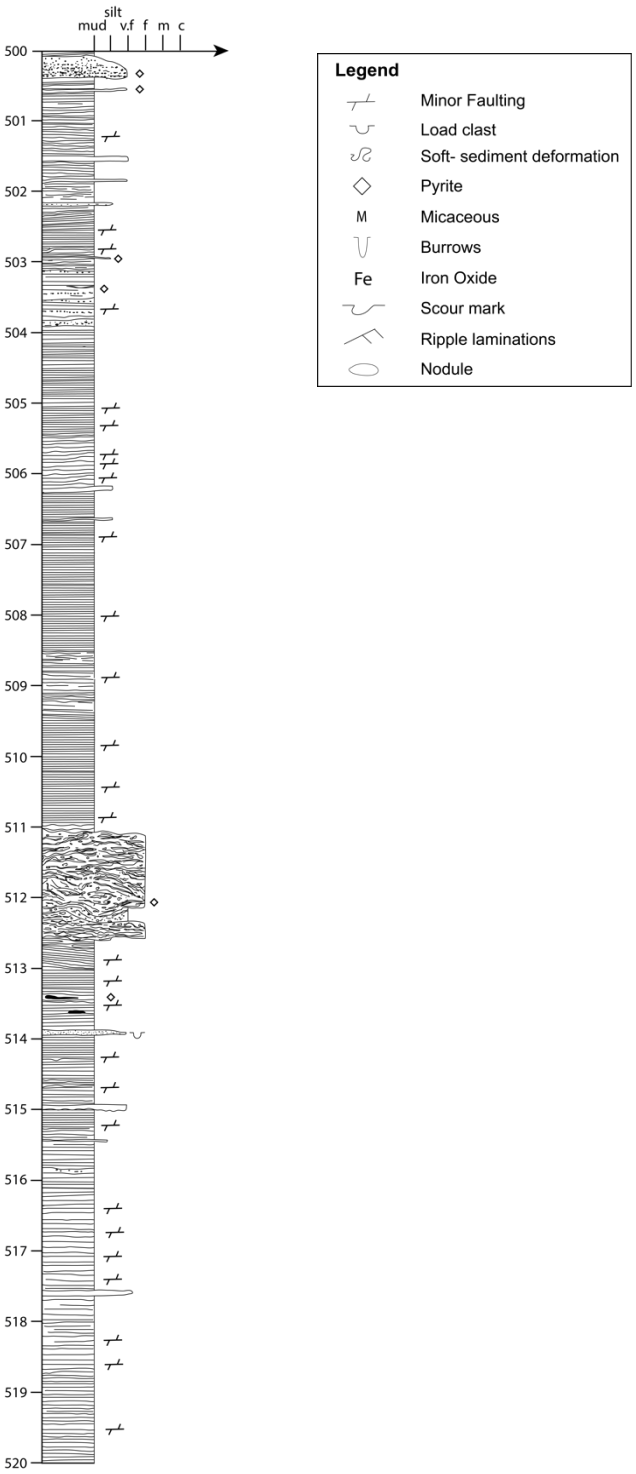
silt
mud v.f f m c
500
501
502
503
504
505
506
507
508
509
510
511
512
513
514
515
516
517
518
519
520
Legend
Minor Faulting
Load clast
Soft- sediment deformation
Pyrite
M
Micaceous
Burrows
Fe
Iron Oxide
Scour mark
Ripple laminations
Nodule

Table 1: Depth in feet with the hopane C_{31} S and R isomer peak values, and the calculated C_{31} 22S/(22S + 22R) index, for Utah State 1.

Depth (ft)	C_{31} S peak area	C_{31} R peak area	C_{31} S / (C_{31} S + C_{31} R)
2272.25	73482335.25	556220857.9	0.12
2275.15	39234607.99	42610168.77	0.48
2279.15	129422887	66284713.51	0.66
2280.3	35277065.44	38688927.91	0.48
2283.6	14928491.34	17734400.7	0.46
2284.2	37855337.04	42900216.46	0.47
2290.15	34212965.44	43505129.39	0.44
2292.12	48601420.81	58286956.74	0.45
2296.22	11015626.13	13409610.71	0.45
2301.17	30874652.79	34331427.82	0.47
2302.07	14093346.23	16706262.49	0.46
2304.7	29662860.31	373124490.5	0.07
2308.3	28914636.04	373371071	0.07
2311.45	53930377.99	748149348.4	0.07
2314.1	23807986.54	435079835.3	0.05
2316.3	60608383.71	1178118562	0.05
2317.4	70857436.75	1274243445	0.05
2318.15	66213020.7	1356461110	0.05
2319.4	6530117.676	111245395.5	0.06
2322.7	77657052.05	1444386937	0.05
2327.6	58079408	800000000	0.07
2330.25	80907372.23	1114660733	0.07

2333.85	72396107.94	459023208.7	0.14
2335.1	103204722.8	831714419.4	0.11
2337.2	65365065.65	452716429.1	0.13
2338.5	110407670.4	775149016.4	0.12
2341.15	42863314.52	255239829	0.14
2344.3	58856864.76	295202256.7	0.17
2348.5	45323135.95	424308149.3	0.10
2351.1	21423700	77297384.85	0.22
2357.3	27045564.97	160817405.4	0.14
2359.3	47650982.06	209257376.9	0.19
2362.6	66138909.42	635856160.7	0.09
2365.15	40251028.36	342606903.4	0.11
2368.07	25719284.15	184147315.1	0.12
2371.5	5578737.777	54492316.16	0.09
2374.7	7471166.863	87331512.93	0.08
2377.15	87396014.81	467716925.3	0.16
2378.9	92200004.09	280103857.5	0.25
2380.6	12180286.14	38624398.64	0.24

Table 2: Depth in feet with the hopane C_{31} S and R isomer peak values, and the calculated C_{31} 22S/(22S + 22R) index, for P-4.

Depth (ft)	C_{31} S peak area	C_{31} R peak area	C_{31} S / (C_{31} S + C_{31} R)
685.3	8566499.89	72429108.33	0.11
697.3	12936732.55	63416523.31	0.17
698.95	10205028.80	60709097.95	0.14
699.7	12744181.30	62886339.84	0.17

700.4	34899303.62	127504063.28	0.21
702.1	24361261.00	148243371.22	0.14
704.5	11364958.87	96351142.48	0.11
706.95	27448327.54	317639219.59	0.08
708.4	9667407.05	178679015.06	0.05
709.8	12628279.51	145962178.22	0.08
711.6	6877763.26	97455090.44	0.07
712.6	9468132.31	152451796.92	0.06
713.9	13877390.21	322752721.28	0.04
714.45	14402477.32	384440425.32	0.04
716.7	10412407.77	349728205.84	0.03
718.6	10976933.58	643153487.85	0.02
720.5	8774156.05	500608378.97	0.02
722.65	5288151.59	193355051.17	0.03
724.9	12947346.40	660891114.38	0.02
727.2	12348509.11	457765828.85	0.03
729.8	10253630.12	487018670.08	0.02
731.85	20820960.58	574248444.70	0.03
738.7	8217084.07	117147364.76	0.07
742.5	4550936.47	57056849.42	0.07
750.6	15734762.29	64612762.33	0.20
755.1	6152659.70	36187744.44	0.15
760.9	3454658.16	24792363.35	0.12
763.15	52083820.98	195268029.16	0.21
766.4	6249017.64	326129628.68	0.02
775.6	4753322.47	72395126.76	0.06
781.7	10268721.48	346442381.88	0.03

Table 3: Depth in feet with the hopane C_{31} S and R isomer peak values, and the calculated C_{31} 22S/(22S + 22R) index, for Skyline 16.

Depth (ft)	C_{31} S peak area	C_{31} R peak area	C_{31} S / (C_{31} S + C_{31} R)
420	9511316.078	101970117.3	0.09
422	3472869.892	62345831.31	0.05
425	3609913.408	28774371.29	0.11
429	4820366.457	30304101.5	0.14
431	3532215.919	46107798.64	0.07
437.9	3283032.219	306264114.8	0.01
444.9	8969486.879	63330934.81	0.12
453.9	5724429.142	155396489	0.04
463.9	Low hopane abundance		
468.1	3750483.3	253209656.4	0.01
472.1	10997433.71	366832512.8	0.03
477.9	9023861.879	315756801.1	0.03
485.8	13153070.05	147542631.6	0.08
493.7	3795703.486	1260893301	0.00
496.3	6342325.886	49405408.18	0.11
503.8	7612908.066	63562010.16	0.11
508.1	4459067.257	90001136.47	0.05
510.6	4371509.924	335711384.4	0.01
515.7	3891458.103	73967357.76	0.05

List of References

Aawasereelert, W., Meyers, S.R., Carroll, A.R., Peters, S.E., Smith, M.E. and Feigl, K.L., 2013. Basin-scale cyclostratigraphy of the Green River Formation, Wyoming. *Geological Society of America, Bulletin,* 125, 216–228.

Abels, H.A., Lauretano, V., van Yperen, A.E., Hopman, T., Zachos, J.C., Lourens, L.J., Gingerich, P.D. and Bowen, G.J., 2016. Environmental impact and magnitude of paleosol carbonate carbon isotope excursions marking five early Eocene hyperthermals in the Bighorn Basin, Wyoming. *Climate of the Past* 12, 1151–1163, https://doi.org/10.5194/cp-12-1151-2016.

Alldredge, A.L. and Silver, M.W.,1988. Characteristics, dynamics and significance of marine snow. *Progress in Oceanography*, 20, 40–82.

Allen, P.A. and Collinson, J.D., 1986. Lakes. In: Reading, H.G. (ed.), *Sedimentary environments and facies*. 63–94, Blackwells, Edinburgh.

Amane, W. and Hideki, N., 1997. Geochemical characteristics of terrigenous and marine sourced oils in Hokkaido, Japan. *Organic Geochemistry,* 28, 27–41.

Anagnostou, E., John, E.H., Edgar, K.M., Foster, G.L., Ridgwell, A., Inglis, G.N., Pancost, R.D., Lunt, D.J. and Pearson, P.N., 2016. Changing atmospheric CO_2 concentration was the primary driver of early Cenozoic climate. *Nature*, *533* (7603), 380–384.

Baars, D.L., Bartleson, B.L., Chapin, C.E., Curtis, B.F., De Voto, R.H., Everett, J.R., Johnson, R.C., Molenaar, C.M., Peterson, F., Schenk, C.J., Love, J.D., Merin, I.S., Rose, P.R., Ryder, R.T., Waechter, N.B. and Woodward, L.A., 1988. Basins of the Rocky Mountain region, in Sloss, L.L., ed., *The geology of North America: Boulder, Colorado, Geological Society of America,* D-2, 198–220.

Baczynski, A.A., McInerney, F.A., Freeman, K.H. and Wing, S.L., Bighorn Basin Coring Project (BBCP) Science Team, 2019. Carbon isotope record of trace *n*-alkanes in a continental PETM section recovered by the Bighorn Basin Coring Project (BBCP). *Paleoceanography and Paleoclimatology*, 34(5), 853–865.

Barke, J., van der Burgh, J., van Konijnenburg-van Cittert, J.H.A., Collinson, M.E., Pearce, M.A., Bujak, J., Heilmann-Clausen, C., Speelman, E.N., van Kempen, M.M.L., Reichart, G., Lotter, A.F. and Brinkhuis, H., 2012. Coeval Eocene blooms of the freshwater fern *Azolla* in and around Arctic and Nordic seas, *Palaeogeography, Palaeoclimatology, Palaeoecology*. 337, 108–119, https://doi.org/10.1016/j.palaeo.2012.04.002.

Berner, R.A., 1969. The synthesis of framboidal pyrite. *Economic Geology*, *64*(4), 383–384.

Bi, X., Sheng, G., Liu, X., Li, C. and Fu, J., 2005. Molecular and carbon and hydrogen isotopic composition of *n*-alkanes in plant leaf waxes. *Organic Geochemistry*, 36(10), 1405–1417.

Birdwell, J.E., Mercier, T.J., Johnson, R.C. and Brownfield, M.E., 2015. In-place oil shale resources of the Mahogany zone sorted by grade, overburden thickness and stripping ratio, Green River Formation, Piceance Basin, Colorado and Uinta Basin, Utah. *US Geological Survey*, 2015–3005.

Birdwell, J.E., Johnson, R.C. and Brownfield, M.E., 2019. Distribution of mineral phases in the Eocene Green River Formation, Piceance Basin, Colorado–Implications for the evolution of Lake Uinta. *The Mountain Geologist*, 56(2), 73–141.

Birgenheier, L.P. and Vanden Berg, M.D., 2011. Core-based integrated sedimentologic, stratigraphic, and geochemical analysis of the oil shale bearing Green River Formation, Uinta Basin, Utah. University of Utah Institute for Clean and Secure Energy, United States Department of Energy. *Oil & Natural Gas Technology Technical Report*. Vol 19.

Birgenheier, L.P., Vanden Berg, M.D., Plink-Björklund, P., Gall, R.D., Rosencrans, E., Rosenberg, M.J., Toms, L.C. and Morris, J., 2019. Climate impact on fluvial-lake system evolution, Eocene Green River Formation, Uinta Basin, Utah, USA. *Geological Society of America Bulletin.* 132, 562–587.

Boggs, S., 1995. *Principles of Sedimentology and Stratigraphy*, Fourth Edition: Pearson-Prentice Hall Pub. Co., Upper Saddle River, NJ, 676.

Bohacs, K.M., Carroll, A.R., Neal, J.E. and Mankiewicz, P.J., 2000. Lake-basin type, source potential, and hydrocarbon character: an integrated sequence-stratigraphic-geochemical framework*. Lake basins through space and time: AAPG Studies in Geology*, 46, 3–34.

Bohacs, K.M., Carroll, A.R. and Neal, J.E., 2003. Lessons from large lake systems-thresholds, nonlinearity, and strange attractors. *Geological Society of America Special Papers*, 75–90.

Bourbonniere, R.A. and Meyers, P.A., 1996, Sedimentary geolipid records of historical changes in the watersheds and productivities of Lakes Ontario and Erie, *Limnology and Oceanography*, 41, doi: 10.4319/lo.1996.41.2.0352.

Bradley, W.H., 1929. The varves and climate of the Green River epoch. *U.S. Geological Survey Professional Paper 158-E.*

Bradley, W.H., 1931. Origin and microfossils of the oil shale of the Green River Formation of Colorado and Utah: *U.S. Geological Survey Professional Paper* 158, 87–110.

Bralower, T.J., Zachos, J.C., Thomas, E., Parrow, M., Paull, C.K., Kelly, D.C., Silva, I.P., Sliter, W.V. and Lohmann, K.C., 1995. Late Paleocene to Eocene paleoceanography of the equatorial Pacific Ocean: stable isotopes recorded at ocean drilling program site 865, Allison Guyot. *Paleoceanography*, *10*(4), 841–865.

Breedlovestrout, R.L., Evraets, B.J. and Parrish, J.T., 2013. New Paleogene climate analysis of western Washington using physiognomic characteristics of fossil leaves, *Palaeogeography, Palaeoclimatology, Palaeoecology,* 392, 22–40.

Brinkhuis, H., Schouten, S., Collinson, M.E., Sluijs, A., Damsté, J.S.S., Dickens, G.R., Huber, M., Cronin, T.M., Onodera, J., Takahashi, K., Bujak, J.P., 2006. Episodic fresh surface waters in the Eocene Arctic Ocean. *Nature*. 441(7093), 606–609.

Brownfield, M.E., Mercier, T.J., Johnson, R.C. and Self, J.G., 2010. Nahcolite resources in the Green River Formation, Piceance Basin, Colorado. In: Johnson RC, Mercier TJ, Brownfield ME, Pantea MP, Self JG (eds) Oil shale and Nahcolite resources of the Piceance Basin, Colorado*. US Geological Survey Digital Data Series* DDS-69-Y.

Buchheim, H.P., 1994. Paleoenvironments, lithofacies and varves of the Fossil Butte Member of the Eocene Green River Formation, southwestern Wyoming. *Rocky Mountain Geology*, 30(1), 3–14.

Burgess, J. D., 1974. Microscopic examination of kerogen (dispersed organic matter) in petroleum exploration. *Geological Society of America Special Paper*, 153, 19–30.

Bush, R.T., McInerney, F.A., 2013. Leaf wax *n*-alkane distributions in and across modern plants: implications for paleoecology and chemotaxonomy. *Geochimica et Cosmochimica Acta*, 117, 161–179.

Carmichael, M.J., Inglis, G.N., Badger, M.P., Naafs, B.D.A., Behrooz, L., Remmelzwaal, S., Monteiro, F.M., Rohrssen, M., Farnsworth, A., Buss, H.L. and Dickson, A.J., 2017. Hydrological and associated biogeochemical consequences of rapid global warming during the Paleocene-Eocene Thermal Maximum. *Global and Planetary Change,* 157, 114–138.

Carrol, A.R. and Bohacs, K.M., 1999. Stratigraphic classification of ancient lakes: Balancing tectonics and climatic controls. *Geology,* 27, 99–102.

Carroll, A.R. and Bohacs, K.M., 2001. Lake-type controls on petroleum source rock potential in nonmarine basins: *AAPG Bulletin*, 85, 6, 1033–1053, https:// doi .org /10 .1306 /8626CA5F -173B -11D7 -8645000102C1865D.

Cashion, W. B., 1967. Geology and fuel resources of the Green River Formation Southeastern Uinta Basin, Utah and Colorado. *U.S Geological Survey Professional Paper,* 548, 48.

Chetel, L.M. and Carroll, A.R., 2010. Terminal Infill of Eocene Lake Gosiute, Wyoming, U.S.A. *Journal of Sedimentary Research,* 80(6), 492–514. doi: https://doi.org/10.2110/jsr.2010.050

Chetel, L.M., Janecke, S.U., Carroll, A.R., Beard, B.L., Johnson, C.M. and Singer, B.S., 2011. Paleogeographic reconstruction of the Eocene Idaho River, North American Cordillera. *Geological Society of America Bulletin,* 123, 71–88.

Chikaraishi, Y. and Naraoka, H., 2003. Compound-specific δD–δ^{13}C analyses of *n*-alkanes extracted from terrestrial and aquatic plants. *Phytochemistry*, 63(3), 361–371.

Clechenko, E.R., Kelly, D.C., Harrington, G.J. and Stiles, C.A., 2007. Terrestrial records of a regional weathering profile at the Paleocene-Eocene boundary in the Williston Basin of North Dakota. *Geological Society of America Bulletin*, 119(3–4), 428–442.

Cole, R., 1998. Possible Milankovitch cycles in the Lower Parachute Creek Member of the Green River Formation (Eocene), North-Central Piceance Creek Basin, Colorado: an analysis, in Pitman, J., and Carroll, A., eds., Modern and Ancient Lake Systems: *Utah Geological Association, Guidebook,* 26, 233–259.

Collister, J.W., Summons, R.E., Lichtfouse, E. and Hayes, J.M., 1992. An isotopic biogeochemical study of the Green River oil shale. *Organic Geochemistry*, 19(1–3), 265–276.

Connan, J. and Cassou, A.M., 1980. Properties of gases and petroleum liquids derived from terrestrial kerogen at various maturation levels. *Geochimica et Cosmochimica Acta,* 44, 1–23.

Cramer, B.S., Wright, J.D., Kent, D.V. and Aubry, M.P., 2003. Orbital climate forcing of δ^{13}C excursions in the late Paleocene–early Eocene (chrons C24n–C25n). *Paleoceanography*, 18(4).

Crowley, K D., Duchon, C.E. and Rhi, J., 1986. Climate record in varved sediments of Green River Formation. *Journal of Geophysical Research,* 91, 8637–8647.

Dansgaard, W., 1964. Stable isotopes in precipitation. *Tellus*. 16(4), 436–468.

Davison, W., 1993. Iron and manganese in lakes, *Earth Sciences Review*, 34, 119–163.

Desborough, G.A., 1975. Authigenic albite and potassium feldspar in the Green River Formation, Colorado and Wyoming. *American Mineralogist: Journal of Earth and Planetary Materials*, 60(3-4), 235–239.

Didyk, B.M., Simoneit, B.R.T., Brassell, S.T. and Eglinton, G., 1978. Organic geochemical indicators of palaeoenvironmental conditions of sedimentation. *Nature,* 272, 216–222.

Diefendorf, A.F. and Freimuth, E.J. 2017. Extracting the most from terrestrial plant-derived *n*-alkyl lipids and their carbon isotopes from the sedimentary record: A review. *Organic Geochemistry,* 103, 1–21.

Dillhoff, R.M., Dillhoff, T.A., Greenwood, D. R., DeVore, M. L. and Pigg, K. B., 2013. The Eocene Thomas Ranch flora, Allenby Formation, Princeton, British Columbia, Canada. *Botany,* 91, 514–529.

Douglas, R.G. and Savin, S.M., 1975. Oxygen and carbon isotope analyses of Tertiary and Cretaceous microfossils from Shatsky Rise and other sites in the North Pacific Ocean. *Initial Reports of the Deep Sea Drilling Project*, *32*(50), 520.

Dunkley Jones, T., A. Ridgwell, D. J. Lunt, M. A. Maslin, D. N. Schmidt, and P. J. Valdes., 2010. A Palaeogene perspective on climate sensitivity and methane hydrate instability, *Philosophical Transactions of the Royal Society A*, 368(1919), 2395–2415, doi:10.1098/rsta.2010.0053.

Dyni, J.R., 1974a. Nahcolite analyses of seven drill cores from the Green River Formation, Rio Blanco County, Colorado. *U.S. Geological Survey Open-File Report*, 45, 74–1027.

Dyni, J.R., 1974b. Stratigraphy and nahcolite resources of the saline facies of the Green River Formation, Rio Blanco County, Colorado. *U.S.G.S Open-File Report* 74–56, 28.

Dyni, J. R., 1987. The origin of oil shale and associated minerals, in Taylor, O.J., ed., Oil shale, water resources, and valuable minerals of the Piceance basin, Colorado - The challenge and choices of development. *U.S. Geological Survey Professional Paper 1310,* 17–20.

Dyni, J.R., 2006. Geology and resources of some world oil-shale deposits. *U.S. Geological Survey Scientific Investigations Report* 2005–5294, 42.

Eglinton, T. I. and Eglinton, G., 2008. Hydrogen isotope fractionation during water uptake by woody xerophytes. Molecular proxies for paleoclimatology. *Earth and Planetary Science Letters,* 275, 1–16.

Eugster, H.P. and Hardie, L.A., 1978. Saline lakes, in Lerman, A., ed., *Lakes—Chemistry, geology, physics.* New York, Springer-Verlag, 237–293.

Evans, D., Sagoo, N., Renema, W., Cotton, L.J., Müller, W., Todd, J.A., Saraswati, P.K., Stassen, P., Ziegler, M., Pearson, P.N. and Valdes, P.J., 2018. Eocene greenhouse climate revealed by coupled clumped isotope-Mg/Ca thermometry. *Proceedings of the National Academy of Sciences*, 115(6), pp.1174–1179.

Feakins, S.J. and Sessions, A.L., 2010. Controls on the D/H ratios of plant leaf waxes in an arid ecosystem. *Geochimica et Cosmochimica Acta,* 74(7), 2128–2141.

Feakins, S.J., 2013. Pollen-corrected leaf wax D/H reconstructions of northeast African hydrological changes during the late Miocene. *Palaeogeography, Palaeoclimatology, Palaeoecology*. 374, 62–71.

Feng J., Sarg J. F. and Tänavsuu-Milkeviciene K., 2016. Source Rock Characterization of the Green River Oil Shale, Piceance Creek Basin, Colorado. *Hydrocarbon Source Rocks in Unconventional Plays Rocky Mountain Region*, 319–351.

Ficken, K. J., Li, B., Swain, D. and Eglinton, G., 2000. An *n*-alkane proxy for the sedimentary input of submerged/floating freshwater aquatic macrophytes. *Organic Geochemistry,* 31, 745–749.

Fischer, A. G. and Roberts, L. T., 1991. Cyclicity in the Green River Formation (lacustrine-Eocene) of Wyoming. *Journal of Sedimentary Petrology,* 61, 1146–1154.

Foreman, B.Z., Heller, P.L. and Clementz, M.T., 2012. Fluvial response to abrupt global warming at the Palaeocene/Eocene boundary. *Nature*, 491(7422), 92–95.

Foster, G.L., Royer, D.L. and Lunt, D. J., 2017. Future climate forcing potentially without precedent in the last 420 million years. *Nature Communications*, 8,14845.

Frantz, C.M., Petryshyn, V.A., Marenco, P.J., Tripati, A., Berelson, W.M. and Corsetti, F.A., 2014. Dramatic local environmental change during the Early Eocene Climatic Optimum detected using high resolution chemical analyses of Green River Formation stromatolites. *Palaeogeography, Palaeoclimatology, Palaeoecology*, *405*, 1–15.

Galeotti, S., Krishnan, S., Pagani, M., Lanci, L., Gaudio, A., Zachos, J.C., Monechi, S., Morelli, G. and Lourens, L., 2010. Orbital chronology of Early Eocene hyperthermals from the Contessa Road section, central Italy. *Earth and Planetary Science Letters*, 290(1–2), 192–200.

Gall, R.D., Birgenheier, L.P. and Vanden Berg, M.D., 2017. Highly seasonal and perennial fluvial facies: Implications for climate control on the Douglas Creek and Parachute Creek members, Green River Formation, Southeastern Uinta Basin, Utah, U.S.A. *Journal of Sedimentary Research,* 87(9), 1019–1047. doi: https://doi.org/10.2110/jsr.2017.54.

Garcin, Y., Schwab, V.F., Gleixner, G., Kahmen, A., Todou, G., Séné, O., Onana, J.M., Achoundong, G. and Sachse, D., 2012. Hydrogen isotope ratios of lacustrine sedimentary *n*-alkanes as proxies of tropical African hydrology: insights from a calibration transect across Cameroon. *Geochimica et Cosmochimica Acta*, 79, 106–126.

Graf, G., 1992, Benthic-pelagic coupling: a benthic view. *Oceanography and marine biology: an annual review,* 30, 149–190.

Grande, L., 1984. Paleontology of the Green River Formation, with a review of the fish fauna. *Bulletin of the Geological Survey of Wyoming*. 64, 333.

Greenwood, D.R. and Wing, S.L., 1995. Eocene continental climates and latitudinal temperature gradients. *Geology,* 23, 1044–1048.

Greenwood, D.R., Pigg, K.B., Basinger, J.F. and DeVore, M.L., 2016. A review of paleobotanical studies of the Early Eocene Okanagan (Okanogan) Highlands floras of British Columbia, Canada and Washington, USA, *Canadian Journal of Earth Science,* 53, 548–564, https://doi.org/10.1139/cjes-2015-0177.

Gutjahr, M., Ridgwell, A., Sexton, P.F., Anagnostou, E., Pearson, P.N., Pälike, H., Norris, R.D., Thomas, E., and Foster, G.L., 2017. Very large release of mostly volcanic carbon during the Palaeocene–Eocene Thermal Maximum. *Nature*, 548(7669), 573–577.

Hills, I.R., Whitehead, E.V., Anders, D.E., Cummins, J.J. and Robinson, W.E., 1966. An optically active triterpane, gammacerane in Green River, Colorado, oil shale bitumen. *Chemical Commications*, 20, 752b–754.

Hiza, M.M., 1999. The geochemistry and geochronology of the Eocene Absaroka volcanic province, northern Wyoming and southern Montana, USA *[Ph.D. thesis]:* Corvallis, Oregon State University, 243.

House, J.I., Prentice, I.C., Ramankutty, N., Houghton, R.A. and Heimann, M., 2003. Reconciling apparent inconsistencies in estimates of terrestrial CO_2 sources and sinks. *Tellus B: Chemical and Physical Meteorology*, 55(2), 345–363.

Huber, M. and Caballero, R., 2011. The early Eocene equable climate problem revisited. *Climate of the Past,* 7, 603–633.

Hughes, W.B., Holba, A.G. and Dzou, L.I., 1995. The ratios of dibenzothiophene to phenanthrene and pristane to phytane as indicators of depositional environment and lithology of petroleum source rocks. *Geochimica et Cosmochimica Acta,* 59, 3581–3598.

Hyland, E.G. and Sheldon, N.D., 2013. Coupled CO2-climate response during the early Eocene climatic optimum. *Palaeogeography, Palaeoclimatology, Palaeoecology,* 369, 125–135.

Hyland, E.G., Huntington, K.W., Sheldon, N.D. and Reichgelt, T., 2018. Temperature seasonality in the North American continental interior during the Early Eocene Climatic Optimum. *Climate of the Past*, 14(10), 1391–1404.

Inglis, G.N., Farnsworth, A., Lunt, D., Foster, G.L., Hollis, C.J., Pagani, M., Jardine, P.E., Pearson, P.N., Markwick, P., Galsworthy, A.M. and Raynham, L., 2015. Descent toward the Icehouse: Eocene sea surface cooling inferred from GDGT distributions. *Paleoceanography*, 30(7), 1000–1020.

Inglis, G. N., Collinson, M. E., Riegel, W., Wilde, V., Farnsworth, A., Lunt, D. J., Valdes, P., Robson, B. E., Scott, A. C., Lenz, O. K., Naafs, B. D. A. and Pancost, R. D., 2017. Mid-latitude continental temperatures through the early Eocene in western Europe, *Earth and Planetary Science Letters,* 460, 86–96, https://doi.org/10.1016/j.epsl.2016.12.009.

Inglis, G.N., Bragg, F., Burls, N.J., Cramwinckel, M.J., Evans, D., Foster, G.L., Huber, M., Lunt, D.J., Siler, N., Steinig, S., Tierney, J.E., Wilkinson, R., Anagnostou, E., de Boer, A.M., Dunkley Jones, T., Edgar, K.M., Hollis, C.J., Hutchinson, D.K., and Pancost, R.D., 2020. Global mean surface temperature and climate sensitivity of the early Eocene Climatic Optimum (EECO), Paleocene–Eocene Thermal Maximum (PETM), and latest Paleocene. *Climate of the Past*, 16, 1953–1968, https://doi.org/10.5194/cp-16-1953-2020.

IPCC., 2014. *Climate Change 2014: Synthesis Report. Contribution of Working Groups I, II and III to the Fifth Assessment Report of the Intergovernmental Panel on Climate Change* [Core Writing Team, R.K. Pachauri and L.A. Meyer (eds.)]. IPCC, Geneva, Switzerland, 151.

Jagniecki, E.A., Jenkins, D.M., Lowenstein, T.K. and Carroll, A.R., 2013. Experimental study of shortite ($Na_2Ca_2(CO_3)_3$) formation and application to the burial history of the Wilkins Peak Member, Green River Basin, Wyoming, USA. *Geochimica et Cosmochimica Acta,* 115, 31–45.

Jansen, B., van Loon, E.E., Hooghiemstra, H. and Verstraten, J.M., 2010. Improved reconstruction of palaeo-environments through unravelling of preserved vegetation biomarker patterns. *Palaeogeography, Palaeoclimatology, Palaeoecology.* 285, 119–130.

John, C.M., Bohaty, S.M., Zachos, J.C., Sluijs, A., Gibbs, S., Brinkhuis, H. and Bralower, T.J., 2008. North American continental margin records of the Paleocene-Eocene thermal maximum: Implications for global carbon and hydrological cycling. *Paleoceanography*, 23(2).

Johnson R. C., 1985. Early Cenozoic history of the Uinta and Piceance Creek Basins, Utah and Colorado, with special reference to the development of Eocene Lake Uinta. In Cenozoic Paleogeography of the West-Central United States (eds. R. M. Flores and S. S. Kaplan). *Rocky Mountain Section (SEPM)* Denver, Colorado, 247–276.

Johnson, R.C., Mercier, T.J., Brownfield, M.E. and Self, J.G., 2010. Assessment of in-place oil shale resources in the Eocene Green River Formation, Uinta Basin, Utah and Colorado, in U.S. Geological Survey Oil Shale Assessment Team, ed., Oil Shale Resources of the Uinta Basin, Utah and Colorado. *U.S.G.S Digital Data Series DDS-69-BB*, 153.

Johnson, R.C. and Brownfield, M.E., 2015. Development, evolution, and destruction of the saline. mineral area of Eocene Lake Uinta, Piceance Basin, western Colorado. *US Geological Survey Scientific Investigations Report,* 2013–5176.

Johnson, R.C., Birdwell J.E. and Mercier, T.J., 2018. Controls on organic matter distributions in Eocene Lake Uinta, Utah and Colorado. *The Mountain Geologist*, 55, 177–216.

Jones, S.M., Hoggett, M., Greene, S.E. and Jones, T.D., 2019. Large Igneous Province thermogenic greenhouse gas flux could have initiated Paleocene-Eocene Thermal Maximum climate change. *Nature communications*, 10(1), 1–16.

Kahmen, A., Schefuss, E., Arndt, S.K., Hoffmann, B., Cernusak, L.A., West, J.B. and Sachse, D., 2012. Leaf wax *n*-alkane δD values as ecohydrological proxies that reflect the δD values of precipitation and leaf water evaporative deuterium enrichment. *In AGU Fall Meeting Abstracts*, B33A-0510.

Keenan, T.F., Prentice, I.C., Canadell, J.G., Williams, C.A., Wang, H., Raupach, M. and Collatz, G.J., 2016. Recent pause in the growth rate of atmospheric CO 2 due to enhanced terrestrial carbon uptake. *Nature communications*, 7(1), 1–10.

Kelts, K., 1988. Environments of deposition of lacustrine petroleum source rocks: an introduction. *Geological Society, London, Special Publications*, 40(1), 3–26.

Kelts, K. and Talbot, M., 1990. Lacustrine carbonates as geochemical archives of environmental change and biotic/abiotic interactions. In *Large Lakes*, 288–315. Springer, Berlin, Heidelberg.

Kemp, P., Lander, D.J. and Orpin, C.G., 1984. The lipids of the rumen fungus *Piromonas communis*. *Microbiology,* 130, 27–37.

Kiehl, J.T., Shields, C.A., Snyder, M.A., Zachos, J.C. and Rothstein, M., 2018. Greenhouse- and orbital-forced climate extremes during the early Eocene. *Philosophical Transactions of the Royal Society A: Mathematical, Physical and Engineering Sciences,* 376(2130), 20170085.

Kiørboe, T., Ploug, H. and Thygesen, U., 2001. Fluid motion and solute distribution around sinking aggregates. I. Small-scale fluxes and heterogeneity of nutrients in the pelagic environment. *Marine Ecology Progress Series,* 211, 1–13. 10.3354/meps211001.

Kirtland Turner, S., Sexton, P. F., Charles, C. D. and Norris, R. D., 2014. Persistence of carbon release events through the peak of early Eocene global warmth. *Nature Geoscience,* 7, 748–751, https://doi.org/10.1038/ngeo2240.

Kocken, I.J., Cramwinckel, M.J., Zeebe, R.E., Middelburg, J.J. and Sluijs, A., 2019. The 405 kyr and 2.4 Myr eccentricity components in Cenozoic carbon isotope records, *Climate of the Past,* 15, 91–104, https://doi.org/10.5194/cp-15-91-2019.

Kraus, M.J. and Riggins, S., 2007. Transient drying during the Paleocene–Eocene Thermal Maximum (PETM): analysis of paleosols in the Bighorn Basin, Wyoming. *Palaeogeography, Palaeoclimatology, Palaeoecology,* 245(3–4), 444–461.

Kraus, M.J., McInerney, F.A., Wing, S.L., Secord, R., Baczynski, A.A. and Bloch, J.I., 2013. Paleohydrologic response to continental warming during the Paleocene–Eocene thermal maximum, Bighorn Basin, Wyoming. *Palaeogeography, Palaeoclimatology, Palaeoecology,* 370, 196–208.

Kuma, R., Hasegawa, H., Yamamoto, K., Whiteside, J.H., 2019. Biogenically induced bedded chert formation in the alkaline palaeo-lake of the Green River Formation. *Science Reports,* 9, 16448. https://doi.org/10.1038/s41598-019-52862-7

Lauretano, V., Littler, K., Polling, M., Zachos, J.C. and Lourens, L.J., 2015. Frequency, magnitude and character of hyperthermal events at the onset of the Early Eocene Climatic Optimum. *Climate of the Past,* 11, 1313–1324.

Lauretano, V., Zachos, J. C. and Lourens, L. J., 2018. Orbitally Paced Carbon and Deep-Sea Temperature Changes at the Peak of the Early Eocene Climatic Optimum. *Paleoceanography and Paleoclimate,* 33, 1050–1065, https://doi.org/10.1029/2018PA003422.

Littler, K., Röhl, U., Westerhold, T. and Zachos, J.C., 2014. A high-resolution benthic stable-isotope record for the South Atlantic: Implications for orbital-scale changes in Late Paleocene-Early Eocene climate and carbon cycling. *Earth and Planetary Science Letters,* 401, 18–30.

Liu, Z., Pagani, M., Zinniker, D., Deconto, R., Huber, M., Brinkhuis, H., Shah, S. R., Leckie, R. M. and Pearson, A., (2009). Global cooling during the eocene-oligocene climate transition, *Science*, 323, 1187–1190, doi:10.1126/science.1166368.

Loizeau, J.L., Span, D., Coppee, V. and Dominik, J., 2001. Evolution of the trophic state of Lake Annecy (eastern France) since the last glaciation as indicated by iron, manganese and phosphorus speciation, *Journal of Paleolimnology,* 25, 205–214.

Longman, J., Gernon, T.M., Palmer, M.R., Jones, M.T., Stokke, E.W. and Svensen, H.H., 2021. Marine diagenesis of tephra aided the Palaeocene-Eocene Thermal Maximum termination. *Earth and Planetary Science Letters*, 571, 117101.

Lourens, L.J., Sluijs, A., Kroon, D., Zachos, J.C., Thomas, E., Röhl, U., Bowles, J. and Raffi, I., 2005. Astronomical pacing of late Palaeocene to early Eocene global warming events. *Nature*, 435(7045), 1083–1087.

Lunt, D.J., Valdes, P.J., Jones, T.D., Ridgwell, A., Haywood, A.M., Schmidt, D.N., Marsh, R. and Maslin, M., 2010. CO_2-driven ocean circulation changes as an amplifier of Paleocene-Eocene thermal maximum hydrate destabilization. *Geology*, 38(10), 875–878.

Lunt, D.J., Ridgwell, A., Sluijs, A., Zachos, J., Hunter, S. and Haywood, A., 2011. A model for orbital pacing of methane hydrate destabilization during the Palaeogene. *Nature Geoscience,* 4(11), 775–778.

Lunt, D.J., Dunkley Jones, T., Heinemann, M., Huber, M., LeGrande, A., Winguth, A., Loptson, C., Marotzke, J., Roberts, C.D., Tindall, J. and Valdes, P., 2012. A model–data comparison for a multi-model ensemble of early Eocene atmosphere–ocean simulations: EoMIP. *Climate of the Past*, 8(5), 1717–1736.

Lunt, D.J., Huber, M., Anagnostou, E., Baatsen, M.L., Caballero, R., DeConto, R., Dijkstra, H.A., Donnadieu, Y., Evans, D., Feng, R. and Foster, G.L., 2017. The DeepMIP contribution to PMIP4: Experimental design for model simulations of the EECO, PETM, and pre-PETM (version 1.0). *Geoscientific Model Development,* 10(2), 889–901.

MacGinitie, H.D., 1969. The Eocene green River flora of northwestern Colorado and northeastern Utah. *University of California Press*, 83, 203.

Machlus, M., Olsen, P.E., Christie-Blick, N. and Hemming, S.R., 2008. Spectral analysis of the Lower Eocene Wilkins Peak Member, Green River Formation, Wyoming: Support for Milankovitch Cyclicity. *Earth and Planetary Science Letters,* 268, 64–75.

Mackenzie, A.S., Patience, R.L., Maxwell, J.R., Vandenbroucke, M. and Durand, B., 1980. Molecular parameters of maturation in the Toarcian shales, Paris Basin, France—I. Changes in the configurations of acyclic isoprenoid alkanes, steranes and triterpanes. *Geochimica et Cosmochimica Acta*, 44(11),1709–1721.

Marzi, R., Torkelson, B.E. and Olson, R.K., 1993. A revised carbon preference index. *Organic Geochemistry*, 20(8), 1303–1306.

McKenna, M.C., 1983. Cenozoic paleogeography of North Atlantic land bridges. In *Structure and development of the Greenland-Scotland Ridge*, 351–399, Springer, Boston, MA.

Mederos, S., Tikoff, B. and Bankey, V., 2005. Geometry, timing, and continuity of the Rock Springs uplift, Wyoming, and Douglas Creek arch, Colorado: Implications for uplift mechanisms in the Rocky Mountain foreland, USA. *Rocky Mountain Geology*, 40(2),167–191.

Meyers, S.R., 2008. Resolving Milankovitchian controversies: the Triassic Latemar Limestone and the Eocene Green River Formation. *Geology*, 36, 319–322.

Miller, K.G., Janecek, T.R., Katz, M.E. and Keil, D.J., 1987a. Abyssal circulation and benthic foraminiferal changes near the Paleocene/Eocene boundary. *Paleoceanography*, 2(6), 741–761.

Moye, F.J., Hackett, W.R., Blakley, J.D., and Snider, L.G., 1988. Regional geologic setting and volcanic stratigraphy of the Challis Volcanic Field, central Idaho, *in* Link, P.K., and Hackett, W.R., eds., *Guidebook to the geology of central and southern Idaho*, Idaho Geological Survey Bulletin 27, 87–97.

Müller, R.D., Seton, M., Zahirovic, S., Williams, S.E., Matthews, K.J., Wright, N.M., Shephard, G.E., Maloney, K.T., Barnett-Moore, N., Hosseinpour, M. and Bower, D.J., 2016. Ocean basin evolution and global-scale plate reorganization events since Pangea breakup. *Annual Review of Earth and Planetary Sciences,* 44, 107–138.

Naafs, B.D.A., Rohrssen, M., Inglis, G.N., Lähteenoja, O., Feakins, S.J., Collinson, M.E., Kennedy, E.M., Singh, P.K., Singh, M.P., Lunt, D.J. and Pancost, R.D., 2018. High temperatures in the terrestrial mid-latitudes during the early Palaeogene. *Nature Geoscience*, 11(10), 766–771.

Nicolo, M.J., Dickens, G.R., Hollis, C.J., and Zachos, J.C., 2007. Multiple early Eocene hyperthermals: Their sedimentary expression on the New Zealand continental margin and in the deep sea. *Geology*, 35(8), 699–702, https://doi.org/10.1130/G23648A.1.

Norris, R.D., Jones, L.S., Corfield, R.M. and Cartlidge, J.E., 1996. Skiing in the Eocene Uinta Mountains? Isotopic evidence in the Green River Formation for snow melt and large mountains. *Geology*, 24(5), 403–406. doi: https://doi.org/10.1130/0091-7613(1996)024

Olsen, P.E. and Kent, D.V., 1999. Long-period Milankovitch cycles from the Late Triassic and Early Jurassic of eastern North America and their implications for the calibration of the early Mesozoic time scale and the long-term behaviour of the planets. *Philosophical Transactions of the Royal Society of London (series A),* 357, 1761–1787.

Olsen, P., McDonald, N. and Kinney, S., 2018. Lake algal-rafted lithic and biotic debris and the origin of insect Lagerstätten, *Geophysical Research Abstracts.* 20, EGU2018-11440-2, EGU General Assembly.

Oriel, S.S. and Tracey, J.I., 1970. *Uppermost Cretaceous and Tertiary stratigraphy of Fossil basin, southwestern Wyoming* (53). Washington, DC: US Government Printing Office.

Pagani, M., Zachos, J.C., Freeman, K.H., Tipple, B. and Bohaty, S., 2005. Marked decline in atmospheric carbon dioxide concentrations during the Paleogene. *Science,* 309, 600–603.

Pagani, M., Pedentchouk, N., Huber, M., Sluijs, A., Schouten, S., Brinkhuis, H., Damsté, J.S.S. and Dickens, G.R., 2006. Arctic hydrology during global warming at the Palaeocene/Eocene thermal maximum. *Nature*, 442(7103), 671–675.

Pearson. P.N. and Palmer. M.R., 2000, Atmospheric carbon dioxide concentrations over the past 60 million years. *Nature,* 406(6797), 695–699.

Pedentchouk, N., Freeman, K.H., Harris, N.B., 2006. Different response of δD values of *n*-alkanes, isoprenoids, and kerogen during thermal maturation. *Geochimica et Cosmochimica Acta.* 70(8), 2063–2072. https://doi.org/10.1016/j.gca.2006.01.013

Pedentchouk, N., Sumner, W., Tipple, B. and Pagani, M., 2008. $\delta^{13}C$ and δD compositions of *n*-alkanes from modern angiosperms and conifers: an experimental set up in central Washington State, USA. *Organic Geochemistry*, 39(8), 1066–1071.

Peters K.E., Walters C.C. and Moldowan J. M., 2005. *The biomarker guide: Volume 1, Biomarkers and isotopes in petroleum exploration and Earth history.* Cambridge University Press, Cambridge, UK.

Peters, K.E., Walters, C.C. and Moldowan, J.M., 2007. *The biomarker guide: Volume 2, Biomarkers and isotopes in petroleum systems and earth history.* Cambridge University Press.

Philp, R.P., 1994. Geochemical characteristics of oils derived predominantly from terrigenous source materials. *Geological Society London Special Publications,* 77, 71–91.

Pietras, J.T., Carroll, A.R. and Rhodes, M.K., 2003a. Lake basin response to tectonic drainage diversion: Eocene Green River Formation, Wyoming. *Journal of Paleolimnology,* 30, 115–125.

Pietras, J.T., Carroll, A.R., Singer, B.S. and Smith, M.E., 2003b. 10 k.y. depositional cyclicity in the early Eocene: Stratigraphic evidence and $^{40}Ar/^{39}Ar$ evidence from the lacustrine Green River Formation. *Geology*, 31, 593–597.

Pietras, J.T. and Carroll, A.R., 2006. High- resolution stratigraphy of an underfilled lake basin: Wilkins Peak Member, Eocene Green River Formation, Wyoming, USA. *Journal of Sedimentary Research,* 76, 1197–1214.

Pietras, J.T., Selby, D., Brembs, R. and Dennett, A., 2020. Tracking drainage basin evolution, continental tectonics, and climate change: implications from osmium isotopes of lacustrine systems. *Palaeogeography, Palaeoclimatology, Palaeoecology,* 537, 109471.

Plewa, K., Meggers, H., Kuhlmann, H., Freudenthal, T., Zabel, M. and Kasten, S., 2012. Geochemical distribution patterns as indicators for productivity and terrigenous input off NW Africa, Deep Sea Research Part I: *Oceanographic Research Papers,* 66, 51–66.

Plink-Björklund, P., 2015. Morphodynamics of rivers strongly affected by monsoon precipitation: Review of depositional style and forcing factors. *Sedimentary Geology,* 323, 110–147, https://doi.org/10.1016/j .sedgeo.2015.04.004.

Rach, O., Kahmen, A., Brauer, A., Sachse, D., 2017. A dual-biomarker approach for quantification of changes in relative humidity from sedimentary lipid D⁄H ratios. Climate of the Past, 13(7), 741–757.

Reagan, M.K., McClelland, W.C., Girard, G., Goff, K.R., Peate, D.W., Ohara, Y. and Stern, R.J., 2013. The geology of the southern Mariana fore-arc crust: Implications for the scale of Eocene volcanism in the western Pacific. *Earth and Planetary Science Letters*, 380, 41–51.

Remy, R.R., 1992. Stratigraphy of the Eocene part of the Green River Formation in the south-central part of the Uinta Basin, Utah. No. 1787-BB.

Ripepe, M., Roberts, L.T. and Fischer, A.G., 1991. Enso and sunspot cycles in varved Eocene oil shales from image analysis. *Journal of Sedimentary Petrology,* 61, 1155–1163.

Risatti, J.B., Rowland, S.J., Yon, D.A. and Maxwell, J.R., 1984. Stereochemical studies of acyclic isoprenoids—XII. Lipids of methanogenic bacteria and possible contributions to sediments. *Organic Geochemistry,* 6, 93–104.

Rodriguez-Pascua, M. and Calvo, J.P., Vicente, G., and Gómez-Gras., 2000, Seismites in lacustrine sediments of the Prebetic Zone, SE Spain, and their use as indicators of earthquake magnitudes during the Late Miocene. *Sedimentary Geology*, 135, 117–135. 10.1016/S0037-0738(00)00067-1.

Roehler, H.W., 1993. Eocene climates, depositional environments, and geography, greater Green River Basin, Wyoming, Utah, and Colorado. *U.S.Geologicalc Survey Professional Paper,* 1506-F.

Röhl, U., Bralower, T.J., Norris, R.D. and Wefer, G., 2000. New chronology for the late Paleocene thermal maximum and its environmental implications. *Geology*, *28*(10), 927–930.

Röhl, U., Brinkhuis, H., Stickley, C.E., Fuller, M., Schellenberg, S.A., Wefer, G. and Williams, G.L., 2004. Sea level and astronomically induced environmental changes in Middle and Late Eocene sediments from the East Tasman Plateau. Washington DC *American Geophysical Union Geophysical Monograph Series,* 151, 127–151.

Rontani, J.F. and Volkman, J.K., 2003. Phytol degradation products as biogeochemical tracers in aquatic environments. *Organic Geochemistry*, 34(1), 1–35.

Sachse, D., Radke, J. and Gleixner, G., 2004. Hydrogen isotope ratios of recent lacustrine sedimentary *n*-alkanes record modern climate variability. *Geochimica et Cosmochimica Acta*, 68(23), 4877–4889.

Sachse, D., Billault, I., Bowen, G.J., Chikaraishi, Y., Dawson, T.E., Feakins, S.J., Freeman, K.H., Magill, C.R., McInerney, F. A., van der Meer, M.T.J., Polissar, P., Robins, R.J., Sachs, J.P., Schmidt, H., Sessions, A.L., White, J.W.C., West, J.B., Kahmen, A., 2012. Molecular Paleohydrology: Interpreting the Hydrogen-Isotopic Composition of Lipid Biomarkers from Photosynthesizing Organisms. *Annual Review of Earth and Planetary Sciences*, 40(1), 221–249.

Sarmiento, L.F. and Rangel, A., 2004. Petroleum systems of the upper Magdalena Valley, Colombia. *Marine Petroleum Geology,* 21, 373–391.

Sayles, R.W., 1922. The dilemma of the paleoclimatologists. *American Journal of Science,* Series 5, 3, 458.

Scalan, E.S. and Smith, J.E., 1970. An improved measure of the odd-even predominance in the normal alkanes of sediment extracts and petroleum. *Geochimica et Cosmochimica Acta*, 34(5), 611–620. doi:10.1016/0016-7037(70)90019-0.

Schieber, J., 2007. Oxidation of detrital pyrite as a cause for marcasite formation in marine lag deposits from the Devonian of the eastern US. *Deep Sea Research Part II: Topical Studies in Oceanography*, *54*(11–13), 1312–1326.

Schimmelmann, A., Lewan, M.D. and Wintsch, R.P., 1999. D/H isotope ratios of kerogen, bitumen, oil, and water in hydrous pyrolysis of source rocks containing kerogen types I, II, IIS, and III. *Geochimica et Cosmochimica Acta,* 63(22), 3751–3766.

Schouten, S., Forster, A., Panoto, F.E. and Damsté, J.S.S., 2007. Towards calibration of the TEX^{86} palaeothermometer for tropical sea surface temperatures in ancient greenhouse worlds. *Organic Geochemistry*, 38(9), 1537–1546.

Senftle, J.T., Landis, C.R. and McLaughlin, R.L., 1993. *Organic petrographic approach to kerogen characterization*. In Organic geochemistry, 355–374. Springer, Boston, MA.

Sessions, A.L., Slyva S.P., Summons, R.E. and Hayes, J.M., 2004. Isotopic exchange of carbon-bound hydrogen over geologic timescales. *Geochimica et Cosmochimica Acta,* 68 (7), 1545–1559. https://doi:10.1016/j.gca.2003.06.004.

Sewall, J.O. and Sloan, L.C., 2006. Come a little bit closer: A high-resolution climate study of the early Paleogene Laramide foreland. *Geology*, 34(2), 81–84.

Sexton, P.F., Norris, R.D., Wilson, P.A., Pälike, H., Westerhold, T., Röhl, U., Bolton, C.T. and Gibbs, S., 2011. Eocene global warming events driven by ventilation of oceanic dissolved organic carbon. *Nature,* 471, 349–352, https://doi.org/10.1038/nature09826, 2011.

Sheliga, C.M., 1980. Sedimentology of the Eocene Green River Formation in Sevier and Sanpete Counties, Central Utah *[Doctoral thesis]* The Ohio State University.

Silliman, J.E., Meyers, P.A. and Bourbonniere, R.A., 1996. Record of postglacial organic matter delivery and burial in sediments of Lake Ontario. *Organic Geochemistry*, 24, 463–472.

Simon, M., Grossart, H., Schweitzer, B. and Ploug, H., 2002. Microbial ecology of organic aggregates in aquatic ecosystems. *Aquatic Microbial Ecology*, 28, 175–211.

Sinninghe Damsté, J.S., Kenig, F., Koopmans, M.P., Köster, J., Schouten, S., Hayes, J.M. and de Leeuw, J.W., 1995. Evidence for gammacerane as an indicator of water column stratification. *Geochimica et Cosmochimica Acta*, 59(9), 1895–1900.

Sluijs, A., and G. R. Dickens., 2012. Assessing offsets between the $\delta^{13}C$ of sedimentary components and the global exogenic carbon pool across early Paleogene carbon cycle perturbations. *Global Biogeochemical Cycles*, 26(4) doi:10.1029/2011GB004224.

Sloan, L.C., 1994. Equable climates during the early Eocene: Significance of regional paleogeography for North American climate. *Geology*, 22(10), 881–884.

Smith, M.E., Singer, B. and Carroll, A.R., 2003. $^{40}Ar/^{39}Ar$ geochronology of the Eocene Green River Formation, Wyoming. *Geological Society of America Bulletin,* 115, 549–565.

Smith, F.A. and Freeman, K.H., 2006. Influence of physiology and climate on δD of leaf wax *n*-alkanes from C3 and C4 grasses. *Geochimica et Cosmochimica Acta*, 70(5), 1172–1187.

Smith, M.E., Carroll, A.R. and Singer, B.S., 2008. Synoptic reconstruction of a major ancient lake system: Eocene Green River Formation, western United States. *Geological Society of America Bulletin,* 120, 54–84. http://dx.doi.org/10.1130/B26073.1.

Smith, M.E., Chamberlain, K.R., Singer, B.S. and Carroll, A.R., 2010. Eocene clocks agree: Coeval $^{40}Ar/^{39}Ar$, U-Pb, and astronomical ages from the Green River Formation. *Geology*, 38, 6, 527530.

Smith, R.Y., Basinger, J.F. and Greenwood, D.R., 2012. Early Eocene plant diversity and dynamics in the Falkland flora, Okanagan Highlands, British Columbia, Canada, *Palaeobiodiversity and Palaeoenvironment,* 92, 309–328, https://doi.org/10.1007/s12549-011-0061-5.

Smith, M.E. and Carroll, A.R., 2015. Introduction to the Green River Formation. *In Stratigraphy and Paleolimnology of the Green River Formation, Western USA*, 1–12, Springer, Dordrecht.

Snell, K.E., Thrasher, B.L., Eiler, J.M., Koch, P.L., Sloan, L.C. and Tabor, N.J., 2013. Hot summers in the Bighorn Basin during the early Paleogene. *Geology*, 41(1), 55–58.

Stap, L., Sluijs, A., Thomas, E. and Lourens, L., 2009. Patterns and magnitude of deep sea carbonate dissolution during Eocene Thermal Maximum 2 and H2, Walvis Ridge, southeastern Atlantic Ocean, *Paleoceanography*, 24, PA1211, doi:10.1029/2008PA001655.

Stein, R.A., Sheldon, N.D., Allen, S.E., Smith, M.E., Dzombak, R.M. and Jicha, B.R., 2021. Climate & Ecology in the Rocky Mountain Interior After the Early Eocene Climatic Optimum, *Climate of the Past Discuss.* [preprint], https://doi.org/10.5194/cp-2021-45.

Sun, Y., Wu, F., Clemens, S. C. and Oppo, D. W., 2008. Processes controlling the geochemical composition of the South China Sea sediments during the last climatic cycle. *Chemical Geology*, 257, 240–246.

Svensen, H., Planke, S., Malthe-Sørenssen, A., Jamtveit, B., Myklebust, R., Eidem, T.R. and Rey, S.S., 2004. Release of methane from a volcanic basin as a mechanism for initial Eocene global warming. *Nature*, 429(6991), 542–545.

Tänavsuu-Milkeviciene K. and Sarg J. F., 2012. Evolution of an organic-rich lake basin - stratigraphy, climate and tectonics: Piceance Creek basin, Eocene Green River Formation. *Sedimentology,* 59, 1735–1768.

Teichmuller, M. and Ottenjahn, K., 1977. Liptinite und lipoide stoffe einem erdolmuttergestein: Souderdruck aus Erdohl und Kohle, 30. 387–398.

ten Haven, H. L., de Leeuw, J. W., Rullkötter, J. and Sinninghe Damsté, J. S., 1987. Restricted utility of the pristane/phytane ratio as a palaeoenvironmental indicator. *Nature*, 330, 641–643.

Thomas, E., Zachos, J.C. and Bralower, T.J., 2000. Deep-sea environments on a warm earth: latest Paleocene-early Eocene. Division III Faculty Publications. Paper 116. http://wesscholar.wesleyan.edu/div3facpubs/116

Tissot, B., Deroo, G., Hood, A., 1978. Geochemical study of the Uinta Basin: Formation of petroleum from the Green River Formation. *Geochimica et Cosmochimica Acta,* 42, 1469–1485.

Tuttle, M.L. and Goldhaber, M.B., 1993. Sedimentary sulfur geochemistry of the Paleogene Green River Formation, western USA: Implications for interpreting depositional and diagenetic processes in saline alkaline lakes. *Geochimica et Cosmochimica Acta*, 57(13), 3023–3039.

van Dijk, J., Fernandez, A., Bernasconi, S. M., Caves Rugenstein, J. K., Passey, S. R. and White, T., 2020. Spatial pattern of super-greenhouse warmth controlled by elevated specific humidity, *Nature Geoscience,* 13, 739–744, https://doi.org/10.1038/s41561-020-00648-2.

Van Gijzel, P., 1979. Manual of the techniques and some geological applications of fluorescence microscopy. In *American Association of Stratigraphic Palynologists,* 12 Annual Meeting Workshop, Dallas.

Vanden Berg, M.D., 2008. *Basin-wide evaluation of the uppermost Green River Formation's oil-shale resource, Uinta Basin, Utah and Colorado*, 128, Utah Geological Survey.

Vanden Berg, M.D. and Birgenheier, L.P., 2017. An examination of the hypersaline phases of Eocene Lake Uinta, upper Green River Formation, Uinta Basin, Utah: *Journal of Paleolimnology*, 58, 353–371. https:// doi.org/10.1007/s10933-017-9983-x.

Venkatesan, M.I., 1989. Tetrahymanol: its widespread occurrence and geochemical significance. *Geochimica et Cosmochimica Acta*, 53(11), 3095–3101.

Volkman, J.K., Barrett, S.M., Blackburn, S.I., Mansour, M.P., Sikes, E.L. and Gelin. F., 1998. Microalgal biomarkers: a review of recent research developments. *Organic Geochemistry,* 29, 1163–79.

Walters, A.P., Meyers S.R., Carroll, A.R., Hill, T.R., Vanden Berg, M.D., 2020. Lacustrine cyclicity In the Early Eocene Green River Formation, Uinta Basin, Utah: Evidence From X-Ray Fluorescence Core Scanning. *Journal of Sedimentary Research*, 90, 429–447. DOI: http://dx.doi.org/10.2110/jsr.2020.24

Wang, C., Adriaens, R., Hong, H., Elsen, J., Vandenberghe, N., Lourens, L.J., Gingerich, P.D. and Abels, H.A., 2017. Clay mineralogical constraints on weathering in response to early Eocene hyperthermal events in the Bighorn Basin, Wyoming (Western Interior, USA). *Geological Society of America Bulletin,* 129, 997–1011.

Washburn, K.E., Birdwell, J.E., Foster, M. and Gutierrez, F., 2015. Detailed description of oil shale organic and mineralogical heterogeneity via Fourier transform infrared microscopy: Energy & Fuels, 29, 4264–4271.

Weiss, H.M., Wilhelms, A., Mills, N., Scotchmer, J., Hall, P.B., Lind, K. and Brekke, T., 2000. NIGOGA - The Norwegian Industry Guide to Organic Geochemical Analyses. Edition 4.0 Published by Norsk Hydro, Statoil, Geolab Nor, SINTEF Petroleum Research and the Norwegian Petroleum Directorate, 102.

Weltje, G.J. and von Eynatten, H., 2004. Quantitative provenance analysis of sediments: review and outlook. *Sedimentary Geology,* 171(1–4), 1–11, ISSN 0037-0738, https://doi.org/10.1016/j.sedgeo.2004.05.007.

West, C. K., Greenwood, D.R., Reichgelt, T., Lowe, A.J., Vachon, J.M. and Basinger, J.F., 2020. Paleobotanical proxies for early Eocene climates and ecosystems in northern North America from middle to high latitudes, *Climate of the Past,* 16, 1387–1410.

Westerhold, T., Röhl, U., Frederichs, T., Agnini, C., Raffi, I., Zachos, J.C. and Wilkens, R.H., 2017. Astronomical calibration of the Ypresian timescale: implications for seafloor spreading rates and the chaotic behaviour of the solar system? *Climate of the Past,* 13, 1129–1152.

Westerhold, T., Röhl, U., Donner, B. and Zachos, J.C., 2018a. Global Extent of Early Eocene Hyperthermal Events: A new Pacific benthic foraminiferal isotope record from Shatsky Rise (ODP Site 1209), *Paleoceanography and Paleoclimatology,* 33, 626–642, https://doi.org/10.1029/2017PA003306.

Westerhold, T., Röhl, U., Wilkens, R.H., Gingerich, P.D., Clyde, W.C., Wing, S.L., Bowen, G.J. and Kraus, M.J., 2018b. Synchronizing early Eocene deep-sea and continental records- cyclostratigraphic age models for the Bighorn Basin Coring Project drill cores, *Climate of the Past,* 14, 303–319, https://doi.org/10.5194/cp-14-303-2018.

Westerhold, T., Marwan, N., Drury, A.J., Liebrand, D., Agnini, C., Anagnostou, E., Barnet, J.S.K., Bohaty, S.M., Vleeschouwer, D.D., Florindo, F., Frederichs, T., Hodell, D.A., Holbourn, A.E., Kroon, D., Lauretano, V., Littler, K., Lourens, L.J., Lyle, M., Pälike, H., Röhl, U., Tian, J., Wilkens, R.H., Wilson, P.A. and Zachos, J.C., 2020. An astronomically dated record of Earth's climate and its predictability over the last 66 million years, *Science,* 369, 1383–1387, https://doi.org/10.1126/science.aba6853.

Whiteside, J.H. and Van Keuren, M.A., 2009. Multiproxy environmental characterization of lake level cycles in the Green River Formation of Utah and Colorado. *Open-File Report 544, Utah Geological Survey*, 26.

Whitlock. C., Marlon. J., Briles. C., Brunelle A., Long. C. and Bartlein P., 2008. Long-term relations among fire, fuel, and climate in the north-western US based on lake-sediment studies. *International Journal of Wildland Fire,* 17, 72–83. https://doi.org/10.1071/WF07025

Wignall, P. B. and Newton, R., 1998. Pyrite framboid diameter as a measure of oxygen deficiency in ancient mudrocks. *American Journal of Science*, *298*(7), 537–552.

Wilf, P., 2000. Late Paleocene-Early Eocene climate changes in south-western Wyoming: Paleobotanical analysis. *Geological Society of America Bulletin*, 112, 292–307.

Wilf, P., Cúneo, N. R., Johnson, K. R., Hicks, J. F., Wing, S. L. and Obradovich. J.D., 2003. High plant diversity in Eocene South America: evidence from Patagonia. *Science*, 300(5616), 122–125.

Wing, S.L. and Greenwood, D.R., 1993. Fossils and fossil climate: the case for equable continental interiors in the Eocene. *Philosophical Transactions of the Royal Society of London. Series B: Biological Sciences*, 341(1297), 243–252.

Wing, S.L., 1998. Late Paleogene–Early Eocene floral and climatic change in the Bighorn Basin, Wyoming: in M. Aubry, S. Lucas, W. Berggren eds. *Late Paleocene–Early Eocene Climatic and Biotic Events in the Marine and Terrestrial Records*, 380–400. Columbia University Press New York.

Wing, S.L., Harrington, G.J., Smith, F.A., Bloch, J.I., Boyer, D.M. and Freeman, K.H., 2005. Transient floral change and rapid global warming at the Paleocene-Eocene boundary. *Science*, 310(5750), 993–996.

Witkowski, C. R., Weijers, J. W. H., Blais, B., Schouten, S. and Sinninghe Damsté, J. S., 2018. Molecular fossils from phytoplankton reveal secular pCO_2 trend over the Phanerozoic. *Science Advances,* 4, eaat4556.

Wolfe, J.A., 1981. A chronologic framework for Cenozoic megafossil floras of northwestern North America and its relation to marine geochronology. *Geological Society of America Special* Paper l84, 39–47.

Wolfe, J.A., 1985. Distribution of major vegetational types during the Tertiary. *The carbon cycle and atmospheric CO_2: Natural variations Archean to present,* 32, 357–375.

Young G.M. and Nesbitt H.W., 1998. Processes controlling the distribution of Ti and Al in weathering profiles. siliciclastic sediments and sedimentary rocks. *Journal of Sedimentary Research,* 68(3), 448–455.

Zachos, J., Pagani, M., Sloan, L., Thomas, E. and Billups, K., 2001. Trends, rhythms, and aberrations in global climate 65 Ma to present. *Science,* 292, 686–693, https://doi.org/10.1126/science.1059412.

Zachos, J.C., Dickens, G.R. and Zeebe, R.E., 2008. An early Cenozoic perspective on greenhouse warming and carbon-cycle dynamics. *Nature,* 451, 279–283.

Zachos, J.C., McCarren, H., Murphy, B., Röhl, U. and Westerhold, T., 2010. Tempo and scale of late Paleocene and early Eocene carbon isotope cycles: Implications for the origin of hyperthermals. *Earth and Planetary Science Letters,* 299, 242–249, https://doi.org/10.1016/j.epsl.2010.09.004.

Zander, J.M., Caspi, E., Pandey, G.N. and Mitra, C.R., 1969. The presence of tetrahymanol in *Oleandra wallichii*. *Phytochemistry,* 8, 2265–226.

Zeebe, R.E., and Lourens, L.J., 2019. Solar System chaos and the Paleocene–Eocene boundary age constrained by geology and astronomy. *Science*, 365(6456), 926–929.